# Measuring mountain glaciers and snow with a spaceborne laser

Désirée Treichler


Thesis submitted for the degree of Philosophiae Doctor (PhD)

Department of Geosciences
Faculty of Mathematics and Natural Sciences
University of Oslo

Oslo, Norway
April 2017

*Series of dissertations submitted to the*
*Faculty of Mathematics and Natural Sciences, University of Oslo*
*No. 1870*

ISSN 1501-7710



Cover: Hanne Baadsgaard Utigard.
Print production: Reprosentralen, University of Oslo.

# Abstract

Under atmospheric warming, the mountain cryosphere is undergoing changes that affect the people living in the mountains and also the surrounding lowlands. However, our knowledge of snow depths and ongoing glacier changes in remote mountain areas is still incomplete. In rough terrain, it is difficult to study volume changes accurately at a regional scale. The ICESat mission sampled the elevation of the Earth's surface along profiles around the entire globe from 2003 through 2009. This thesis shows how ICESat's sparse, but accurate elevation samples can be spatially integrated to estimate snow depths and average glacier volume changes in remote mountainous areas. The focus lies on two study sites: southern Norway, where glacier changes and snow depths are relatively well known, and High Mountain Asia (HMA), where our knowledge of the mountain cryosphere is very limited. To introduce the subject, the thesis contains an extensive review of methods to measure surface elevations with remote sensing methods, followed by an introduction to the ICESat mission and data, including the upcoming successor mission ICESat-2, and concludes with a summary and discussion of ICESat applications for glaciers and snow.

The original goal of the ICESat mission was to measure surface elevation changes of the large, flat ice sheets, and its application in rough topographies was hampered by two main limitations: (i) ICESat's comparably large spatial footprints of ~70 m in diameter cause uncertainty in the elevation measurement due to within-footprint topography, and (ii) the spatial offsets of up to hundreds of metres between ground tracks of the same repeat-orbit make that elevations from different overpasses cannot be compared directly. These challenges are overcome by grouping several samples, so that uncertainties are averaged out, and by using a digital elevation model (DEM) to model the surface between repeat-tracks. Rather than comparing elevations directly, ICESat's elevations are first compared to the DEM elevations at the same location to receive local elevation differences (dh). For samples on snow-covered terrain, the dh correspond to snow depth. On glaciers, decreasing (increasing) dh over time indicate glacier thinning (thickening).

The method to use ICESat data for regional snow depths is new. It was developed and applied for the first time within this thesis. In southern Nor-

way, it yields average March/June snow depths for a given elevation band every few kilometres along ICESat's ground tracks. The spatial patterns of increasing snow depths closer towards the west coast and at higher elevations are correctly represented. Unexpectedly, the main source of uncertainty lies not with ICESat's large footprints and the terrain variations therein, but within the reference DEM: spatially varying, systematic vertical bias in three tested DEMs severely hamper accurate snow depth estimates. We present a way to correct such bias locally by using ICESat's elevation samples acquired during snow-free seasons. After such correction, the uncertainty of the method is ca. 0.5 m for spatially averaged estimates compared to measured and modelled data of the same area. Given a high resolution DEM without vertical bias, even snow depth estimates for single footprints agree within ca. 1 m with measured snow depths.

ICESat data has been used on mountain glaciers before, but the methods lacked validation and its representativeness was questioned. On the example of southern Norway, this work shows that ICESat's sampling is indeed able to capture a regional glacier elevation change signal that corresponds to the regionally averaged glacier mass balance — but certain conditions have to be fulfilled: not only the combined sample of the entire acquisition period, also the sample of each individual campaign needs to correctly represent the regional glaciers and other influencing factors. This is not necessarily the case, since the ICESat ground tracks vary in space. The spatial sample distribution thus differs for each campaign. Inconsistent sampling of the glacier hypsometry or spatially varying vertical DEM offsets bear the greatest bias potential. A new per-glacier correction is introduced that effectively removes the influence of such DEM bias. The improved method is applied in HMA, where a new spatial zonation reveals a spatially diverse pattern of glacier changes with more detail than previous estimates. Locally very different behaviour can be attributed to greatly varying glacier sensitivity to precipitation and changes thereof. In the 2003–2008 period, glaciers were thinning everywhere in HMA except for the Kunlun Shan and northwestern Tibetan Plateau: In this extremely dry region, a step-increase of precipitation around the year 2000 caused glaciers to thicken in the period covered by ICESat.

The methods presented in this thesis can also be employed in other remote mountain areas to estimate snow depths or glacier changes at a regional scale. Accurate elevation data that do not contain spatially varying DEM bias, e.g. from airborne lidar or upcoming global DEMs such as the TanDEM-X DEM, have the potential to greatly decrease the uncertainty of the methods. Data from the ceased ICESat mission only provides a snapshot of the short time span between 2003 and 2009, but the methods will be useful also for data provided by the upcoming ICESat-2 mission.

# Acknowledgements

Before committing to four years' worth of dealing with space lasers, it seems I first had to try out all other possibilities, including moving from Europe to the end of the world. July in Tasmania is a good month to write a PhD application to Norway, just over New Year is maybe a less obvious time to move there. But the shock freeze welcome back at the antipode included only the weather, and I never regret the move.

My greatest thanks go to the section for geography and hydrology at the University of Oslo: you are the most fantastic colleagues. I could not have found a better group with a warmer atmosphere or more cooperative spirit to embark on a PhD project. Andy, my main adviser, and Bernd, section leader: I really appreciate your guidance, support, confidence, and the freedom you gave me. I learned so much more than about space lasers only.

Many other people were important on the way here, especially my family who always encouraged me to look at the world with open eyes. It would probably never have come to my mind to send that PhD application if it weren't for my friends and former colleagues at the Remote Sensing Laboratories at the University of Zürich, in particular Zbyněk, Andy, Felix, and the friends of the Schlitzwandbagger. Thanks to the geology and GIS crew at Nagra and the geoscience group at the University of Tasmania, you had an important role on my way here. Thanks also to the physical geography group at the University of Fribourg, and Inka and the glaciology group at ICIMOD, for hosting me last year and giving me new ways to look at glaciers and many other things, too. Since I arrived in the North, I have met many great people that shared my bubbling enthusiasm, supported me when needed, fed me chocolate, climbed mountains with me and the rest of the fjellgjengen, posed for skiing pictures, fed me more chocolate, sung with me in Grorud, biked with me in forests, pouring rain, Kathmandu's dirt roads, or to Bygdøy to go paddling, read through my drafts, and deserve an applause. Anne, Marianne, Kjersti, and especially Espen and my family, I greatly appreciate your support also when the idea of writing acknowledgements seemed very far away. Dear family and friends here in Norway, in Switzerland, and all across the globe: thank you.

# Contents

# Part I

# Overview

# Chapter 1

# Introduction

## 1.1 The role of glaciers and snow

Atmospheric warming has a heavy impact on the entire cryosphere, the frozen part of the Earth. With the world's growing population, the interest in studying the different elements of the cryosphere is higher than ever before: To prepare for further changes to come, we need knowledge and in-depth understanding of the status quo.

Glaciers and snow are attractive landscape elements many people relate to personally. Especially in mountain areas, they are the source of great recreational joys — but also of hazards such as avalanches or glacier lake outburst floods, threatening the live and infrastructure of mountain communities (Kääb, 2005; Richardson and Reynolds, 2000). Snow cover interacts with the climate through albedo feedbacks. Its role as a boundary layer between the air and the ground determines permafrost conditions and affects the local vegetation and ecosystem (Dietz et al., 2012). And only where there is sufficient snow, glaciers can exist. They helped shape valleys and moraines, and their persistent existence may have a stabilising effect on steep valley rock walls (Fischer et al., 2006, 2013). Both forms of frozen water have an extremely important role in the world's hydrological cycle (Viviroli et al., 2007). Meltwater from glaciers and snow shape the annual river runoff cycle, also for areas and communities far downstream. That water is needed for drinking, electricity and irrigation. Thereby, the runoff timing and flow volumes are key for a constant, reliable supply — or floods and water shortage during low flows. Finally, even far away from glacierised catchments, coastal communities and authorities alike are concerned about sea level rise, partly caused by the ice that melted from thinning and retreating glaciers in distant mountain areas (Meier et al., 2007; Gardner et al., 2013; Marzeion et al., 2015).

(a) Skiers on Uranosbreen, Norway (1800 m a.s.l.)

(b) Carrying up gear to build a weather station on Yala glacier, Langtang Himal, Nepal (5300 m a.s.l.).

Figure 1.1: Glaciers in Norway and the Himalayas

The role and importance of glaciers and snow is not the same everywhere in the world, nor is the status quo of knowledge. Norway is probably one of the countries where they are monitored best: through a dense network of weather stations, regular snow measurements, and a well set-up glacier mass balance program with records reaching many decades back (Fleig et al., 2013; NVE, 2016). This is maybe not surprising, as these phenomenons dominate the landscape — and thus the life of the people — for large parts of the year. They are a part of the country's cultural identity, and an important resource. Irrigation may not be a prime issue in that rather rainy clime, but floods or hydropower are — also economically, hence the intense monitoring efforts.

In most other great mountain areas, the situation is a different one — in High Mountain Asia (HMA) in particular. There, most people live on the plains below the mountain ranges surrounding the Tibetan Plateau (TP), where conditions are much less harsh than in the rugged, difficult to access mountain areas (fig. 1.1b). When asked about glaciers, people in HMA and surrounding areas do not enthuse about beautiful landscapes and skiing as the Norwegians do (fig. 1.1a), they think mostly of water. Melt water from the mountain cryosphere is of the utmost importance in the arid, continental climate with adjacent lowlands (Kaser et al., 2010). The lowland populations of HMA depend greatly on the water originating from high elevations all year long, not only during the peak precipitation seasons. Whereas spring snow melt mainly has a delaying effect on runoff on a seasonal scale (e.g. Gurung et al., 2017), glaciers act as a long-term storage system for water — providing consistent supplies for years or even centuries (Jansson et al., 2003; Bolch et al., 2012).

While the public interest and impact of cryosphere-related changes may be huge, the scarcity of data is of a real concern. The remoteness and inaccessibility of many mountain areas in the world cause severe limits to our knowledge both about snow amounts at high altitudes and the state and fate of glaciers. In HMA, there are few direct measurements from weather stations, barely any information on snow depths, and only a handful of glaciers have been visited and studied repeatedly (WGMS, 2016). Even in Norway with its comparably dense network of measurements, interpolation and modelling are needed to paint a regional, spatially resolved picture of snow depths or glacier changes.

For regional studies, remotely sensed data is the solution to data gaps from missing in-situ observations — in particular data from spaceborne missions. Inaccessibility and remoteness do not impede a satellite in orbit. Spaceborne data has of course a major shortcoming: it completely fails to provide the in-situ impressions and understanding gained from a field visit. Its great strength, on the other hand, lies in giving a spatial overview by covering a much larger area more extensively than field observations possibly can. With this advantage, remote sensing data is the method of choice to map the current state and ongoing changes of mountain glaciers and snow.

Spaceborne remote sensing data contribute to our knowledge about the cryosphere in several ways: i) the current extent of glaciers and snow-covered area is visible in optical imagery, ii) glacier movements are retrieved from e.g. correlating time-offset optical or radar imagery, iii) optical or radar backscatter data can provide information on snow/ice surface conditions such as impurities or moisture content that determine the surface energy balance, and iv) mass changes are provided directly from gravimetric data on very coarse scale or v) indirectly from volumetric changes using elevation data with different timestamps. This work focuses on the latter of the five. Changes in ice/snow volumes have the most direct use from a hydrology/runoff point of view, as they directly translate into water that flows down the rivers that sustain lowland populations. In mountainous areas, glacier volume changes are commonly derived from Digital Elevation Models (DEMs) from spaceborne stereo-photogrammetry or interferometric Synthetic Aperture Radar (SAR), albeit with some limitations discussed later. Laser altimetry provides an alternative way to estimate not only regional glacier volume changes but also snow depths.

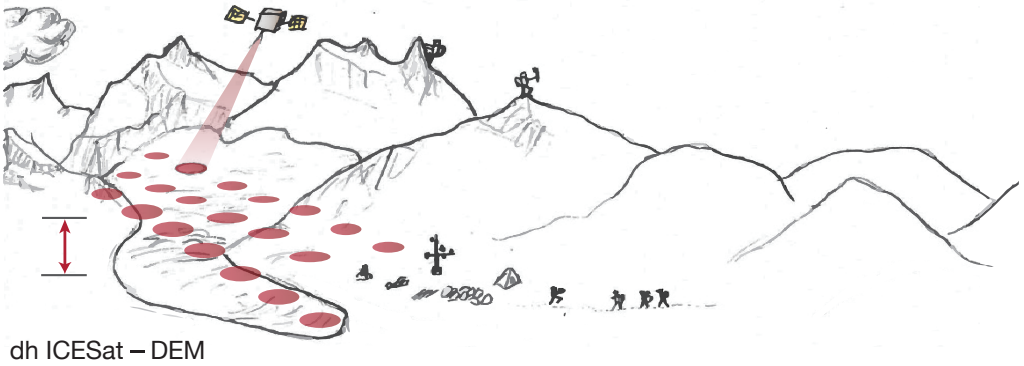


Figure 1.2: Elevation differences (dh) between ICESat footprints and a reference DEM on a mountain glacier.

## 1.2 Objectives

It is the purpose of this work to show how spaceborne laser altimetry can be used to monitor mountain glaciers and snow on a regional scale. Thereby, reference elevations from DEMs are compared with surface elevation measurements from ICESat (fig. 1.2), a laser satellite operational between 2003 and 2009. For ICESat data acquired on snow-covered, stable ground, the elevation differences (dh) between the two datasets correspond to snow depths. Glaciers change their surface elevation according to mass balance and flow dynamics, thus increasing (decreasing) dh with time indicate glacier thickening (thinning). Uncertainties in both elevation datasets require grouping of measurements and corrections to remove bias. These topics are expanded on in the publications.

The two study areas — Norway and HMA — differ not only in the role glaciers and snow have for the local communities, but also in availability of reference and validation data. 'Regional', as we use the term here, thus occupies a scale range stretching roughly from a river catchment to an entire continent. The work resulted in three publications, two of which are published and one in preparation. The main research objectives are:

- Show how space laser altimetry can provide valuable volumetric information on the cryosphere in mountainous terrain, namely glaciers and snow.
- Illustrate the potential of such satellite-based measurements on a spatial scale range dominated by modelled data, through the unique combination of very localised, direct surface elevation measurements and regional summarising.

- Discuss uncertainties in (global) elevation datasets that affect ICESat-based volume change studies, and propose solutions to reduce bias caused by these uncertainties.

## 1.3 Outline

To introduce the publications, this prologue provides an overview over space-based methods to measure surface elevation, available elevation products, and associated uncertainties (chapter 2). A separate chapter (3) is dedicated to the ICESat mission and data. Existing methods for glacier and snow applications are reviewed, with special attention to the challenges from applications in mountainous terrain (this work) versus flatter surfaces such as ice sheets (most previous studies). Chapter 4 summarises the two journal articles and the manuscript that are the result of this work. Finally, chapter 5 places the main findings in a broader context and proposes directions for future work.

# Chapter 2

# Methods to measure the surface elevation of snow and ice

The last century was the century where the Earth was mapped (Collier, 2002). After World War I, the introduction of the airplane suddenly expanded the possibilities to fill white spots on the maps. The wealth of satellite data emerging in recent decades, and continuing to grow exponentially, again revolutionised our knowledge of the Earth's surface. Both imagery data (e.g. photogrammetry), ranging methods (laser, radar) and combinations thereof (SAR interferometry) are being used — locally and increasingly also globally.

This chapter provides an overview of methods to measure the Earth's surface elevation and the data they produce. The focus lies on data and products relevant for the regional-scale applications presented in this work, i.e. satellite-based elevation data and products available globally or for the two study sites.

## 2.1 Stereo methods

Photogrammetry is the practice of measuring objects or landscapes from photographic imagery, using perspective. Geometry and perspective are principles that were known already to Leonardo Da Vinci in the fifteenth century. Photogrammetry is thus the oldest of the techniques described here, and undoubtedly the most familiar to everyone: our eyes use the same trick to see a three-dimensional world from two images with slightly different perspective, a process also called stereoscopy (fig. 2.1). Not long after photography was invented stereo-photography came, too. Soon enough, cameras were put on board airplanes, later on board satellites such as SPOT or ASTER, to take pictures of

the Earth from multiple perspectives so that our planet could be mapped and measured thoroughly.

For decades, operators used stereoscopes (and their eyes) to measure perspective-related differences and displacements of two overlapping images — before computers came, doing essentially the same from digital imagery, but faster. These displacements, also called stereo parallaxes, reveal object heights and terrain elevation differences, given that the camera position and view angles are known (e.g. Toutin, 2001). The process of generating a DEM from satellite or aerial imagery requires good image contrast and the presence of distinct features that can be matched.

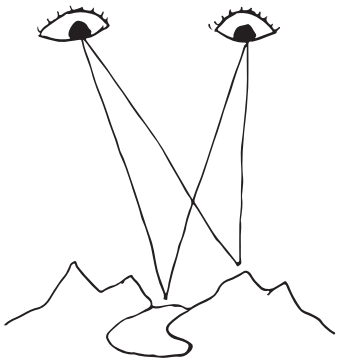

Figure 2.1: The principle of stereo-photogrammetry

Regional-scale DEMs from photogrammetric methods are nearly always based on optical imagery but also radar images can be used for this purpose. Those techniques and common DEM products are introduced below. On a much smaller spatial scale, Structure from Motion (SfM) techniques in combination with drones and other unmanned aerial vehicles (UAV) are on the rise for the production of high-resolution Digital Surface Models (DSMs) (Toth and Jóźków, 2016). Thereby, a moving camera takes dozens to thousands of pictures of a scene or an object that are subsequently combined into a single surface model, a process that until recently was too computationally expensive to be practical. DSM from SfM techniques are employed for local studies on (parts of) glaciers (Bhardwaj et al., 2016a; Girod et al., 2017) or snow depths in small catchments (Bühler et al., 2016), but are currently not useful or practical for the regional scale this work is focused on.

### 2.1.1 Optical stereo-photogrammetry

Stereo-photogrammetry requires at least two images of the same area. For air-/spaceborne applications, the most practical way to achieve this is to use the motion of the carrier to acquire images along-track, with a different perspective on the surface topography and just a few seconds apart. The systems have typically several sensors acquiring imagery simultaneously, but pointing in different directions — for example a nadir- and a backward-looking camera (e.g. ASTER), or a forward- and a backward-looking camera (e.g. SPOT-5). Newer spaceborne systems achieve the same result using only one camera with pointing ability so that several images can be acquired from different view angles during a single overpass (e.g. Pléiades). A small view angle, i.e. the camera pointing nearly straight down (nadir direction), is preferable to avoid steep topography being shaded from the camera view. At the same time, the distance between the two acquisition points (baseline) needs to be sufficient to cause a difference in perspective. The base-to-height ratio (B/H ratio) thus defines the sensitivity of the stereo geometry to elevation differences (Toutin, 2008). Stereo systems can cause steep mountain slopes to be obscured from view in one of the images which makes it impossible to interpret the surface/elevation of these areas (e.g. ASTER, sect. 2.1.3). To avoid areas with undefined topography in DEMs, tri-stereo systems have three look angles, pointing in forward, nadir and backward direction. This ensures that also steep topography is covered by at least two images. Tri-stereo and multi-stereo geometries with even more look angles are used in modern airborne sensors and some spaceborne systems (e.g. Pléiades, sect. 2.1.5).

It is also possible to create DEMs from cross-track stereo imagery, acquired from neighbouring orbits (e.g. SPOT 1–4, or the Landsat/Sentinel-2 satellites). However, this setup is rarely used nowadays as it is more error-prone and less accurate (e.g. Altena and Kääb, 2017). The time offset of days rather than seconds makes the images less similar and thus harder to correlate, and the more complicated viewing geometry requires two-dimensional correlation in comparison to the more efficient (and more fail-proof) one-dimensional correlation of along-track stereo pairs (Colvocoresses, 1982).

To create accurate DEMs, camera lenses and sensors must not have distortions, or these must be known and removed mathematically. Otherwise the distortions will be mistaken as parallaxes and bias the calculated terrain elevations. The same is true for any other factor that influences the viewing geometry — for spaceborne systems, for example, the effect of Earth's curvature and rotation between two time-lagged image acquisitions along orbit (Toutin, 2004). To generate accurate DEMs from satellite stereo pairs, image metadata about the sensor optics and accurate position and pointing direction is usually

combined with a satellite orbital model (Toutin, 2004) and ground control that ties the DEM to an absolute reference system. Ground control may consist of manually set Ground Control Points (GCPs) or earlier acquired imagery that is used as a reference for image co-registration. Typical elevation errors of stereo-photogrammetric DEMs are blunders in areas lacking correlation (water, featureless surfaces) or that are obscured from view in one of the two images. Elevation-dependent elevation bias is also fairly common, i.e. that valleys are consistently too low and mountain tops too high at the same time, or vice versa. Such bias is caused by imperfect parametrisation of the geometric setting, such as from an unfavourable distribution of GCPs (e.g. Berthier et al., 2004; Kääb, 2008), and can be corrected by fitting a linear or polynomial relationship to elevation differences and elevation (Nuth and Kääb, 2011). In general, relative elevation accuracy compared to the surrounding area in the DEM is higher than the absolute elevation accuracy of a point.

Optical stereo-photogrammetry has two main limitations: i) the need for cloud-free conditions, and ii) correlation failure where image contrast is low. Optical sensors use the visible and near-infrared (VNIR) part of the light spectrum which does not penetrate through clouds. Since surface topography stimulates cloud formation, mountain areas have naturally more cloud cover and thus less favourable conditions for optical mapping. Most non-commercial satellite missions have fixed view angles and repeat cycles of around two weeks — which greatly reduces the number of (potentially) cloud-free scenes that can be used for DEM generation, a major disadvantage especially for studies of the mountain cryosphere. For that reason, many commercial satellites (sect. 2.1.5) can adjust their pointing direction to target requested areas whenever the opportunity arises.

The process of DEM generation requires the existence of distinct features or patterns that can be matched by correlation algorithms. This is in particular an issue on very bright and featureless surfaces such as fresh snow that causes sensors to saturate. Thus, DEMs tend to be less accurate on glacier accumulation parts or other snow-covered areas — another disadvantage in particular for mountain cryospheric applications. The problem is greatest for older sensors as these tend to have lower radiometric resolution due to limited on-board storage and downlink bandwith capacities (sect. 2.1.3, 2.1.4). Despite these disadvantages, DEMs from optical stereo-photogrammetry remain the most common and widespread elevation datasets globally. In sections 2.1.2–2.1.5, a few sensors and products that are relevant in the context of this work are introduced in greater detail.

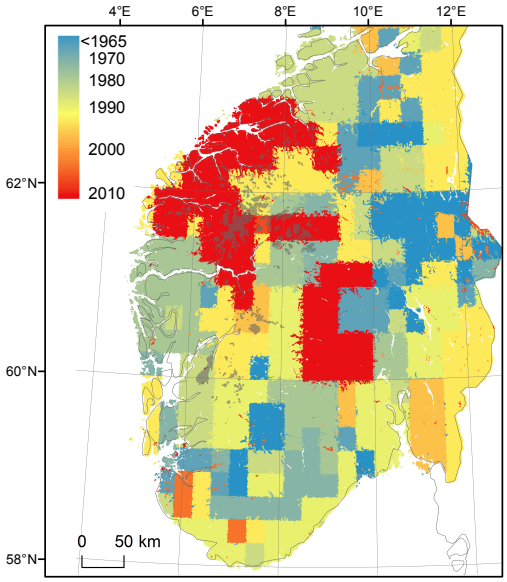


Figure 2.2: Patchwork of approximate DEM ages (colour scale) in the southern Norway study area, using the update timestamp of the elevation contours at 1:50 000 map scale (layer N50_høyde_L) as a proxy. Darker areas indicate glaciers. The DEM is updated continuously and this map (DEM from ~2012) does not necessarily reflect the latest DEM timestamps.

### 2.1.2 Topographic maps from aerial imagery

Worldwide, most national topographic maps and DEMs are based on airborne stereo imagery. Explorer spirit and the surge of new technological advances resulted in the first complete mapping of the globe in the course of the last century, to a substantial degree thanks to analogue aerial photography (Collier, 2002). Since then, national campaigns with modern, digital camera systems may have made the national elevation data more accurate, finely resolved, and up to date, or not — depending on the size and budget of a country. In any case, different processing sub-units of national maps/DEMs usually stem from different dates, and elevation quality tends to be of lower quality for mountain areas than for populated places. Also in Norway, data from 1:50 000 maps are the source for the national elevation data, albeit merged with more detailed information, where available (primarily in the densely populated areas), and updated continuously (Kartverket, 2016). The dataset is thus a patchwork in time (fig. 2.2), with elevation measurements of some remote areas in Norway dating back to the sixties. Historical maps and elevation datasets are invaluable for glacier change studies, as long as the spatial units of a certain time stamp are well known. Where this is not the case and surface elevations change over time,

date differences in elevation data can hamper glacier elevation/volume change studies (e.g. in Switzerland; Fischer et al., 2015, or in Norway; Publication I). The topographic maps of Norway serve as the main reference DEM for ICESat-based dh in Publications I and II.

### 2.1.3 ASTER stereo imagery and GDEM

The Advanced Spaceborne Thermal Emission and Reflection Radiometer (ASTER) on board the Terra (EOS AM-1) spacecraft is an along-track pushbroom stereo sensor that provides nadir imagery at resolutions between 15 m and 90 m in the VNIR, short-wave infrared (SWIR) and thermal infrared (TIR) (Yamaguchi et al., 1998). The instrument is a joint project between Japanese institutions and the US space agency NASA. It has been in orbit since 1999, providing a unique record of stereo-imagery time series with consistent quality. The backward-looking camera responsible for its stereo capabilities has only one near-infrared (NIR) band and acquires images with 27.6° off-nadir angle, approximately one minute after the nadir-pointing sensors scanned the same area on the ground (Hirano et al., 2003). The setup allows for vertical accuracies of ±15–30 m (Toutin, 2008), twice as much in mountainous terrain (Kääb, 2002). The large off-nadir angle leads to heavy distortions on steep north-facing slopes not visible in the back-looking band. Since ASTER is an older instrument, it suffers from a low radiometric resolution (8 bit), resulting in lack of contrast on snow. It also experiences spacecraft attitude angle variations that lead to geometric distortions both within and between the nadir- and backward-looking images. The so-called jitter from satellite vibrations, at wavelengths of approximately 4 km and 30 km along-track, is not measured by on-board angle monitoring systems and causes noise and elevation bias of up to tens of metres that severely hamper the use of ASTER DEMs e.g. for glacier volume change studies (Nuth and Kääb, 2011; Girod et al., 2016). Despite all errors and uncertainties, ASTER DEMs have been widely and successfully used within glaciology (Toutin, 2008).

In effort to get rid of errors, not least from non-systematic distortions, time series stacks of DEMs were used to produce the time-averaged ASTER Global Digital Elevation Model (GDEM). DEM time stacks were also used to retrieve (glacier) surface elevation change trends from linear regression of multi-temporal ASTER DEM elevations (Berthier et al., 2016) using a similar approach as this work (Publications I and III), and recently as well to remove the bias in individual DEMs by means of a time-integrated DEM generation processing chain (Girod et al., 2016). The latter has great potential to retrospectively improve the quality of ASTER DEMs to a degree that makes this

data more suitable for glacier volume change studies, or other applications with similar accuracy requirements and the need of a distinct timestamp.

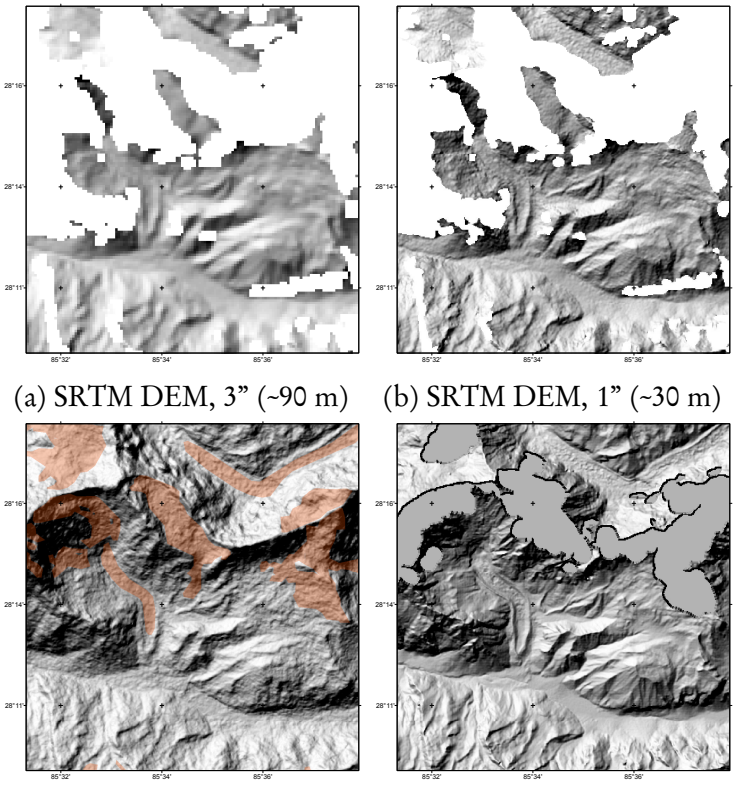

(a) SRTM DEM, 3” (~90 m)

(b) SRTM DEM, 1” (~30 m)

(c) ASTER GDEM2 (30 m), glaciers emphasized in red

(d) ALOS DSM (30 m)

Figure 2.3: Langtang, Nepal: Hillshade views of global DEMs of comparable spatial resolution. The white/flat grey areas correspond to data gaps. The moraines of south-flowing, debris-covered Lirung glacier are clearly visible. Yala glacier (fig. 1.1) is located at the right edge of the image, south-facing.

The ASTER GDEM versions 1 and 2 (version 3 is upcoming; Gesch et al., 2016) are freely available, global (up to 83° latitude) elevation datasets at 30 m posting (the effective spatial resolution is two to three times lower; Tachikawa et al., 2011a). They were produced without ground control points from stacked and averaged DEMs based on more than a million ASTER scenes acquired since 2000 (Tachikawa et al., 2011b). The GDEM2 is considered an improvement in actual spatial resolution and vertical accuracy, but is still noisy (fig. 2.3c) and has elevation errors of several metres, including errors of up to tens of metres in rugged terrain. Both products are of limited use for glacier volume change studies due to the averaging of surface elevations from an

entire decade. They continue to be used within glaciology nevertheless, for example to model glacier surface topography for which absolute elevation accuracy is less of a concern (e.g. Frey and Paul, 2012) — but have also been used to fill in no-data voids in one of the SRTM DEM products (sect. 2.3.2), which is more problematic for volume change studies as it introduces uncertainty about the surface elevation time stamp into the dataset that is not obvious to the user.

### 2.1.4 ALOS PRISM stereo-imagery and World 3D-30m DSM

The Panchromatic Remote-sensing Instrument for Stereo Mapping (PRISM) instrument on board the Japanese commercial Advanced Land Observing Satellite (ALOS) acquired panchromatic tri-stereo imagery at 2.5 m spatial resolution (Shimada et al., 2010) between 2006 and 2011. Like the ASTER GDEM, time stacks of ALOS/PRISM data were merged into a global DSM at a much finer resolution of 5 m, called ALOS World 3D DSM (Takaku et al., 2014) — albeit for purchase only at that resolution. A coarser version of the DSM at 30 m spatial resolution, called ALOS World 3D-30m DSM (AW3D30), is distributed free of charge and seems to outperform both the ASTER GDEM and SRTM DEM products (sect. 2.3.2) in terms of actual spatial resolution and vertical accuracy (fig. 2.3d, Tadono et al., 2016). The temporal merging of six years of data plus large data gaps in particular in mountainous areas (due to cloud cover and correlation failure on snow — owing to the limited 8-bit radiometric resolution; Shimada et al., 2010), i.e. the same limitations as for the ASTER GDEM, make also this DEM of limited use for glacier volume change studies. On stable terrain, however, the ALOS DSM (even at 30 m resolution) is a promising candidate as a reference DEM for regional snow depth studies such as presented for Norway in this thesis (Publication II).

### 2.1.5 High-resolution sensors

Several commercial satellite companies offer stereo/tri-stereo imagery at high spatial resolutions of ca. 0.3–6 m that are suitable for local DEM studies. Designed to be maximally flexible in targeting customised locations, most of these satellites have only one sensor that can be pointed forward/backward (and also to the side) to acquire the same target area on ground twice or more during a single overpass (e.g. the IKONOS or WorldView satellites). Interest in this originally quite costly data has grown in the last few years due to improved accessibility (Berthier et al., 2014). The most versatile for DEM applications are systems that allow tri- or multi-stereo acquisitions, such as the Pléiades twin

satellites and also the most recent satellites in the SPOT series. These platforms are especially interesting for researchers in Europe which are given preferential purchase conditions through the ISIS programme of the French Space Agency CNES. The Pléiades satellites were launched in 2011 and 2012 and provide a tri-stereo VNIR imagery at 0.7–2.6 m spatial resolution (Gleyzes et al., 2012). A radiometric resolution of 12 bit makes the data superior to e.g. ASTER or ALOS data over bright areas such as glaciers, where Pléiades data is being used increasingly (Berthier et al., 2014). A recent study shows that the horizontal and vertical accuracy are sufficient even for snow depth studies (Marti et al., 2016), albeit for much smaller areas (a mountain creek catchment) than the regional scale of this work (Publication II).

The Satellite Pour l'Observation de la Terre (SPOT) program consists of a series of high-resolution, commercial satellites with a multispectral pushbroom sensor in the VNIR. SPOT 1–4 provided imagery at 10–20 m spatial resolution as early as in the 80s and 90s that were widely used to create DEMs from cross-track stereo-photogrammetry. In 2002, the launch of SPOT-5 with multiple imaging systems on-board opened up for along-track stereo-photogrammetry at 2.5–10 m resolution (Toutin, 2006), later continued by SPOT-6 and 7 that also provide tri-stereo mode and an even higher spatial resolution of 1.5–6 m. Their high vertical accuracy make DEMs from SPOT-5 and its successors suitable for local glacier volume change studies (e.g. Berthier and Toutin, 2008). During the fourth International Polar Year (2007–2009), the SPOT-5 stereoscopic survey of Polar Ice: Reference Images and Topographies (SPIRIT) project enabled the collection of a large archive of SPOT-5 stereo-imagery over polar icemasses that so far lacked topographic data of sufficient quality (Korona et al., 2009).

While important for local DEM differencing studies, the small spatial extent of high-resolution stereo imagery make them not directly applicable on the regional scale of this work.

### 2.1.6 Radargrammetry

Stereo-photogrammetry from two radar images, also called radargrammetry, essentially follows the same principle as for optical stereo-photogrammetry. While far less frequently used, the technique has already been applied to airborne imagery to generate DEMs in cloud-infested areas (Leberl, 1976) and has again become popular with the availability of new SAR satellites (Toutin and Gray, 2000). Side-looking radar is sensitive to topography as the sent radar pulses are first reflected off higher elevations and slopes facing the sensor (fig. 2.4). Topography in radar imagery looks thus as if it had been folded towards the sensor — the so-called foreshortening, most pronounced on the far side of

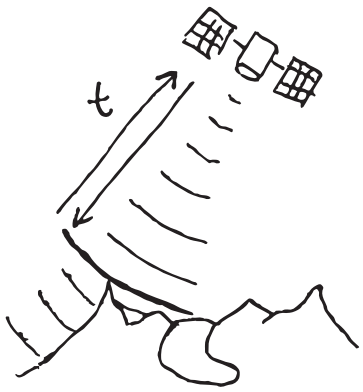


Figure 2.4: A side-looking radar determines the distance to the ground from the time (t) that has passed between the sent and received microwave pulse. The signal is first reflected off areas close to the sensor and at higher elevations.

the image in across-track direction. SAR systems are thus more sensitive to incidence angles than VNIR sensors, and DEM accuracy decreases linearly with increasing slope (Toutin, 2002). Radargrammetry is less prone to image decorrelation than interferometry (sect. 2.3) and in relatively flat terrain, the newest civil SAR systems achieve elevation accuracies of 4–5 m (e.g. COSMO-SkyMed, RADARSAT-2 and TerraSAR-X with metric spatial resolution; Capaldo et al., 2015). Radar waves penetrate clouds and are independent of daylight which makes them useful for DEM acquisition, in particular in cloudy areas or during the polar night. To date, only a few glacier volume change studies used radargrammetry (e.g. Papasodoro et al., 2016; Toutin et al., 2013) and no regional-scale radargrammetry DEM products exist.

## 2.2 Altimetry

Altimetry is the measurement of height or altitude, in this context by using active systems such as lidar (in the VNIR part of the light spectrum) and radar (microwaves). The time lag between the emitted laser/radar wave pulse and the recorded pulse (reflected off the surface) corresponds to the two-way travel time between sensor and ground surface (fig. 2.5). Rather than image data, these systems record point clouds (scanners) or profiles (profiler systems that usually point straight down). Individual elevation data is acquired within a ground footprint that is very small for airborne lidar, up to tens of metres in diameter for spaceborne lidar, and hundreds of metres to several kilometres for spaceborne radar.

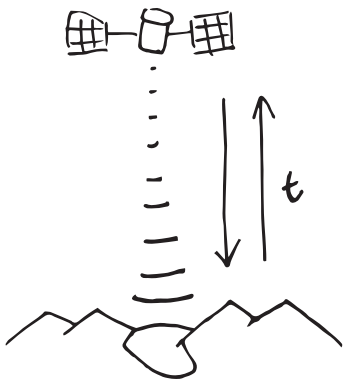


Figure 2.5: Altimetry uses the two-way travel time (t) of a sent and received pulse to derive the distance to the ground.

Airborne lidar systems and radar altimetry (in particular spaceborne) are frequently used to monitor the cryosphere. These techniques are introduced in detail below. In contrast, there are (were) very few spaceborne laser missions. Apart from ICESat, to which a separate chapter is dedicated (chapter 3), only two other lidar altimetry systems have been in space: The Lidar In-space Technology Experiment (LITE), an experimental system on board the 12-day STS-64 mission in September 1994 (Winker et al., 1996), and the Cloud-Aerosol Lidar and Infrared Pathfinder Satellite Observations (CALIPSO) mission targeted to atmosphere applications, a profiling system in orbit since April 2006 (Winker et al., 2009). Apart from aerosol/atmosphere studies, CALIPSO has been used to detect thick layers of blowing snow in Antarctica (Palm et al., 2011) — which is probably the closest link to the cryospheric applications discussed in this work. Volume change studies of glaciers or snow depths are unfortunately made impossible by its vertical resolution of only 30 m. Spaceborne lidar systems are an active research and development topic within the atmospheric sciences and further missions are in preparation (Reitebuch et al., 2009; Burrows et al., 2011). While terrestrial lidar/radar systems that are e.g. mounted on a tripod are frequently used, too, they are less relevant for the scope of this work and thus not further discussed here.

### 2.2.1 Airborne lidar

Lidar stands for Light Detection and Ranging, a principle that has been known already since the first half of the 20th century. However, lidar systems only became affordable and more widely used in the last 15 years and the technology still continues to advance (Bhardwaj et al., 2016b; Toth and Jóźków, 2016).

Airborne lidar systems used for geoscience applications are usually so-called laser scanners that use rotating mirrors to distribute narrow-beam laser pulses over a larger swath instead of a single profile line. In newer systems, the entire waveform of the received pulse is recorded rather than a single arrival event. Pointing direction and the position of the aircraft need to be known with very high accuracy to compute the exact location of where each sent/received pulse was reflected off the ground. Nowadays, Global Navigation Satellite Systems (GNSS), such as the Global Positioning System (GPS), and an Internal Measurement Unit (IMU) are used on board the aircraft. They are often combined with post-acquisition co-registration with existing elevation data or GCPs, typically measured with differential GPS (DGPS) techniques in the field (Toth and Jóźków, 2016). The spatial resolution is determined by the density of the resulting point cloud, typically 0.5–10 pts/$m^2$. Point clouds are often integrated to gridded DSMs to remove redundancy and for easier computational handling in combination with other gridded data. Airborne lidar DSMs achieve centimetre-scale elevation accuracy and are thus useful for applications with high accuracy requirements or small elevation differences. The technique is thus especially popular for snow depth and snow distribution studies and has also been used in dozens of glacier volume change studies (Deems et al., 2013; Bhardwaj et al., 2016b). As active systems, lasers are not dependent on neither GCPs nor daylight, and sample sunlit and shaded areas equally well — i.e. they may be used on featureless, bright surfaces, also during the polar night or in unfortunate illumination conditions. This is an advantage compared to photogrammetry, where especially SfM techniques from drones achieve similar spatial resolutions and accuracies (Bühler et al., 2015; Toth and Jóźków, 2016).

The price tag of airborne lidar acquisitions make this technique affordable mainly for private companies or national authorities. Several states in Europe mapped their entire country with lidar data, among these are also Sweden and Finland. Norway has now started such a project (Kartverket, 2017) as the need of accurate elevation data is large in that rugged country. The technique is established not least within cryospheric applications: the Norwegian Water Resources and Energy Directorate (NVE) mapped selected glaciers with laser scans in 2009 and 2013 for mass balance studies (NVE, 2016) and the Hardangervidda area in 2008/2009 for snow studies (Melvold and Skaugen, 2013). The latter dataset served as high-resolution reference data for a small spatial area in Publications I and II.

Apart from pulse-based laser scanning, a few other laser systems exist (Toth and Jóźków, 2016) that are not currently used on board aircrafts — except for one: The Multiple Altimeter Beam Experimental Lidar (MABEL) is a photon-counting airborne instrument that was built as a simulator for the ICESat-2

mission (section 3.3). Rather than sending out strong laser pulses at lower frequency (pulse-based systems), photon-counting lasers send out weak pulses at higher frequency and record each individual photon arriving at the detector (Degnan, 2002). Noise filtering techniques are used to extract the ground reflection signal from ambient photon background noise (Horan and Kerekes, 2013). MABEL is primarily used to understand and prepare methods for the upcoming ICESat-2 data (e.g. Horan and Kerekes, 2013; Kwok et al., 2016; Brunt et al., 2016).

### 2.2.2 Radar altimetry

Radar (Radio Detection and Ranging) has been known since the interwar period, in the beginning mainly for military applications (Barton, 1984). The first microwave satellite dedicated to Earth observation was NASA's SEASAT, operational during three months in 1978, that carried a radar altimeter, among other instruments (Born et al., 1979). The last three decades experienced a surge of spaceborne radar altimetry missions, primarily targeted to measure sea surface level and oceanographic parameters but also other vast, flat surfaces such as sea ice or ice sheets. Flat surfaces are needed because of the large footprint of single-pulse radar systems: Microwaves cannot be focused to the same degree as laser beams, thus footprints are typically several kilometers in diameter — and the recorded surface elevation corresponds to the first (strong) reflector hit by the transmitted pulse anywhere in that footprint (e.g. Levinsen et al., 2016). While altimeters point straight down, the Point of Closest Approach (POCA) does not necessarily correspond to the nadir point wherever there is topography (fig. 2.5) or surface reflectivity varies strongly spatially.

To improve the information content and spatial resolution, systems such as the Synthetic Aperture Interferometric Radar Altimeter (SIRAL) on board CryoSat-2, an environmental research satellite by the European Space Agency ESA, use frequency-modulated pulses with SAR processing and interferometric methods (see sect. 2.3) that allow for improved along-track resolution and more accurate location of surface returns (Wingham et al., 2006). The multi-frequency received waveforms provide more information per footprint and thus not only the POCA elevation but also secondary elevation measurements, usually referred to as the swath (Gray et al., 2013). This allows the application of CryoSat-2 data also for smaller ice bodies with more prominent (but convex) topography, e.g. ice caps in Iceland (Foresta et al., 2016). Valley glaciers in mountains with large elevation differences are more problematic, not least due to on-board software that determines the expected elevation range, i.e. when

the receiver antenna is 'listening' — which is usually at the elevation of mountain crests/peaks, not valley bottoms (Dehecq et al., 2013). CryoSat-2 data are therefore not suitable as reference elevations for ICESat applications, but provide results at a comparable spatial scale. Similar to ICESat applications in mountainous terrain, radar altimetry processing requires a-priori knowledge about the surface topography and data processing methods are still improving.

Radar systems have similar advantages over optical photogrammetry as lidar systems do and are thus a natural choice on featureless, flat ice surfaces. In addition, radar waves penetrate clouds. Least affected by rain and clouds are the low-frequency bands (C, X) which however also have larger penetration depths in snow and ice (sect. 2.3.1). Most radar altimeters use a dual-band system with a high-frequency band (Ku-band, fig. 2.8) for increased range accuracy and a second, low-frequency band (C, S) to assess the biasing influence of atmospheric water vapour and the ionosphere on radar wave transmission times.

Within airborne radar altimetry, the most common application is the derivation of ice thickness from (low-frequency) radar that penetrates dry ice. Also sub-surface ice layers that correspond to past summer surfaces in (dry) firn may be mapped, for example with the experimental ASIRAS instrument that was developed as the airborne equivalent of CryoSat-2's SIRAL instrument (Lentz et al., 2002). The same may be achieved with ground-based radar systems at lower costs but also limited spatial coverage (e.g. Brandt et al., 2008).

## 2.3 SAR Interferometry

Imaging microwave systems came up after World War II with the invention of side-looking radar systems that illuminate a wide swath (fig. 2.4), shortly followed by side-looking Synthetic Aperture Radar (Toth and Jóźków, 2016). SAR systems use frequency-modulated pulses (the chirp) and the Doppler effect to greatly improve spatial resolution compared to single-pulse altimetry. Modern civil spaceborne sensors can achieve metre-scale spatial accuracies. The first spaceborne SAR instrument was on board the SEASAT mission (Fu and Holt, 1982), followed by ESA's European Remote Sensings (ERSs) satellites in the 90s.

Of the received microwave pulses, SAR systems record the travel time, amplitude (the strength of the signal), and phase as the fraction ($0$–$2\pi$) of the radar wavelength. The latter is of little use for one image alone, but very valuable for an image pair acquired from two slightly offset positions, the so-called baseline (Graham, 1974, fig. 2.6). Phase differences between such an interferometric image pair correspond to a difference in range, typically caused by topography. By

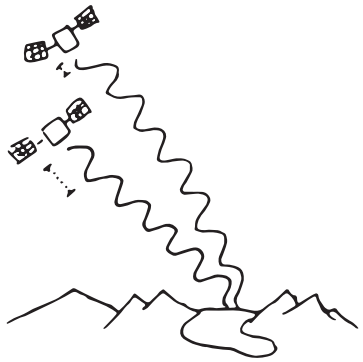

Figure 2.6: The phase difference in the recorded microwaves of two sensors relates to terrain heights and movement.

unwrapping the 0–$2\pi$ phase cycles (fringes), Interferometric Synthetic Aperture Radar (InSAR) is used to produce very accurate DEMs — or also to detect surface movement in line of sight (slant range). Temporal baselines, i.e. image pairs from different dates, reveal surface displacement such as from slope movements or an earthquake, given the surface elevations are known from before (fig. 2.7).

InSAR requires much smaller temporal and spatial baselines (tens to hundreds of metres) than radargrammetry (sect. 2.1.6). A large temporal offset increases the probability for changes in the surface properties in the scene, such as from precipitation or vegetation growth, that lead to image decorrelation (Zebker and Villasenor, 1992). The rather short revisit times of some of the 90s' SAR missions and in particular the 1995–1996 tandem mode of the two ERS satellites (one day revisit) thus provided the first important source of interferometric data for global DEM production (Rott, 2009). For the same reason, airborne interferometric systems usually have two antennas mounted at a distance to each other (single-pass interferometry), a setup that eliminates any temporal decorrelation problems.

The ideal length of the spatial baseline depends on the surface topography/ roughness and microwave frequency used. Longer baselines cause narrower fringes and are thus more sensitive to topography, but when a critical baseline is exceeded, the fringes can no longer be separated (e.g. from ca. 1150 m on flat surfaces for ERS' C-band at a wavelength of ~5.6 cm; Ferretti et al., 2007). Shorter radar wavelengths and larger elevation differences cause fringes to become denser (fig. 2.7) and require thus shorter baselines (Rott, 2009).

Interferometric SAR allows for DEM generation with high spatial and elevation resolution and consistent performance. Airborne SAR systems with interferometry capabilities are less frequently used than spaceborne InSAR sys-

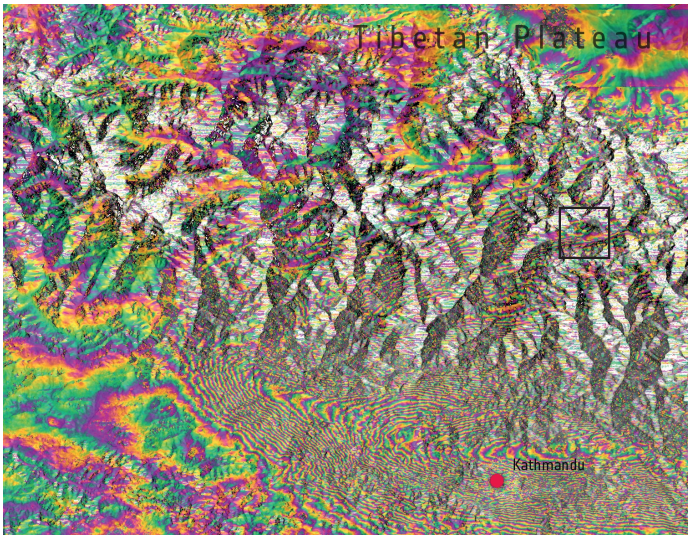


Figure 2.7: An interferogram from two time-offset Sentinel-1A scenes shows how surface elevation changed due to the Gorkha Earthquake that struck Nepal on 25 April 2015. The cyclic colour fringes represent the relative phase difference, they are narrowest where surface elevation changed most. The black square corresponds to the Langtang area in fig. 2.3. *Image credits: ESA*

tems (e.g. RADARSAT, TerraSAR-X, Sentinel-1), not least due to the high cost of airborne missions (Toth and Jóźków, 2016). Together with the 24/7 advantage of SAR compared to optical systems, it is not surprising that the technique has provided some of the most accurate and frequently used global DEM products, namely from the TanDEM-X and the Shuttle Radio Topography Mission (SRTM) that are introduced below. However, in steep terrain, SAR performance is not perfect either. Foreshortening and layover (areas shaded from view in the side-looking geometry) lower data quality or cause gaps. Penetration of radar waves into snow and ice add uncertainty to glacier surface elevations. This issue has some implications for the use of InSAR-based DEMs as a reference surface for ICESat applications (Publication III).

### 2.3.1 Penetration of electromagnetic radiation

Electromagnetic radiation to some degree penetrates into a material before all of it is reflected or absorbed, but the penetration depth varies greatly depending on the material and the wavelength/frequency. For the very short wavelengths in the VNIR part of the electromagnetic spectrum, penetration depths are in general very small and usually assumed to be zero — i.e. laser pulses are assumed to be reflected off the surface of a material, and with our eyes we usually see the

surfaces of objects except for very few transparent materials. Even for snow, a material that transmits light relatively well, the vast majority of reflected VNIR light comes from the top few cm (Deems et al., 2013). There is however little data on this subject, and studies are on-going (Harding et al., 2015; Brunt et al., 2016) on how the penetration may affect surface elevation measurements and thus large-scale volume change studies with ICESat-2 (sect. 3.3).

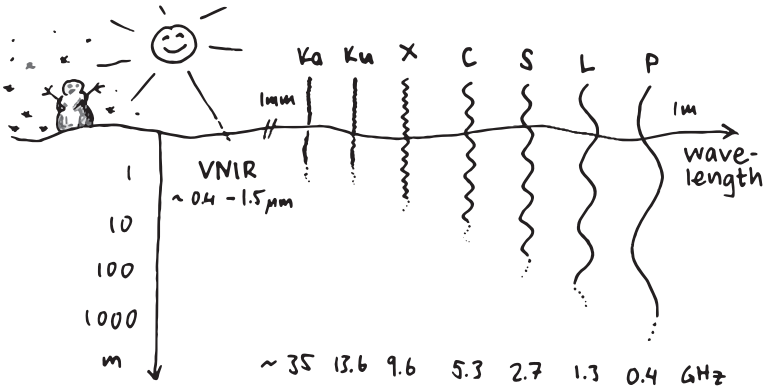


Figure 2.8: Microwave bands, frequencies (after Toth and Jóźków, 2016) and magnitude of penetration into dry ice/snow (approximate, after Müller, 2011; Gay and Ferro-Famil, 2016).

The penetration situation is an entirely different one in the case of microwaves with millimetre- to metre-scale wavelengths (fig. 2.8). Microwave penetration depth into materials with volume scattering — vegetation, snow/ice, granular materials like sand, etc. — is greatest for low-frequency bands (L, C) and lower for the higher frequencies that are typically used for radar altimetry (Ku-, Ka-band). Penetration into snow/ice depends highly on the surface roughness, material composition, granular structure and temperature (Müller, 2011; Gay and Ferro-Famil, 2016). Also the presence of liquid water strongly affects radar backscatter (Rott and Mätzler, 1987). For cold ice, penetration depths $>100$ m were observed for L-band (Rignot et al., 2001) whereas the Ku-band microwaves of Cryosat-2's SIRAL are commonly assumed to only penetrate through (dry) snow layers and reflect off the snow/ice interface (e.g. Armitage and Ridout, 2015). Dedicated InSAR missions operate in frequencies in between those extremes, such as the X-band (TanDEM-X, secondary SRTM-X antenna pair) or C-band (SRTM-C main antennas). These bands have metre-scale penetration depths on glaciers — assumingly larger in cold, dry accumulation areas than on the rougher and wetter glacier tongues (Berthier et al., 2006, Publication III). For the C-band, penetration depths $<10$ m have been observed on glaciers (Rignot et al., 2001; Dall et al., 2001; Rott et al., 1993).

Microwave penetration into snow/ice has to be taken into account for DEM differencing studies. As long as data from the same sensor or frequency are compared, the vertical offset to the snow/ice surface can be less of a problem as the ice/snow material composition (and thus microwave penetration depth) are relatively stable for one location (Müller, 2011). However, if the snow/ice surface was melting during one of the two acquisitions the penetration depths will be different. Where InSAR-based glacier elevations are compared to DEMs from optical methods or lidar, penetration always needs to be estimated and considered, otherwise volume changes will be severely underestimated (e.g. Gardelle et al., 2012a,b; Vijay and Braun, 2016).

### 2.3.2 SRTM

The goal of the Shuttle Radio Topography Mission (SRTM) was to obtain a global high-resolution DEM. This was achieved for all land surfaces between 56° and ~60.3°N with a C-band InSAR system on board the Space Shuttle Endeavour over the course of 11 days in February 2000 (Farr et al., 2007; Farr and Kobrick, 2000). The mission included a second, X-band InSAR system with narrow swath (no complete coverage) for quality control (Rabus et al., 2003). To avoid temporal decorrelation, the single-pass system had a 60 m mast where a second (slave) antenna was mounted.

The nominal vertical accuracy of the SRTM-C elevation data is 5–10 metres (Rodriguez et al., 2006) but in particular in steep terrain foreshortening and layover caused large data gaps. The SRTM DEM is freely available in several versions: at 3-arc-seconds spatial resolution with no-data voids in steep terrain (SRTM3, fig. 2.3a), the same as a void-filled version (using the ASTER GDEM), and at 1-arc spatial resolution (SRTM1, fig. 2.3b) where some voids are filled, some not. The void-filled data are useful for applications that require complete coverage (e.g. hydrological studies) but fail as a reference dataset for DEM differencing studies on glaciers or ICESat applications since they have spatially varying quality and elevation time stamps. The DEMs are a merged product of 1–4 interferometric pairs at each location (Farr et al., 2007), and both vertical and horizontal shifts of processing sub-units are thus possible, for example from phase unwrapping errors or imperfect co-registration. Such systematic vertical offsets have been found in mountain areas around the globe (e.g. Kääb, 2005; Surazakov and Aizen, 2006; Berthier and Toutin, 2008). Compared to the several releases of improved, re-processed SRTM3 versions, only one version of the global SRTM1 C-band DEM has been released so far, and the elevation quality of the latter is therefore not necessarily superior.

The SRTM DEM may be subject to an elevation-dependent bias (Berthier et al., 2006; Schiefer et al., 2007), although the existence of this bias is still disputed (e.g. Paul and Haeberli, 2008; Larsen et al., 2007; Gardelle et al., 2012a). On glaciers, C-band penetration causes an unknown vertical bias in DEM elevations. This is inconvenient, as in particular in HMA and other remote areas the SRTM DEM is often the best quality elevation dataset available. It is thus frequently used for DEM differencing studies in combination with a more recent optical stereo-photogrammetric DEM. Subsequently, penetration introduces considerable uncertainty into geodetic glacier mass balance studies in particular in remote areas where data for validation are lacking. The severity of the penetration bias is still discussed (e.g. Berthier et al., 2006; Gardelle et al., 2012a). Approaches to estimate the penetration depth include comparison to ICESat data (e.g. Kääb et al., 2015; Shangguan et al., 2015) or to the SRTM-X DEM with lower expected penetration (e.g. Gardelle et al., 2012b, 2013).

The X-band DEM is only available for narrow stripes close to the equator. It has similar nominal elevation accuracies as the C-band DEMs (Rabus et al., 2003), but its absolute elevation accuracy is lower than expected prior to the mission. Unexpectedly large shaking of the mast where the slave antenna was mounted exceeded the X-band wavelength and thus introduced phase ambiguity (Rabus et al., 2003).

Nevertheless, the globally consistent quality, single timestamp, and relatively high elevation accuracy and spatial resolution, have made the SRTM DEM the standard reference DEM for many local and global studies, including ICESat applications in HMA (e.g. Kääb et al., 2012; Gardner et al., 2013, Publication III). Unfortunately, the mission did not include polar areas and the SRTM DEM thus only covers the southernmost, non-glacierised part of Norway. There, the SRTM DEM is used to assess the elevation accuracy of ICESat data (Publications I and II) and snow depths in the Hardangervidda area (Publication II).

### 2.3.3 TanDEM-X and WorldDEM

TanDEM-X was launched in 2010 as the second satellite in an X-band InSAR constellation together with TerraSAR-X, which has been in orbit since 2007. After four years of global acquisitions, they now provide a global coverage of high-resolution elevation data with unprecedented accuracy — due to the quasi-polar orbit also beyond the 60° limit of the SRTM (Zink et al., 2014). The two satellites follow each other tightly with a flexible baseline (typically a few hundred metres) and the possibility for both pursuit-monostatic and bistatic modes (Krieger et al., 2007). In the bistatic constellation, one of the satellites acts as a (passive) slave, i.e. the setup corresponds to a single-overpass interferometer — but with a flexible baseline. In the monostatic mode, the satellites operate

independently from each other without the need for synchronisation and still very little temporal decorrelation (e.g. over vegetation and water). In addition to the 24/7 advantage of microwave sensors compared to optical systems, the TanDEM-X data is also far superior to the SRTM DEMs. The X-band is more sensitive to topography and less affected by penetration than the SRTM's C-band, and the on-going satellite mission allows far more adapted and targeted data acquisition compared to the short time window and fixed geometry of the SRTM. TanDEM-X thus marks a clear step-up in global satellite elevation data quality and sets a new accuracy standard for global DEMs (Zink et al., 2014).

The recently released WorldDEM is a hydrologically corrected, mosaicked product from several TanDEM-X InSAR DEMs at each location. It covers the entire globe at 12 m horizontal resolution and 2–4 m relative elevation accuracy (Riegler et al., 2015; Collins et al., 2015). However, the DEM is not freely available, thus for projects with a tight budget it will likely not push the less accurate global DEMs from ASTER, ALOS, and the SRTM out of the market. For glacier applications, the lower penetration depths of the X-band compared to earlier, predominantly C-/L-band InSAR missions is an advantage, but TanDEM-X penetration can still reach several metres in dry snow (Dehecq et al., 2016). As with the other global DEMs, the readily mosaicked WorldDEM is less useful for glacier volume change studies due to merging of surface elevations with different time stamps. DEMs from individual scenes are preferred for this purpose. Assumingly similar penetration depths into ice/snow call for comparison with SRTM elevation data (e.g. Jaber et al., 2013, 2016; Rankl and Braun, 2016; Vijay and Braun, 2016). The high elevation accuracy of TanDEM-X data make it a suitable candidate as a reference DEM for snow depth studies.

## 2.4 Other methods: Gravimetry

Spaceborne gravimetry sensors measure the geoid of the Earth by recording changes in along-track gravimetric forces between the Earth and the spacecraft. The local gravity-defining mass consists not only of the solid Earth but also movable masses such as water — or glacier ice. Glacier volume changes correspond to mass changes (given the snow/ice density is known, see also section 3.2.4). Regional glacier elevation change studies are thus often compared to gravimetric studies that measure mass changes directly. Gravimetry data, such as from the Gravity Recovery and Climate Experiment (GRACE) mission, has been used to estimate glacier mass loss, in particular in the HMA region (e.g. Matsuo and Heki, 2010; Jacob et al., 2012; Gardner et al., 2013) — though at a coarser spatial resolution than ICESat-based studies. However, gravimetry does not directly translate into surface elevation, and in particular in HMA,

glacier-related changes are only responsible for a small part of the mass change signal gravimetry-based studies need to decompose (e.g. Yi and Sun, 2014). Consequently, such studies deal with entirely different assumptions and challenges than described here. These are beyond the focus of this work and thus not further discussed.

# Chapter 3

# ICESat data and methods

The Ice, Cloud and land Elevation Satellite (ICESat) was a NASA space laser altimetry mission that provided local samples of surface elevation along near-repeat ground tracks between 2003 and 2009. On a near-polar orbit at 600 km altitude, the mission collected data between 86° N and 86° S. The satellite carried the Geoscience Laser Altimeter System (GLAS) instrument on board, with three profiling lasers that were expected to operate for ca. 18 months each and thus allow a continuous operation for five years in a 183 day repeat orbit (Zwally et al., 2002). Unfortunately, the first laser failed only 38 days into operation, and also the second laser decreased in power more rapidly than expected (Abshire et al., 2005). The acquisition strategy was therefore altered to a 91-day repeat orbit and a campaign-based mode with approximately month-long campaigns in autumn, winter and late spring on the northern hemisphere (Schutz et al., 2005, table 3.1). Despite the non-ideal setting, this updated strategy ensured that the main mission goal of ice sheet change detection was reached — and the GLAS data also proved extremely useful for numerous other applications. Examples are vegetation studies and global biomass estimation (e.g. Harding and Carabajal, 2005; Lefsky, 2010), improved determination of sea ice freeboard (e.g. Kwok and Rothrock, 2009), valuable information on dynamic rapid thinning on the ice sheet margins (Zwally et al., 2011; Pritchard et al., 2012), atmospheric characteristics (e.g. Spinhirne et al., 2005), water levels (Urban et al., 2008), mass changes of ice caps and mountain glaciers (e.g. Moholdt et al., 2010b; Kääb et al., 2012) — and a consistent reference for co-registration and mosaicking of other elevation data, including the ALOS World DSM (Takaku et al., 2014, sect. 2.1.4) and TanDEM-X World DEM (Zink et al., 2014, sect. 2.3.3).

While the profile-like elevation data is spatially far less extensive than the predominantly gridded products introduced in chapter 2, ICESat still provides the most consistent global elevation measurement available to date (Nuth and

Kääb, 2011). Thanks to the success and wealth of data provided by ICESat, a follow-on mission was initiated that will conduct similar measurements with newer technology (Abdalati et al., 2010). This chapter provides a background on the GLAS sensor, data products, and methods that are relevant for the cryosphere applications in Publications I–III, and briefly introduces the upcoming successor mission ICESat-2.

Table 3.1: ICESat operational periods. L1A/L1B and a small part of L2A had an 8-day repeat orbit instead of the 91-day repeat orbit for all other campaigns. The late spring campaign was only flown in the years 2004–2006 and the autumn 2008 campaign had to be split due to failure of laser 3 before the campaign was completed. The orbit could only be completed in December using laser 2 that was already low in power and expired 11 days into the autumn 2009 campaign.

| Laser | Campaign | First day | Last day |
|---|---|---|---|
| 1AB | Winter — 8-day | 20 Feb 2003 | 19 Mar 2003 |
| 2A | Autumn — 8-day | 25 Sep 2003 | 04 Oct 2003 |
| 2A | Autumn — 91-day | 04 Oct 2003 | 19 Nov 2003 |
| 2B | Winter | 17 Feb 2004 | 21 Mar 2004 |
| 2C | Late spring | 18 May 2004 | 21 Jun 2004 |
| 3A | Autumn | 03 Oct 2004 | 08 Nov 2004 |
| 3B | Winter | 17 Feb 2005 | 28 Mar 2005 |
| 3C | Late spring | 20 May 2005 | 26 Jun 2005 |
| 3D | Autumn | 21 Oct 2005 | 24 Nov 2005 |
| 3E | Winter | 22 Feb 2006 | 28 Mar 2006 |
| 3F | Late spring | 24 May 2006 | 26 Jun 2006 |
| 3G | Autumn | 25 Oct 2006 | 27 Nov 2006 |
| 3H | Winter | 12 Mar 2007 | 14 Apr 2007 |
| 3I | Autumn | 02 Oct 2007 | 05 Nov 2007 |
| 3J | Winter | 17 Feb 2008 | 21 Mar 2008 |
| 3K | Autumn | 04 Oct 2008 | 19 Oct 2008 |
| 2D | Autumn | 25 Nov 2008 | 17 Dec 2008 |
| 2E | Winter | 09 Mar 2009 | 11 Apr 2009 |
| 2F | Autumn | 30 Sep 2009 | 11 Oct 2009 |

## 3.1 Instrument and data

The ICESat mission was intended to serve two main research topics: ice sheet changes, including other aspects of the polar cryosphere (sea ice), and atmospheric science. Land elevation and vegetation cover were secondary mission goals. The GLAS instrument was designed to fit these aims, and processing of its measurements resulted in several data products that suit different purposes/surface types. Zwally et al. (2002), Abshire et al. (2005), Schutz et al.

(2005) and Jester (2012) provide details on the functionality, design and data products that are summarised here.

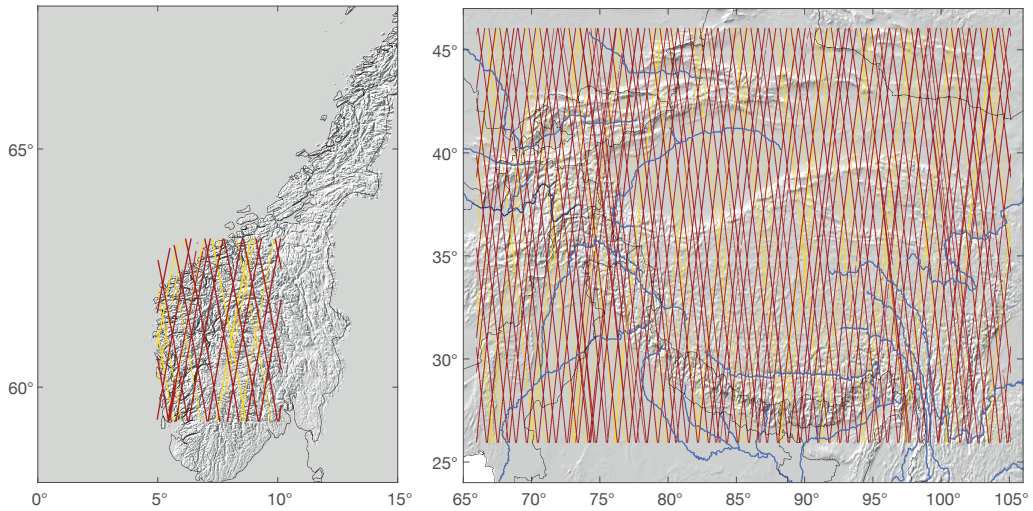


Figure 3.1: ICESat footprints in southern Norway and HMA. Red: repeat orbit autumn 2003–2009 (only a 33-day subset of the 91-day repeat orbit was served), yellow: ground tracks of the calibration orbit with 8-day repeat cycle, only served in winter/autumn 2003. Note the different map scale and narrower track spacing (due to the higher latitudes) in Norway.

### 3.1.1 GLAS

The GLAS sensor operated at two wavelengths, a green channel (532 nm) for cloud/aerosol vertical distribution, and a near infrared channel (1064 nm), less affected by the atmosphere, for surface elevation measurements. GLAS operated at 40 Hz, i.e. 40 pulses per second that result in a footprint spacing of 172 m on the ground. The ground footprints are of elliptic shape with a diameter of ca. 70 m on average (fig. 3.7). The actual footprint varies, both with the laser in use (ca. 52 x 95 m for L1–L2c, 47 x 61 m for L3 and L2d–L2f; Abshire et al., 2005; NSIDC, 2016) and the slope/roughness of the footprint. Strong reflectors in the laser far field contribute to the signal. The 1064 nm nominal pulse width is 6 ns and the digitising resolution of the return waveform is 1 ns which corresponds to 15 cm in range (fig. 3.2). The on-board digitiser searches the received waveform backward in time within a range window, estimated from an 1-km resolution gap-filled version of the SRTM DEM, and stores it in 544 bins. Over land surfaces, bins 393 to 544 are compressed and digitised at 4 ns

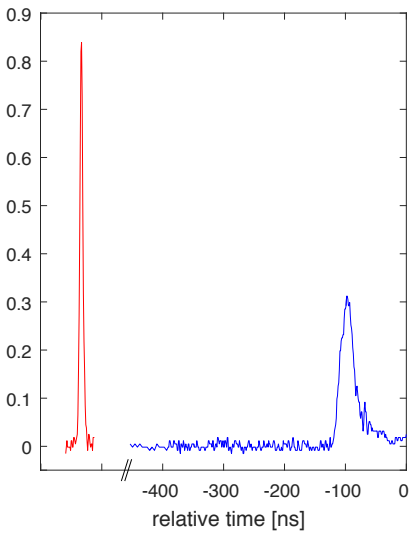


Figure 3.2: Emitted pulse (nominal width 6 ns) and received return waveform for a footprint of laser 3K (3 March 2008) on snow-covered Hardangervidda at 59.89° N/7.28° E, with an average footprint slope of ca. 4°. Bins 1–392 are digitised at 1 ns, corresponding to 15 cm in range, bins $>$ 393 (here truncated at 450 ns) at 4 ns.

to extend the receiving range window to 150 m, in order not to truncate the (stretched/skewed) return waveform from steep slopes (Jester, 2012).

Mean surface elevations per footprint are determined by fitting modelled Gaussian curves to the return waveforms. The delay between the peak/centroid of the sent and received waveform is then used to determine the range, considering the off-nadir pointing angle and other parameters recorded by the system. Smooth ice sheets typically produce single-peak waveforms, but complex land topographies may have several reflecting surfaces/objects, resulting in multi-peak and skewed waveforms that require a composition of several modelled curves (Brenner et al., 2011). Different algorithms and methods were designed for a particular expected/assumed surface type, and resulted in the different science data products.

Uncertainties in the determined range are caused, for example, by atmospheric forward scattering or detector saturation. The latter can occur with near-specular reflections with high-energy returns that exceed the detector gain. Corrections for range bias caused by saturation have been computed for ice-sheet-type surfaces (Fricker et al., 2005). The saturation detection algorithms and corrections are not necessarily valid for complex land surfaces (NSIDC, 2012, Publication I). Due to the rapid energy loss of the lasers, the return waveforms of later campaigns have a lower intensity (Abshire et al., 2005). The

elevation measurements of these returns may still be accurate but the higher signal-to-noise ratio introduces larger uncertainty.

The uncertainty budget from the GLAS instrument and atmospheric influences is about 0.1 m (Zwally et al., 2002). Measurements on flat surfaces yielded elevation accuracies/precision $< 3$ cm (Salar de Uyuni, Fricker et al., 2005) to $< 0.7$ m on gently sloping ice surfaces (Brenner et al., 2007; Moholdt et al., 2010b, from crossover tracks; sect. 3.2.1). Naturally, these numbers increase by a magnitude for rough mountain surfaces where elevations can vary greatly even within a single footprint (Publications I–II).

Except for the winter 2003 campaign, when a 8-day repeat orbit was flown for calibration targets (fig. 3.1), ground tracks were repeated during each campaign. However, GLAS footprint locations do not repeat exactly. Campaign ground tracks were kept within ca. $\pm 250$ m (Howat et al., 2008) of the reference track for polar acquisitions $> 59°$ latitude (Schutz et al., 2005), i.e. including the Norway study site. They can be off by $> 1$ km at lower latitudes. Comparison of ICESat elevations of different years requires that terrain differences between the annually varying ground tracks are taken into account (sect. 3.2).

### 3.1.2 Data products

Several data products and levels were generated from the raw data collected on ICESat and transmitted to the NASA Goddard Space Flight Center. The fifteen Level-1/2 products are targeted for different applications. They are freely available from the U.S. National Snow and Ice Data Center (NSIDC) as binary (GLA) or HDF5 (GLAH) data. Level-1A products (GLA01–GLA04) contain uncorrected global altimetry data (GLA01) — including the transmitted and received waveform (fig. 3.2), key parameters and statistics — and atmosphere/engineering/laser pointing data, respectively. Three Level-1B products contain waveform characterisation (GLA05), pre-corrected elevation data including surface characteristics (GLA06), and (atmospheric) backscatter data (GLA07). These lay the basis of the Level-2 data targeted for specific applications. Four of the eight Level-2 products address the atmospheric sciences (GLA08–GLA11), the other four contain elevation data for ice sheets (GLA12), sea ice (GLA13), land surface (GLA14), and oceans (GLA15). The individual footprints were split between the four altimetry products according to a surface type mask. At the time of writing, data dictionaries with a description of all attributes are available at http://nsidc.org/data/icesat/data-dictionaries-landing-page.html. The products were updated multiple times with improved processing algorithms and to incorporate additional parameters and corrections. The (assumingly) final release numbers are 33 and 34 for the atmosphere and altimetry products, respectively. The data are divided into granules that cover

a fraction of an orbit for the more extensive Level-1 products, and 14 orbital revolutions for Level-2 products.

This work uses the GLAH14 product (land surface elevations, Zwally et al., 2012), where a flexible number of up to six Gaussian curves is used to model the return waveform. The surface elevation corresponds to the centroid of the fit Gaussians. The land elevation algorithm is the most appropriate choice for applications in the varied terrain of mountain landscapes, also for small glaciers that can have considerably more rugged surfaces than flat ice sheets. The previous ICESat-based mountain glacier surface studies (Kääb et al., 2012; Gardner et al., 2013; Neckel et al., 2014) also used this dataset whereas ICESat glacier studies in polar regions (e.g. Svalbard) rather used GLA06, which is adequate for smooth surfaces. The standard surface elevations of GLA06 are computed with algorithms for ice sheet elevations that use one or two Gaussians. However, differences between the two elevation products are of decimetre-scale only (they reach up to 3 m in alpine terrain, Nuth, 2011) and average out when large numbers of footprints are summarised (Kääb et al., 2012).

## 3.2 ICESat-based methods to quantify surface elevation change

ICESat's primary mission goal was to quantify changes of the ice sheets to determine sea level rise contribution, but this goal was hampered by the non-exact repeat orbits (Markus et al., 2017). Even on the flat surfaces of the ice sheets, surface slopes of 0.5° are common. On such a slope, a spatial offset of 150 m (a common value) between ground tracks of different years would correspond to 1.3 m elevation difference, and tracks of different years can thus not be compared to each other without knowledge of the local surface slope (e.g. Moholdt et al., 2010b, fig. 3.4a). This problem is enhanced at the ice sheet margins where slopes are steeper — and the greatest changes are happening. On rough surfaces in mountainous terrain, direct comparison of ICESat elevations is nearly impossible altogether and a detailed reference elevation model is needed to model the surface below and between the footprints (Kääb et al., 2012). This section introduces the methods that are used on different (ice) surfaces to measure surface elevation change over time (dh/dt), and also touches on challenges such as representativeness of ICESat tracks for an entire area and the question of volume–mass conversion.

### 3.2.1 Methods for flat surfaces

Surface slopes are approximately constant locally on the flat ice sheets, even at the ice margins and on sufficiently large ice caps. However, deriving the surface slope of a footprint directly from the return waveform is difficult as slope has the same broadening effect on the return waveform as surface roughness. The two effects cannot be separated and these parameters in the GLAS data were thus only calculated assuming either no slope or no surface roughness (Brenner et al., 2011). Surface roughness comes from up to a metre high sastrugi in the ice sheet interior or crevasses on the outlet glaciers that reach tens of metres in depth (Brenner et al., 2011; Nuth, 2011).

Consequently, several years of data were necessary to separate the real elevation change from differences induced by slope or surface roughness. Except for the few areas where ICESat tracks intersect directly, methods to derive dh/dt from ICESat data on flat surfaces aim at estimating the slope between repeat-tracks. The different approaches are introduced below.

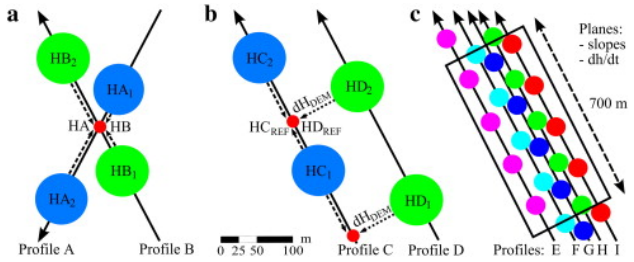


Figure 3.3: Methods to estimate dh/dt on ice sheets and large arctic glaciers: Linear interpolation between two footprint pairs of crossing ground tracks (a), projection of a track segment between neighbouring footprints onto a nearby ground track with the help of a reference DEM to estimate the surface slope (b), least-squares regression to fit planes for surface slope and average dh/dt to repeat-track observations. *Image credits: Moholdt et al. (2010b)*

**Crossover points** Elevations at crossover points of the ascending and descending tracks can be compared directly by interpolation from adjacent footprints on the two tracks (fig. 3.3a, e.g. Brenner et al., 2007). This is the most accurate method to locally assess elevation uncertainty from crossing tracks of the same campaign, dh/dt from comparing tracks of the same season, or seasonal elevation changes from comparing autumn/winter campaigns of the same mass balance year (e.g. Moholdt et al., 2010b). However, the crossover method results in a very sparse spatial dh/dt distribution that may have limited representativeness for regional ice volume change.

**Along-track planes** Sets of neighbouring footprints span a plane that corresponds to the local slope, only biased by elevation changes over time and roughness variations. The method used by Howat et al. (2008) and Moholdt et al. (2010b) fits a local slope plane and a dh/dt plane to reference track segments of 700 m, using linear regression (fig. 3.3c). The approach requires enough ground tracks to generate redundancy for parameter estimation and it is sensitive to the spatial arrangement of the tracks. Several other methods have been proposed that are based on a similar idea of a plane or relative relationship: Yi et al. (2005) used a two-dimensional equivalent approach with an orthogonal cross-track profile instead of a plane, using interpolated elevations from adjacent footprint pairs on each track. The approach of Zwally et al. (2011) uses one footprint of each repeat track, without interpolation, and thus lies in-between the plane- and profile-based methods. Fricker and Padman (2006) and Fricker et al. (2007) analysed the track elevation anomaly compared to an averaged reference profile, and Pritchard et al. (2009) generated ribbons of triangular irregular networks (TINs) from tracks of subsequent years and then compared the triangular planes with elevations of other tracks crossing the facets.

All of these plane-based methods assume that the surface slope is constant over time and in space, at least within the area spanned by repeat-track offsets and a given along-track segment (i.e. up to several hundred metres across tracks by at least 172 m along-track). Schenk and Csatho (2012) found that quadratic or higher-order surfaces are needed to model surfaces of ~1 $km^2$ areas in the rougher coastal areas of the ice sheets. They propose a method that fits such surfaces to crossover areas of ascending/descending tracks, and also to crossover areas with data from airborne laser scanners. Contrary to the assumption of most other plane-based methods, that dh/dt is constant over time, their integrated approach allows for more complicated thickening/thinning signals.

The plane/surface-based methods performed very well on the ice sheets and also on Svalbard's ice caps and glaciers. Attempts have thus been made to fit both planes and higher-level polynomial surfaces to short stretches of multi-annual tracks on mountain glaciers (e.g. on Tibetan glaciers, Huang et al., 2016). There, the plane-based approach clearly failed, and also the fitting of higher-level polynomials is rather problematic as the increased number of parameters to fit hamper a clear separation of elevation change rates. Such an approach is thus error-prone, not least because ICESat's elevation uncertainty for each 70-m-diameter footprint is greatly increased on mountain glaciers with small-scale surface topography and roughness compared to the flat ice sheets.

**DEM projection** Other methods use a DEM to gain a-priori information about the surface slope. Slobbe et al. (2008) compare elevations of overlap-

ping footprints and estimate the local slope between footprint centres from a DEM to remove bias in the steeper ice sheet margin areas. Also Scambos et al. (2004) use a DEM to determine the slope along the flowline of an outlet glacier, so that they can connect elevations of two tracks crossing the glacier by projecting up-glacier along the flowline. Similarly, Moholdt et al. (2010a,b) projected footprints orthogonally onto a nearby repeat-track and removed the artificial dh caused by the surface slope with the help of a reference DEM (fig. 3.3b). Gardner et al. (2013) used a slightly modified version of the latter method in HMA. This turned out to be difficult due to the large cross-track separation in the mid-latitudes (up to several km), leaving only few areas where tracks were close enough to provide a reliable measurement of dh/dt. The fewer measurements, the higher the chance that these are not representative for the area studied.

The use of reference DEMs is not problem-free as it introduces additional uncertainty. For large areas, the surface elevations of the ice sheets were (are) not known very accurately prior to the ICESat era. Optical DEM-generation methods fail due to lack of image contrast except for the rougher ice sheet margins and some outlet glaciers, where the SPIRIT project greatly increased the DEM coverage (sect. 2.1.5). Elevation data from radar altimetry has a very coarse resolution. It is also affected by microwave penetration into the ice/firn, although that may only result in a constant vertical offset while large-scale surface slopes can still be correctly represented.

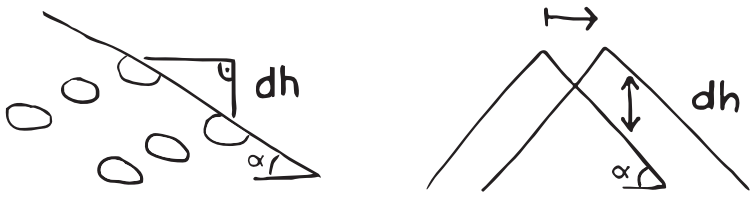


(a) ICESat repeat track offset (b) Imperfect DEM co-registration

Figure 3.4: Artificial dh induced by (a) a sampling offset of a quasi-repeat-track on a sloping surface, and (b) a horizontal shift between two elevation datasets. The artificial dh corresponds to the shift/offset distance divided by $\tan\alpha$.

### 3.2.2 Methods for rough surfaces

The assumption of a flat, sloping surface over an extended area is not valid for small mountain glaciers or footprints on land surfaces (figs. 1.2, 3.5). Landscape topographies are difficult to approximate by mathematical surfaces. A better solution is thus to use a-priori knowledge about the surface by using a reference elevation DEM.

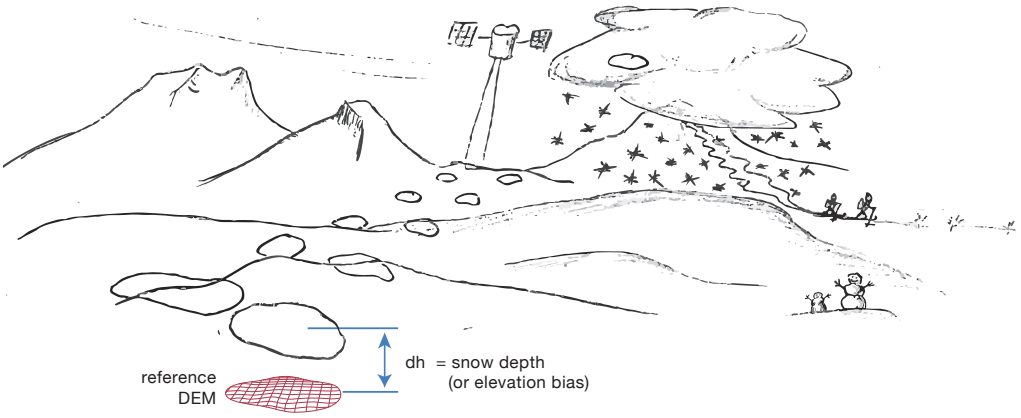


Figure 3.5: ICESat footprints on a snow-covered mountain landscape, compared to reference DEM elevations. In the mid-latitudes, ICESat's ground tracks of different years can be separated by as much as a kilometre.

This approach has been proposed by Kääb et al. (2012) to measure glacier thinning in the Himalayas. Thereby, ICESat elevations are treated as point-based surface elevation measurements and compared to the surface elevation from an accurate reference DEM at the same spatial locations (fig. 3.5) to receive elevation differences (dh). With this, the recorded elevations are normalised to the reference elevation surface, and the dh correspond to actual elevation differences — plus uncertainties. An example for this is given in fig. 3.6 which shows the elevations of ICESat and a reference DEM in blue/red of a track over Svartisen ice cap in northern Norway. In particular where the track crosses outlet glaciers, ICESat recorded consistently lower elevations than the (older) DEM. The elevation differences (black, in cm) do not only provide information about such surface elevation changes, they are also used to filter out footprints on clouds and footprints affected by errors in either elevation dataset (cyan).

**A single footprint** In the case of the SRTM DEM with ~90 m grid cells, the reference elevation has to be interpolated — with associated large uncertainties. At the same time, the resolution is similar to ICESat's footprint size. Reference DEMs with finer resolution have several grid cells per footprint and thus a better potential to represent the within-footprint topography accurately. GLAH14 elevations correspond to the centroid of several Gaussian curves, thus the entire histogram of elevations within one footprint contributes to finding the footprint elevation. Statistical measures of central tendency in the contributing elevations are suitable for the processing of large numbers of footprints (Publication I). Snow tends to smooth rough landscapes so that snow depths

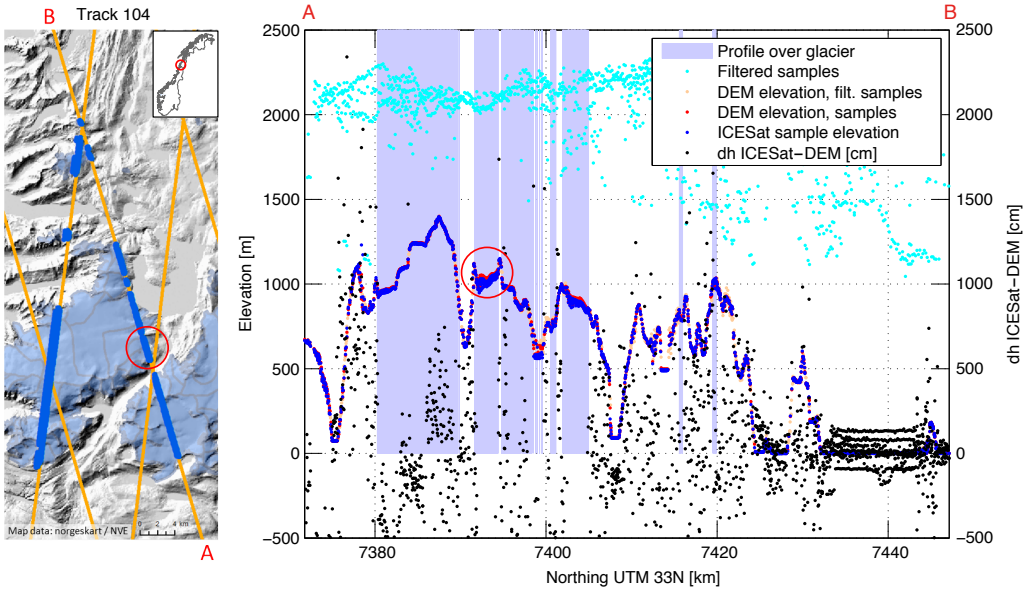


Figure 3.6: ICESat track over Svartisen ice cap in northern Norway (A–B in map, left), with reference elevations from the Norwegian national DEM. Footprints are classified into valid ground samples (blue: ICESat GLAH14 elevations, red: reference elevations) and filtered cloud samples (cyan/orange). All data from 2003–2009 are shown. Over some glacier areas (blue background), ICESat elevations are consistently lower, indicating glacier surface lowering (e.g. area in red circle). The ICESat–DEM dh (black) are mostly within ±5 m over solid ground, out of range for outlet glaciers (consistently $< -5$ m) or samples on clouds, and capture a tide signal on the fjord (~7440 km N).

vary greatly spatially (e.g. Melvold and Skaugen, 2013), also within one ICESat footprint (fig. 3.7, Publication II). Snow-covered landscapes and glaciers have a smoother surface than rough mountain landscapes without snow cover, and the return waveforms are therefore narrower and simpler (e.g. Kääb, 2008; Molijn et al., 2011). To ensure that dh between ICESat and reference elevations correspond to an actual measurement of elevation difference, accurate co-registration of the two elevation datasets is essential (Nuth and Kääb, 2011, fig. 3.4). Especially on sloping terrain, horizontal shifts even of sub-pixel magnitude can cause large artificial dh (e.g. a 10-m shift on a 5-degree slope causes a vertical offset of 0.87 m).

**Double-differencing** Under the assumption that the uncertainties of single footprints are random, averaging of a large enough number of dh (black dots in fig. 3.6, in cm) reveals true surface elevation changes. This technique is also called double-differencing and a standard procedure within GNSS, e.g. for dif-

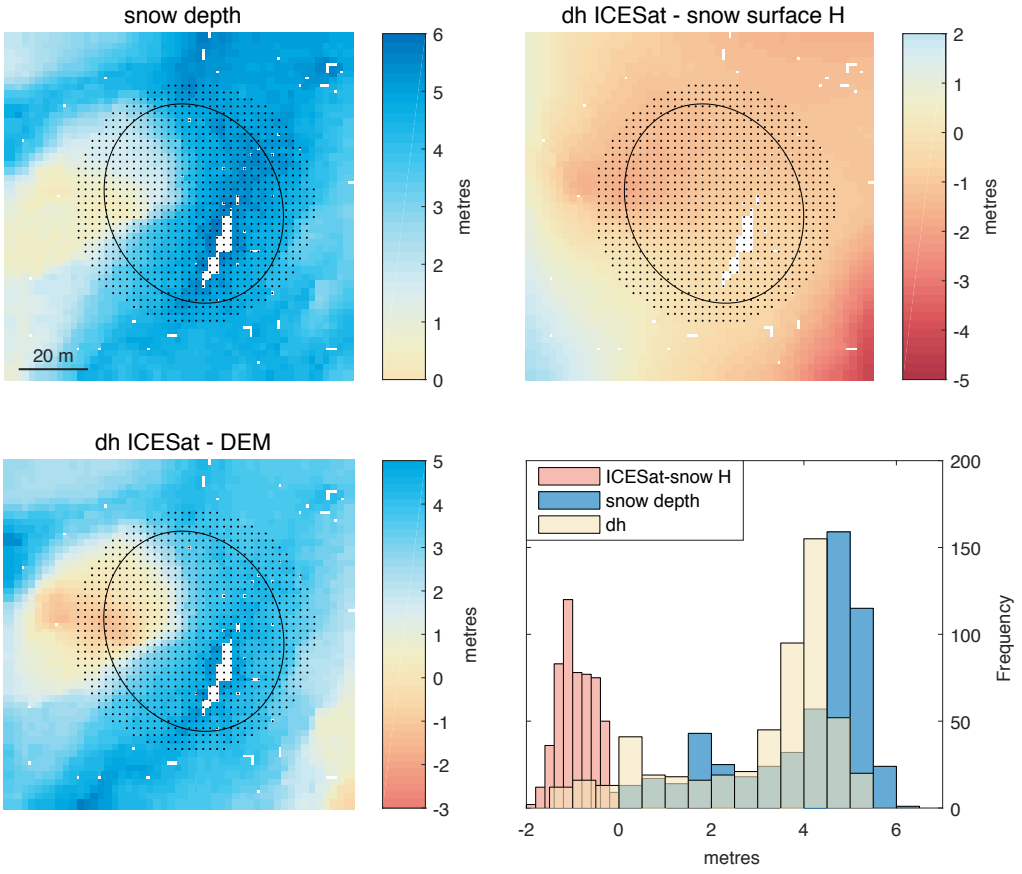


Figure 3.7: An example for an ICESat footprint on snow-covered Hardangervidda at 59.887° N/7.28° E, compared to lidar surface elevations from snow-free conditions and maximum snow depth respectively. Shown are the lidar snow depths in April 2008 (top left), the difference between ICESat's footprint elevation from 3 March 2008 and the snow-free DEM, which roughly corresponds to snow depth (bottom left), and the difference between ICESat and the snow surface elevation H, which should be zero (top right) respectively. The back dots represent the cells within an assumed circular footprint (70 m), the ellipses correspond to the actual footprint as from GLAS metadata. The histograms show the dh within the elliptic footprint, which are offset by ca. 1 m compared to lidar snow depths (bottom right). The lidar data was provided by NVE (Melvold and Skaugen, 2013) and used also in Publication II.

ferential GPS. On snow-covered surfaces, averaging of dh from ICESat's winter campaigns corresponds to the mean snow depth of the years covered (fig. 3.7, Publication II). On glaciers, where we expect a thinning/thickening signal, fitting a linear trend through individual dh and time gives an estimate of the average annual surface elevation change (fig. 3.8).

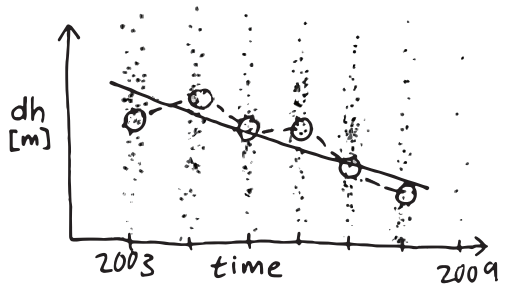


Figure 3.8: Double differencing: fitting a linear trend through ICESat autumn campaign dh and time. Campaign medians (o) might not always follow the trend precisely because annual mass balances vary, and due to uncertainties. The 2009 campaign is usually left out due to its low sample numbers.

Thereby, the annual elevation change signal is about a magnitude smaller than the individual dh. These are t-distributed (fig. 3.9) with a rather large variance due to spatially variable glacier behaviour and differences even within a single glacier (e.g. stronger melt at the tongues), and also due to uncertainties in either elevation dataset. More aggressive filtering based on |dh| might erroneously remove extreme, but valid surface elevation change measurements from e.g. surging glaciers. Therefore, robust trend-fitting algorithms that are insensitive to outliers are the method of choice. In this work (Publications I, III), three methods are employed that are commonly used for time series data with high variance/uncertainty:

- Robust linear regression, which minimizes an iteratively weighted sum of squares so that outliers are identified and down-weighed. This method assumes a normal distribution, which is not a good assumption for data with additive uncertainties (here: large natural variance, plus random uncertainty from within-footprint roughness, plus potential systematic bias from vertical shifts in the reference DEM).

- A linear t-fit, which assumes t-distributed samples (fig. 3.9) and thus accounts for additive uncertainties and outliers in the assumed sample distribution rather than relying on iterative filtering or down-weighing of samples (Lange et al., 1989).

- The non-parametric Theil-Sen linear regression (Theil, 1950; Sen, 1968, Publication III only) that corresponds to the median of the slopes of all possible sample pairs pairs. This method is thus not only less sensitive to outliers but also depends less on the samples at either end of the studied time period.

Since the uncertainty in the individual dh is large whereas the campaign medians follow the linear fit well (fig. 3.8), one might ask why the linear regression is not performed on the campaign medians instead. Rather than increasing the robustness of the fitted relationship, the contrary would be the case. Curve fitting methods assume that there is a true relationship between two variables that is blurred by uncertainties in the individual measurements (i.e., the dh), and that these uncertainties can be described by a statistical distribution (e.g. a normal distribution or t-distribution). Campaign medians still contain uncertainty as they deviate from a perfect linear relationship, not least due to annual variations in glacier mass balance. Taking the campaign medians instead would reduce the sample number from typically hundreds to thousands of individual dh to only six, one for each year of data acquisition. These few values would fit the underlying, assumed distribution poorly compared to the full set of dh (fig. 3.9). A linear regression based on campaign medians would thus greatly increase the trend standard error and herewith the uncertainty in the linear fit.

DEM differencing with ICESat data is described in detail in Publication I. All three linear fitting methods used assume that the regional glacier mass balance was approximately constant throughout the five mass balance years captured by ICESat (the 2009 campaign is usually left out due to incomplete coverage).

It would be inappropriate to use trend-fitting methods on snow samples — the studied period is far too short to capture a long-term precipitation trend. For a larger area, snow depths are commonly assumed to have a lognormal distribution (e.g. Liston, 2004) — in our case, elevation uncertainty comes in addition to the signal. dh distributions of snow samples are similar to those of snow-free terrain (fig. 3.9), but shifted/skewed skewed towards positive dh. Regional snow depths can thus be retrieved from spatial/temporal averaging of samples. The methodology as well as the relevance of such regional-scale snow depths compared to other methods for snow studies are discussed in detail in Publication II.

### 3.2.3 Applications and uncertainties on rough surfaces

The double-differencing technique has been applied to estimate glacier elevation change rates for glacierised areas across the globe (Gardner et al., 2013; Neckel

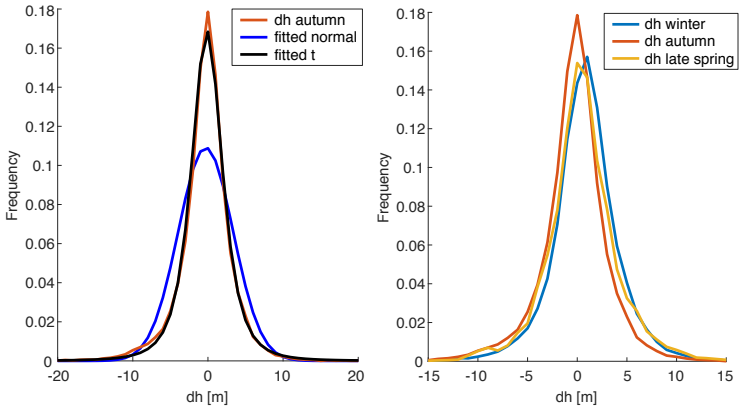


Figure 3.9: dh distributions of off-glacier samples in the southern Norway study site visualise per-footprint elevation uncertainty (Publications I, II). Left: the fitted t-distribution with its narrow peak and long tails matches the sample distribution far better than the fitted normal distribution. Right: Snow cover causes a slight offset/skewness towards positive dh in winter/late spring dh distributions.

et al., 2014; Kääb et al., 2015; Farinotti et al., 2015; Phan et al., 2017). Increasingly, attempts are made to use the method for local glacier complexes or even individual glaciers (Kropáček et al., 2014; Bao et al., 2015; Ke et al., 2015a,b; Li et al., 2015, 2016). The majority of the studies uses both the autumn and winter campaigns, either by fitting separate linear regressions through winter/autumn campaigns only, or by combining the two seasons and fitting a trend through all campaigns. Both can be problematic where snow depths vary yearly — and Publication II shows that ICESat is clearly sensitive to snow cover. The method to derive snow depths from ICESat data was developed in this work and has not yet been applied elsewhere.

The remote sensing approach to assess glacier changes from ICESat spiced with a pinch of statistics makes it easy to forget about the question of representativeness of ICESat's sparse spatial sampling for glaciers in an entire region, let alone for a single glacier only. Also the influence of uncertainties in all contributing elevation datasets or other aspects that affect dh is not immediately obvious from the elevation data. These are, for example, bias from recent snow fall, reference DEM age, or radar penetration into ice/snow in the reference DEM.

Publication I addresses the issues above with regard to the glaciers in southern Norway, a control scenario in a small region with well-studied glacier evolution but a reference DEM that is inconsistent in age and affected by local vertical bias. In the presence of such spatially varying vertical bias, it plays a role how point-based elevation samples are grouped spatially. The role of elevation

bias and spatial grouping for snow depth studies is examined in Publication II. Publication III uses the new insights from the first two studies to assess glacier changes in HMA, a much larger region where the same challenges exist as in Norway, but where little reference and validation data are at hand: glacier behaviour is not well known, the terrain even more rugged, and only the coarse-resolution SRTM DEM is available with various sources of elevation uncertainty (sect. 2.3.2). Additionally, the sheer size of the study area in combination with sparse spatial sampling requires careful grouping of samples to ensure representative elevation change rates.

### 3.2.4 From elevation changes to mass changes

In many cases, the final number of interest in relation to glacier thinning rates is the contribution to river discharge or sea level rise. For this, an estimate of water equivalent (i.e. a mass change) rather than elevation change is needed. However, geodetic methods such as DEM differencing or double-differencing of ICESat data only provide information on elevation change. To convert dh/dt to mass change, two conditions need to be fulfilled: (i) the elevation change measurements need to be representative for the area of interest so that they can be converted to a volume change, and (ii) the density of the ice/firn needs to be known in order to convert volume to mass.

In terms of representativeness, ICESat data has the advantage that it samples many glaciers with individual thickening/thinning signal. For the large glaciers and ice caps in Svalbard, Moholdt et al. (2010b) found that this yields a robust area-averaged estimate of elevation changes. Extrapolation from measurements on few, selected glaciers to larger regions is rather less reliable as the risk of sampling bias is higher (Berthier et al., 2010; Cogley, 2012). This work assesses whether the representativeness of ICESat data is also given for the small mountain glaciers in southern Norway (Publication I).

Of key importance for representativeness is the correct sampling of the glacier hypsometry. A glacier is characterised by a mass transport from the accumulation area at higher elevations to the ablation area in the lower part. In order to capture an elevation change signal related to geodetic mass balance, we need to sample the entire glacier to consider both surface elevation changes from ice melt and glacier dynamics. A sampling bias towards either of the glacier parts would not fulfill the condition of mass continuity. To ensure correct hypsometric representation is an important and inherent condition of any volumetric-geodetic glacier method, including ICESat studies (e.g. Arendt et al., 2002; Kääb, 2008; Moholdt et al., 2010b). It would be physically incorrect to draw conclusions on the glaciers' mass balance from a linear fit on dh and time based on a subset of samples that does not reflect a glacier's hypsometry or, in

the case of the larger spatial regions assessed in this work, the hypsometry of the glacier population in that region.

Naturally, the different parts of glaciers have different densities. Snow/ice density varies greatly in space and for different layers of the snow pack/firn at high elevations, and increases towards the compressed ice layers of the tongues. In particular in the accumulation areas, one cannot know from remote sensing data alone whether an elevation change is due to a change in the ice column or in snow or firn thickness, newly accumulated snow or firn, or if the density profile changed over time, for example due to firn compaction or superimposed ice. Conversion between volume and mass changes thus always requires a density assumption. This is the case for any glacier DEM differencing studies and discussed in detail by Huss (2013). Kääb et al. (2012) and Gardner et al. (2013) use ICESat-based double differencing to estimate sea level rise contributions of mountain glaciers and used overall densities of 850 and 900 $\mathrm{kg\,m^{-3}}$, respectively, to convert the dh/dt signal to water equivalent. Kääb et al. (2012) also applied an alternative density scenario with $600\,\mathrm{kg\,m^{-3}}$ for firn and $900\,\mathrm{kg\,m^{-3}}$ for ice areas but found this affected the results by only 5%.

The focus of this work lies primarily on methods to derive elevation differences from ICESat data, not on conclusions from mass changes — the conversion between volumetric and mass changes does not depend on ICESat parameters but on local conditions and is thus an entirely different problem. Where a conversion between dh/dt and mass changes is necessary to compare ICESat-based results to values from the literature, e.g. from mass balances measured in-situ (Publications I, III), we rely on the findings of Huss (2013). That study finds that a value of $850\,\mathrm{kg\,m^{-3}}$ is an appropriate estimate for multi-annual changes and stable mass balance gradients. Strictly speaking, these conditions are not perfectly in place (we find that glaciers in both study areas are not in balance, and that mass balances vary annually), but the simple assumption provides a reasonable first guess for validation purposes. The value proposed by Huss (2013) has become a de-facto standard for glacier volume/mass conversion for volumetric-geodetic mass balance studies and has thus been used also in some of the glacier mass balance numbers we reference to in this work (e.g. NVE's mass balance series in Publication I).

Also for many snow applications targeted at downstream hydrology, snow water equivalent (SWE) rather than snow depth is the final parameter of interest. ICESat can provide information on snow depths, but not on density — which is also the case for most other methods to measure snow, such as airborne lidar or distance-measuring instruments on meteorological stations in the field. However, also snow depth on its own is an important parameter, especially

to assess heat flux, soil temperatures and surface energy balance (Harris et al., 2009). An extensive review of methods to measure snow-related parameters is provided in Publication II.

## 3.3 ICESat-2

The invaluable data provided by ICESat called for a follow-on mission. ICESat-2 is currently scheduled to be launched in 2018 into a near-circular orbit at 500 km altitude and 92° inclination, and is ranked as one of NASA's top priorities. It has primary goals that are similar to those of the original ICESat mission, yet go beyond these (Markus et al., 2017): quantification of the mechanisms and dynamics of regional ice-sheet changes and the ice-sheet contributions to sea-level change, accurate sea ice freeboard measurements that capture freeze and melt cycles and improve the understanding of ice/ocean/atmosphere interaction, and global biomass estimation for a complete global carbon budget. As bonuses, so to speak, ICESat-2 is expected to measure atmosphere/cloud properties, wave heights, snow depths, or mountain glacier changes — to name just a few examples. Such a complete assessment of everything related to elevations or height changes on the Earth require a step up from both the spatial/temporal resolution and spatial coverage delivered by ICESat (Abdalati et al., 2010). Detailed science requirements for coverage and resolution as well as elevation accuracies are defined in Markus et al. (2017).

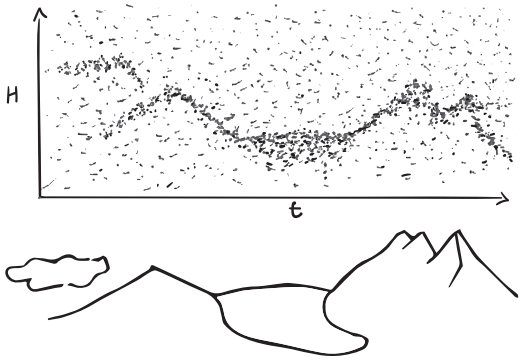


Figure 3.10: A photon density cloud: how the Advanced Topographic Laser Altimeter System (ATLAS) instrument on-board ICESat-2 might 'see' a mountain glacier landscape.

To meet these requirements, ICESat-2 will have a denser cross- and along-track sampling and smaller footprints. Rather than relying on high-energy pulses such as from GLAS, it will carry the ATLAS instrument, a high-frequen-

cy photon-counting laser (sect. 2.2.1; the ATLAS instrument is described in detail in Markus et al., 2017). The single-wavelength (532 nm), low-energy system greatly increases the number of pulses that can be fired with the same amount of energy, a major advantage over the system used for the ICESat mission. A green wavelength rather than NIR (used by GLAS) was chosen, aiming at the higher sensitivity and efficiency of photon-counting detectors for green wavelengths (Degnan, 2002), hopefully without compromising data quality of vegetation or water surface targets (Abdalati et al., 2010; Swatantran et al., 2016). The data provided by ICESat-2 will therefore be entirely different to GLAS' waveforms and consist of zillions of time/location recordings of individual photon detections (fig. 3.10). Analysis of single footprints will not be possible: even for high-reflectivity targets, only a handful of photons will be detected per sent pulse, and separation of the background photons and the surface returns require density filtering of the along-track profile point clouds (e.g. Horan and Kerekes, 2013; Markus et al., 2017).

ATLAS' high-frequency (10 kHz) pulses enhance along-track resolution to continuous profiles with overlapping footprints every 0.7 m. The nominal footprint diameter is <17.5 m and ATLAS has not only one, but six of them, as its laser beam is split into sub-beams (fig. 3.11). These are arranged in a 2 x 3 array that form three profile pairs separated by 90 m / 3.3 km (fig. 3.12). One of the beams in each pair points slightly ahead (2.3 km, thus a slight yaw of the spacecraft defines within-pair beam separation). Like ICESat, the follow-on mission does not have a metre-scale pointing ability that would allow exact repeat tracks, but its improved pointing control is expected to be < 45 m (with the pointing location known within 6.5 m) and the beam pair should therefore always embrace the fixed reference ground track. Beam pairs allow the detection of the cross-track slope from a single overpass on the flat ice shields — a major source of uncertainty for the ice sheet elevation change studies of the single-beam ICESat mission.

The beam pairs consist of a weak and a strong (four times the energy, ~120 µJ) laser pulse in order to minimise energy consumption. The weak beam should generate a detectable amount of photons on the highly reflective ice sheets (0.4–3 photons per shot; Markus et al., 2017) but possibly not on dark and rough (land) surfaces (Brown et al., 2016). Together with a spare laser and multiple detectors, the split-beam approach ensures redundancy in case of instrument failure or other problems with ATLAS' extremely precise and finely aligned optical elements.

The split beam triples the number of elevation profiles for a single overpass compared to ICESat (fig. 3.11). A continuous operation on the 91-day repeat orbit with three sub-cycles is planned, which results in 1387 ground tracks and again triples the data provided by ICESat: The complete repeat orbit

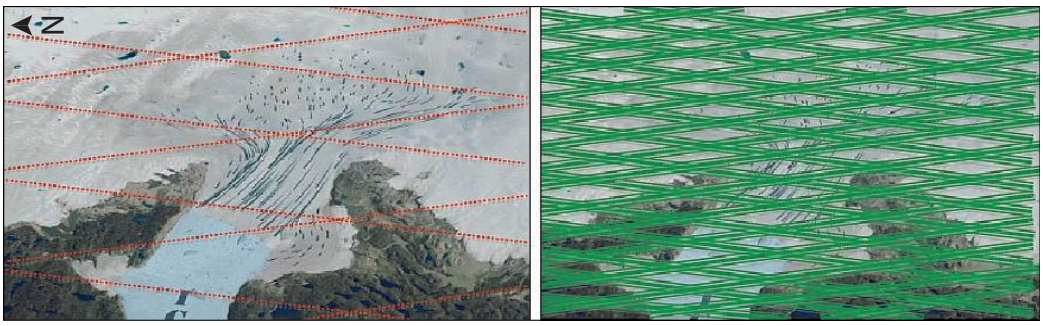


Figure 3.11: Jakobshavn Glacier, Greenland, with ICESat reference tracks (left) and planned ICESat-2 coverage (right) with denser reference tracks and split beams. *Image credits: Brunt et al. (2013)*

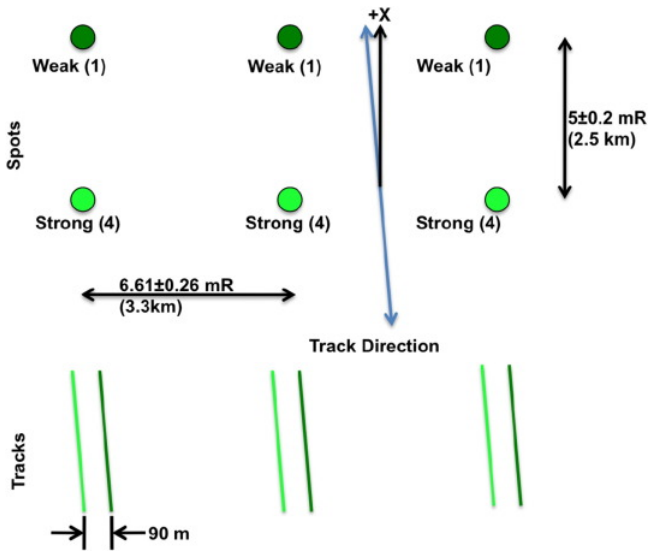


Figure 3.12: ICESat-2 will have six laser beams arranged in a 2 x 3 array. They form three pairs with a weak and a strong beam each. *Image credits: Markus et al. (2017)*

adds two additional ground tracks in between ICESat's campaign-mode reference tracks (corresponding to only one sub-cycle). One ICESat-2 sub-cycle will thus provide global coverage with ICESat-like orbit spacing up to 88°, so that the requirement of e.g. monthly sea ice thickness maps is met.

However, only the polar regions will have exact repeat-track observations. In mid-latitudes, vegetation and mapping applications are prioritised. At this stage of global vegetation height (and surface elevation) knowledge, these applications require complete coverage rather than repeated observations. Systematic off-nadir pointing during the first two years of operation will lead to a track density of 2 km at the equator. Consequently, some areas will be sampled during the transition between the coverage- and repeat-track modes (fig. 3.13) which takes ca. 20 seconds (Escobar et al., 2015).

Like ICESat, ICESat-2 will provide science data products at different levels and include housekeeping data, with latencies of 3–7 weeks for geolocated photon data and higher-level elevation products (Brown et al., 2016). Currently, data processing algorithms and corrections are being prepared with the help of ATLAS' airborne sibling MABEL and other lidar instruments (Escobar et al., 2015). MABEL has been flown over ice targets (e.g. Kwok et al., 2016; Brunt et al., 2016) and other surfaces (e.g. Gwenzi and Lefsky, 2014; Jasinski et al., 2016). The ICESat-2 mission requirement is a three-year operation, but the goal is five years — and the satellite will carry fuel for seven years (Brown et al., 2016).

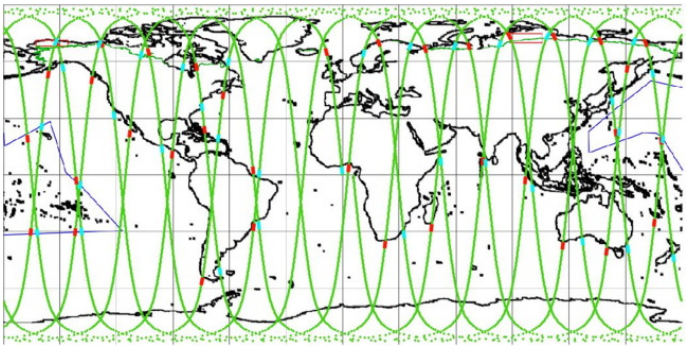

Figure 3.13: One day of ICESat-2 orbits with transitions from polar repeat-track mode to mid-latitude full-coverage mode (blue; red the other way round). *Image credits: Markus et al. (2017)*

# Chapter 4

# Summary of Research

This chapter summarises the research done within this work. The three publications describe applications of ICESat for the mountain cryosphere that were shared with the scientific community (appendix A). Publications I and III are about glaciers, Publication II about snow depths. The publications are introduced and discussed chronologically. This reflects how the methods evolved as our knowledge of the potential and limitations of this data in rough mountain terrain increased.

## 4.1 Publication I: ICESat laser altimetry over small mountain glaciers

Previous studies that used ICEsat data to assess glacier volume changes did so in large, remote areas where few other measurements of glacier mass balance exist (e.g. Kääb et al., 2012; Gardner et al., 2013). Questions have thus been raised about the representativeness of ICESat data for the glaciers in a given region. The spatial sampling of ICESat, which crosses arbitrary glaciers randomly and often right across rather than e.g. along their center line, is very different to classical in-situ mass balance measurements. There, a selected glacier, declared representative for a region, is monitored carefully, spatially extensively and regularly. ICESat's sparse sampling is also very different to classical geodetic mass balance measurements from DEM differencing of the complete extent of one or several glaciers in an area. This study addresses concerns about the representativeness, validity and uncertainties of ICESat-derived dh/dt in a controlled test setup. In size, number and density of its glaciers, Southern Norway represents a varied glacierised mountain area that is suitable but challenging for ICESat applications, and its glaciers are rather well studied — including

winter/summer mass balance measurements on eight glaciers during the 2003–2008 ICESat period. The area is thus suitable as a test site for the potential and limitations of ICESat data in analysing regional glacier elevation change of small mountain glaciers.

We compare the distributions of elevation, slope, aspect, and glacier size of the ~1100 ICESat footprints on glaciers in southern Norway to the respective distributions of all glaciers in the study area, and find that they are indeed representative — also for individual ICESat autumn campaigns, except for the (excluded) autumn 2009 campaign whose few samples are spatially too tightly clustered. Notably, we find that ICESat also samples the many small ice patches that are not commonly monitored in-situ. The spatial sample distribution varies; the same glaciers are not sampled each year, both due to cloud cover and the spatial offsets between the repeat tracks.

The sample is sufficiently large to perform spatial and thematic subsetting that yields plausible results: for example, smaller glaciers are thinning more than large glaciers. We only use ICESat's autumn campaigns: ICESat's winter campaigns indicate substantial snow cover that varies greatly in thickness each year and reaches several metres, in particular in the western, more maritime half of the study area. The onset of winter snow fall is visible in the December part of the 2008 autumn campaign (table 3.1). Correcting for this effectively removes a false positive trend in off-glacier samples. The detected snow signal led to Publication II, where we analyse ICESat's potential in determining snow depths in more detail.

We test two different linear fitting methods; a robust linear regression and a t-fit that better represents the t-distribution of our samples (fig. 3.9), and find that the differences between the two are small. As a reference DEM for the double-differencing approach, we use the Norwegian National DEM at 10 m and 20 m resolution. To analyse the influence of spatial resolution and other uncertainties inherent in the reference DEM, two additional DEMs are tested on the non-glacierised Hardangervidda mountain plateau (they are not available for the entire study area): the SRTM DEM at 3-arc-sec resolution, and a high-resolution lidar DEM. From all three DEMs, we compute dh to autumn samples (snow-free, i.e. no elevation difference expected) of ICESat as a spatially consistent elevation dataset. We find that elevation errors caused by within-footprint topography can reach several metres, but these errors cancel out as soon as several samples are grouped. To that end, it is of little importance what resolution the reference DEM has and which statistical/interpolation method is used to derive dh from DEM grid cells within one ICESat footprint. It does turn out, however, that the DEMs are affected by systematic vertical bias that is varying spatially. Such vertical bias is caused by small spatial shifts in the merging process of several elevation datasets to a larger DEM, and fairly common (fig. 3.4b,

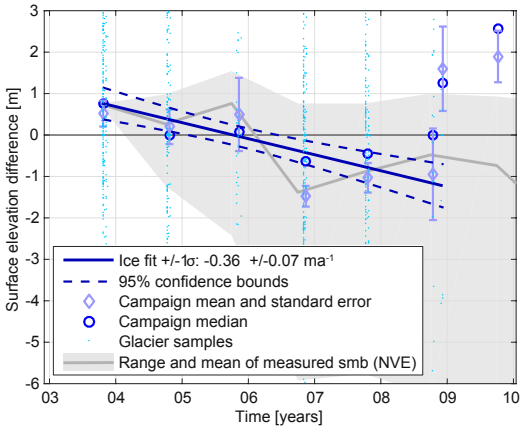


Figure 4.1: Glacier elevation change from ICESat and NVE's in-situ surface mass balance (smb) measurements of eight glaciers in southern Norway.

Van Niel et al., 2008; Nuth and Kääb, 2011). In comparison, ICESat-related biases, such as from waveform saturation, are negligible. Consequently, the elevation uncertainties of the reference DEMs exceed ICESat elevation uncertainty by a magnitude, and it is the reference DEMs rather than ICESat elevation uncertainty that are limiting the accuracy of the method. Spatially more consistent DEMs have the potential to greatly reduce the influence of such bias. A promising candidate is the TanDEM-X World DEM, even at a lower spatial resolution.

For samples on glaciers, additional uncertainty comes from the varying DEM age of the Norwegian national DEM (which is a product of spatio-temporal merging, see fig. 2.2). Because ICESat's spatial sample distribution is not exactly the same each year, the composition of vertical offsets (from older glacier DEM surfaces and vertical DEM bias) is different for each autumn campaign. To remove the diluting effect that these uncertainties have on the fitted linear regression, we develop a new per-glacier bias correction that corresponds to the median dh of all autumn footprints on one glacier. This correction decreases the error/uncertainty in glacier dh by about 50% and greatly reduces the uncertainty in the derived dh/dt. At $-0.36 \pm 0.07 \mathrm{m\,a^{-1}}$, we receive a very plausible regional estimate that matches the average of in-situ timeseries (fig. 4.1). Only with the per-glacier correction in place do the median dh of individual ICESat campaigns match the annual in-situ mass balance signal. The correction has the potential to improve ICESat-derived glacier change rates in other areas as well, for example to remove bias from vertical offsets and penetration in the SRTM DEM.

The study thus shows that ICESat data is representative for an area comparable to southern Norway, but that good control on biasing factors is necessary. The most important is a consistent distribution of the samples for individual campaigns — not only in space or hypsometry, but also in terms of spatially varying bias from the reference DEMs. The research provides a road map for other studies that wish to assess glacier elevation changes using elevation data from ICESat, and possibly also ICESat-2.

## 4.2 Publication II: Snow depth from ICESat laser altimetry — A test study in southern Norway

To date, no method exists to measure snow depths directly at regional scales. Applications that require information on snow depths or SWE (e.g. river runoff, permafrost) have to rely on coarse-scale passive microwave data that does not work well in mountain areas, or on modelled and interpolated data from e.g. sparse in-situ measurements and remotely sensed information on snow cover extent. The closely related SWE is considered an essential climate variable, but international efforts to generate global SWE maps have not yet resulted in satisfactory results (e.g. ESA's GlobSnow project, Luojus et al., 2010) — not least because microwave data fails to appropriately estimate SWE $> 100$ mm. Consequently, estimation of snow depths in mountainous terrain is arguably the most important unsolved problem in snow hydrology (Dozier et al., 2016; Lettenmaier et al., 2015). In Publication I, we clearly saw the effect of snow cover on Norwegian glaciers in ICESat's March campaigns, and also for off-glacier samples in the December 2008 campaign. Here, we present a feasibility study for ICESat-derived regional snow depths in the already familiar southern Norway study area. The research is based on the same data as in Publication I, but in this study we only use off-glacier samples on stable ground to ensure that the dh capture the effect of snow cover.

To account for uncertainty in elevation data, ICESat samples are grouped into spatial subsets, elevation bands, and/or over time. In time series for the entire 2003–2009 period and different elevation bands, the effect of snow cover in March and June campaigns is clearly visible. We correctly reproduce both annual differences in snow amounts and the increase of snow depth with elevation. The values for different elevation bands agree well with measured (root mean square error (RMSE) 0.47 m) and modelled (RMSE 0.61 m) snow depths from snow depth sensors on meteorological stations and the seNorge distributed snow model, respectively. However, time series are only possible for a large spatial area — resolving the effect of elevation as well requires that samples of

Figure 4.2: Snow smoothens the landscape around Fondsbu, Jotunheimen.

the entire study area are grouped. Since the spatial sampling distribution is not the same for each campaign, the spatially varying offsets in the reference DEMs have a similar biasing influence as the effect seen on glaciers in Publication I. To remove this bias, we propose a local vertical co-registration that is similar to the per-glacier correction in Publication I: First, we split samples into smaller spatial subsets but group them over the entire time period, i.e. all winter campaigns together. Then, we bias-correct the March/June snow depths with the median of the autumn dh per spatial unit or elevation band. This bias correction is somewhat less reliable than in Publication I, where glaciers form obvious spatial units. For off-glacier areas, we do not know the spatial extent of (vertically offset) processing sub-units of the DEM. After correction of the local DEM biases, we retrieve a spatially resolved map with a snow depth estimate every few km along-track within a given elevation band. The spatial pattern clearly captures the increasing snow depths towards the rainy Norwegian west coast and matches the modelled snow depths in southern Norway with decimeter-scale accuracy.

For the Hardangervidda area, additional elevation data from the SRTM and high-resolution DEMs are available — plus lidar-based snow depth measurements for April 2008/2009 on six stripes crossing the area (Melvold and Skaugen, 2013). In the western part of Hardangervidda, ICESat-based average March snow depths agree better with the lidar measurements (RMSE $\leq$0.15 m for all three DEMs) than modelled snow depths (RMSE 0.61 m). The modelled data consistently overestimate snow depths. This can be attributed to a lack of measurements in this area, since the seNorge model is forced with temperature/precipitation measurements from weather stations. In eastern Hardangervidda, the coarse resolution SRTM DEM performs better (RMSE 0.41 m) than the 10 m Norwegian DEM (RMSE 0.64 m), even after bias-correction. The high

resolution lidar DEM is the least affected by vertical DEM bias, thus even the dh of single footprints show good agreement with lidar-measured snow depths from the same year (R2 0.59, RMSE 0.94 m, average snow depths are up to 8 m, see also fig. 3.7).

The study shows that spatially averaged mean snow depths can be retrieved from ICESat data. Currently, the main limitation lies in the reference DEMs — but good quality reference DEMs of spatially consistent quality may still be acquired in the future even in areas where no such data exists today. Due to the need of sample grouping, the spatial resolution of ICESat-derived snow depth maps is rather coarse. However, especially in more remote areas than southern Norway, ICESat's measurement density is far superior to the sparse in-situ measurement networks. The data could thus be very valuable in combination with a spatially distributed model such as the seNorge snow model, not least by contributing to a better parametrisation of e.g. snow depth–elevation gradients. Also combination with SWE estimates from passive microwave data could be fruitful, as these data are most accurate for low SWE values ($< 100$ mm, Luojus et al., 2010) whereas ICESat is more reliable for large snow depths, where the relative influence of DEM bias is smaller. This study focuses on areas above the tree line, and further research in a different setting is needed to assess ICESat's performance in areas with coniferous or leaf-shedding vegetation. The method presented here could be further improved and localised, for example by using full waveform ICESat data in combination with a high-resolution DEM. Data from the follow-on mission ICESat-2 has an even higher potential, once this satellite is operational.

## 4.3 Publication III: A spatially resolved pattern of glacier volume changes in High Mountain Asia for 2003–2008 and its relation to precipitation changes

Glacier changes in High Mountain Asia directly affect downstream water availability for billions of people, yet they are still not well measured. To date, ICESat still provides the spatially most extensive and complete measurement of glacier elevation changes in the area (Cogley, 2012). Climate change affects both temperatures and precipitation patterns in the complex topography of the region. To assess the state and fate of HMA's glaciers, we need to understand not only how they react to warming temperatures but also to changes in precipitation. This study extends the previous work of Kääb et al. (2012, 2015) in

the Pamir–Karakoram–Himalaya to the TP and Tien Shan areas, with an improved, robust method using the insights gained from Publication I. We present a spatially diverse pattern of glacier elevation changes in HMA and provide an interpretation on how these are driven by spatially greatly varying sensitivity to precipitation, and changes thereof.

Previous work in the area (appendix A) relied on large regions or a regular grid to group ICESat samples, which blurs local signals. We introduce a new, better adapted zonation where ICESat samples are grouped in units of similar glacier behaviour, glacier type, and topographic setting. As a reference DEM for the double-differencing approach, we use the SRTM DEM at 3-arc-seconds resolution (sect. 2.3.2). The other freely available, global alternatives are not suitable as a consistent reference: Both the ASTER GDEM (sect. 2.1.3) and the ALOS World DSM are a time-averaged product, and the latter has large data gaps due to persistent cloud coverage in parts of HMA.

However, not only does the SRTM DEM contain locally varying bias in HMA, but the much greater microwave penetration depths in the accumulation areas compared to low penetration at the tongues cause very steep gradients of dh and elevation. The dh–elevation gradients reach 1–3 m dh per 100 m elevation, and correct sampling of the local glacier hypsometry is therefore especially important for accurate results. We assess four different methods to correct for imperfect hypsometric sampling and find that in 50 of 100 spatial units, the effect of hypsometry missampling on elevation change rates exceeds 0.1 m $a^{-1}$. Converted to water equivalent, such a bias would be large enough to affect hydrological studies on river runoff, more often than not the main motivation to assess glacier volume changes in HMA. We also test the effect of the per-glacier correction developed in Publication I to remove vertical bias from DEM offsets, microwave penetration, or locally extreme dh on surging glaciers. The correction has a similar improving effect as in Publication I for some spatial units but not everywhere, as it tends to remove parts of the thinning/thickening signal. A decision whether or not this correction should be applied has thus to be taken for each spatial unit individually, depending on the local sampling pattern and influence of the different sources of bias.

An assessment of the split autumn 2008 campaign reveals that glacier elevation change rates are more sensitive than previously assumed to snow cover during the last ICESat campaign in December 2008. Correction for up to 1.5 m snow in December 2008 makes the dh/dt up to −0.25 m $a^{-1}$ more negative. We test three different linear regression algorithms and find that all of them are particularly sensitive to offsets/bias in the first/last campaigns. Good control on biasing effects is therefore important for an accurate estimate of local glacier elevation change signals. Since the linear regression is disproportionally determ-

ined by the first/last campaign, this also means that representative sampling is most important for these two campaigns.

In contrast, the overall pattern of glacier changes is robust against all bias corrections, and neither is it affected by changes in sample compositions or reference elevations, for example from using the SRTM DEM at 1-arc-second resolution. The spatial pattern corresponds well to the findings of earlier studies. In several places, however, our spatially resolved zonation reveals local differences and anomalies that have not been described previously. Much of the spatial pattern can be attributed to the glaciers' sensitivity to precipitation.

Along the entire Himalayan range, glaciers on the first orographic ridge that are exposed to abundant precipitation were thinning less in 2003–2008 than glaciers in the dryer climate of the inner ranges. On the TP, analysis of MERRA-2 precipitation data shows a step-increase in precipitation around the year 2000 that is likely the cause of the glacier thickening we observe in the Eastern Pamirs, Kunlun Shan and central TP by 0.1–0.7 $\mathrm{m\,a^{-1}}$. The signal picked up by ICESat for the years 2003–2008 is located further east than the much discussed Karakoram anomaly. The mass gain stands in great contrast to an overall trend of mass loss in all the surrounding, more peripheral mountains. The anomaly has a crisp boundary in the Eastern Pamir that continues just north of the central Karakoram, but transitions smoothly to an only slight thickening in the central TP. We find indications that TP glaciers are dynamically adapting their geometry to a different precipitation/temperature regime, as the elevation change signal in the accumulation areas is stable or positive whereas the ablation areas were thinning. Glaciers in the south/east of the TP were thinning, with increasing rates towards southeast. The precipitation anomaly possibly extended as far as to the northern slopes of the Tarim Basin, where glaciers were thinning less than their neighbours just north. Thinning rates in the Tien Shan vary spatially but are on average more negative than in other parts of HMA. Other areas with strongly negative elevation change are the Nyainqêntanglha Shan/Hengduan Shan and Western Himalayas, where glaciers sit at lower elevations than elsewhere and seem to already have lost their accumulation areas (Kääb et al., 2015). Glacier melt is inevitable where temperatures increase so much that the equilibrium line altitude rises above the glacier's accumulation area — even when precipitation is abundant.

The glacier change signal seen by ICESat only captures the short period of 2003–2008, which is not representative for a long-term trend, and should thus not be extrapolated into the future. In particular the thickening signal centered above the Kunlun Shan is likely a short-term reaction to the recent precipitation increase and might not persist in a climate with further rising temperatures. Also, the assumption of a linear regression, corresponding to constant mass balance during five years, might not be appropriate everywhere

(e.g. Schenk and Csatho, 2012). However, coupled with other climate-related observations, the spatially resolved pattern of glacier changes presented in this study can contribute to a better assessment of ongoing changes in a large and important region that is still not very well understood.

# Chapter 5

# Conclusions and outlook

## 5.1 General conclusions

The first satellite-based laser altimetry mission, ICESat, provided a wealth of elevation data across the globe that is of a very different nature than a classical, gridded DEM, yet unsurpassed in its accuracy and global consistency. The sparse spatial sampling do not make this data the most obvious choice to monitor the mountain cryosphere, and neither is it what the mission was intended for. This work shows that the data indeed contains a valuable, unique and representative sample of glacier surface elevations and snow depths for the years 2003–2009 that cannot be supplied by other sources.

Within this thesis, a new method to use ICESat data to estimate average regional snow depths was developed and applied for the first time. The test study in southern Norway shows good agreement with locally measured and modelled snow depths. No other method exists to measure snow depths directly at this scale and accuracy. While small-scale spatial variations are averaged out and the temporal resolution is restricted to an average estimate each for March and June, ICESat-derived snow depths could be combined with distributed snow models or passive microwave data to create spatially distributed maps.

An existing method for regional elevation changes of small mountain glaciers (Kääb et al., 2012) was validated and improved in a test study on the well-studied mountain glaciers of southern Norway. We find that it is essential that also individual campaigns paint a representative picture of the glaciers in the region, not only the combined sample of the entire acquisition period. In particular, accurate sampling of glacier hypsometry for all individual campaigns is a key requirement. The improved method better reproduces temporally/spatially varying glacier thickening and thinning signals with greatly reduced uncertainty. In HMA, where other measurements of glacier changes are

sparse, the updated, spatially resolved map of glacier changes presents a diverse pattern of glacier reactions to climate change which reveals local differences that have not previously been discussed in a larger spatial context. We find indications that changes in precipitation play a large role in explaining this pattern. Set in the context of other climate-related observations, the regionally complete snapshot of glacier evolution during 2003–2009 can contribute to our understanding of the ongoing changes in this large region.

Also in other remote areas, the ICESat-based methods developed in this thesis can help to improve our knowledge of the state and fate of mountain glaciers and snow. However, the application of ICESat in rough mountain areas is dependent on, and limited by, the availability of a DEM that provides an accurate and spatially consistent reference surface.

## 5.2 The role of DEM bias

ICESat's profile-like sampling and uncertainties within the large footprints require that several samples are grouped, in a way that is representative for the observed phenomenon. In addition, the large horizontal offsets between repeat ground tracks make that the ICESat elevations from different times only are comparable after they have been set in relation to a reference surface. ICESat studies on ice sheets with comparably smooth topography try to avoid using an external DEM for good reasons: Our results show that external elevation datasets, usually in the form of gridded DEMs, are the major source of uncertainty and bias.

The main challenge comes from spatially varying, systematic vertical offsets of unknown sub-units in the reference elevation data. DEMs covering the larger spatial areas that are interesting for ICESat applications are usually a composite of several input datasets. The global DEMs are based on satellite data such as from ASTER, SRTM, or ALOS PRISM, and many individual scenes were used to create them. On a smaller scale, national DEMs are commonly composed from terrestrial or remotely-sensed elevation data. When individual data are combined into a larger dataset, horizontal and vertical shifts of production subunits are easily introduced. Imperfect co-registration of sub-pixel magnitude can quickly cause elevation bias of the same magnitude as the surface change signals studied in this work, in particular on sloping terrain. Additionally, the individual input datasets may already contain inherent bias, as all DEM generation methods have their weaknesses. Examples for mountainous terrain are the elevation-dependent bias of stereo-photogrammetric data (in our Norway study site), or phase-unwrapping errors in InSAR DEMs. Specifically for glaciers, microwave signal penetration into dry ice/snow (observed in the SRTM

DEM for HMA's glaciers) and merging of elevation data with different time stamps (Norwegian national DEM) can cause metre-scale offsets. Correction of these systematic biases is hampered by the fact that we do not know the spatial extent of the areas that have a certain vertical offset.

In relation to ICESat-based studies, the biasing effect from locally varying vertical offsets comes from the fact that ICESat's sampling distribution is not the same each year. Partly, this is caused by data loss due to varying cloud coverage, but also because ICESat's repeat-tracks were offset by up to several kilometres in the mid-latitudes. All other elevation uncertainties studied in this work are negligible in comparison: ICESat's strength is its global consistency, and sensor-related elevation uncertainties are one magnitude smaller than the biases in the reference DEMs. Admittedly, errors for individual footprints can grow large in the case of complex within-footprint topography — but these errors turned out not to be systematic and average out when samples are grouped. Due to their smoother surfaces, elevation accuracy of ICESat is better on glaciers and snow-covered landscapes than on snow-free terrain.

Within this thesis, correction methods were developed that reduce the influence of locally varying DEM biases. These are a per-glacier correction (Publication I) and the local bias-correction of March/June snow depths using elevations measurements of the snow-free ground (Publication II). Both corrections essentially correspond to a vertical local co-registration between ICESat and DEM elevations. The improved methods greatly reduce the uncertainty in glacier elevation change rates and March/June snow depths. Uncertainty could be further decreased if we had spatially more consistent DEMs, or better knowledge of processing sub-units of the merged DEM products. Reprocessing of the ICESat data with e.g. the TanDEM-X DEM, once a free version of this data becomes available, could thus further improve our estimates — in particular for snow depths.

## 5.3 Perspectives

ICESat's potential in providing glacier volume changes is already well exploited. The data holds information for the short period of 2003–2009 only, and new satellites provide a wealth of data about more recent developments. Worldwide, most glaciers have been thinning rapidly since the end of the ICESat acquisition period — and with it changing the surface shape of the glaciers. Even a very accurate global DEM acquired now, nearly a decade after ICESat expired, might not substantially alter the estimates we already have, but could still re-

duce the uncertainty. In terms of spatial resolution, the limit is likely reached at least in HMA — smaller spatial units would no longer ensure representative sampling for individual campaigns. For a particular area, however, experts familiar with the local conditions may still achieve results of similar quality as we did for Norway, by securing good control over local biasing effects or by a more appropriate spatial grouping of samples.

In contrast, snow depth applications still have large potential. The average snow depths that ICESat can provide are better than available estimates for many remote areas, and they will not be as quickly outdated as glacier volume changes. In mountainous areas, the samples available for snow depth studies are one to two magnitudes greater than for mountain glacier applications. Even in areas where accurate DEMs are currently lacking, these may still be acquired on stable land surfaces. It can be expected that ICESat's performance for snow depths will be better than what we achieved in this work for regions with more accurate elevation data, for example in countries that have, or will have, national lidar DEMs. Also DEMs from TanDEM-X data or newer, high-resolution tristereo optical sensors are valuable candidates. At a smaller spatial scale, the use of waveform-fitting techniques in combination with a high-resolution DEM from e.g. SfM techniques or airborne/terrestrial lidar could even provide retrospective snow depth estimates for single footprints.

### 5.3.1 ICESat-2

Even greater potential to monitor the mountain cryosphere with a spaceborne lidar lies with the upcoming ICESat-2 mission. It will have distinct advantages compared to ICESat: greatly increased spatial resolution, smaller footprint, continuous sampling. In their introduction to the ICESat-2 mission, Markus et al. (2017) explicitly mention snow thickness measurements, permafrost monitoring and mass balance measurements of mountain glaciers as targeted application fields. Naturally, the question arises whether the new setup solves the challenges faced with ICESat as well for applications outside the polar regions, in particular for the mountain areas this work focuses on.

ICESat-2 will have better pointing accuracy to allow near-exact repeat tracks — but only within ca. 45 m, and only in the polar regions. At lower latitudes, strategic off-pointing will be done at least during the first two years. This includes the two study areas or other regions with an extensive mountain cryosphere, like Canada and Alaska (Escobar et al., 2015). Parts of these will lie in the transition zone between repeat-track and coverage mode. In these areas, a reference DEM will still be needed, both for snow depth and glacier studies. Even if repeat-track acquisitions will later be extended to lower latitudes, an

offset of 45 m in rough or sloped mountain terrain could still be too large to directly compare ICESat-2 elevations from repeat overpasses without a-priori knowledge of the surface.

On the other hand, off-nadir pointing would increase the spatial coverage for snow depth maps and increase the number of sampled glaciers. To measure a volume change signal of mountain glaciers, it will still be necessary to group samples in larger spatial units to accurately represent the regional glacier hypsometry and other relevant factors.

The pair-wise arrangement of ground tracks opens up new possibilities. While it is not sure that also the weak beam of the beam pairs will provide enough data for accurate surface measurements on snow-free mountain surfaces (Brown et al., 2016), this should be the case for snow-covered areas or glaciers. In addition, parallel tracks separated by 90 m would enable a more precise local co-registration to a reference DEM. Repeated acquisitions of profile pairs on snow-free terrain could allow the generation of an accurate local surface model even in the absence of a reference DEM. Profile pairs on snow might contain information on how snow depths vary on small scales, an important variable for permafrost studies or for accurate estimates of total snow volume with regard to hydrological discharge modelling.

The data acquired by ICESat-2 will be very different to what ICESat provided and it is difficult to accurately foresee its elevation accuracy on rough mountain surfaces. Better laser beam focusing will result in nominally smaller footprints, but the photon-counting approach requires along-track density filtering methods — on rough terrain, this still leaves a considerable elevation range as potential reflection locations for the recorded photons with subsequently high local elevation uncertainty. If ICESat-2 reaches centimetre-scale accuracies, the data could become interesting to monitor further aspects of the mountain cryosphere, namely permafrost processes and phenomena such as thermokarst, creep, or frost heave and thaw settlement.

Globally, the increased coverage of ICESat-2 will make this data invaluable as a consistent elevation reference. As with ICESat, other regional/global DEMs from multiple source datasets can use such a reference to remove sub-grid shifts of processing sub-units. ICESat-2 thus has a potential to improve the spatial accuracy of other elevation datasets.

Thus, it seems that for applications outside the polar areas, some of the challenges faced with ICESat data will continue with ICESat-2 — at least as long as the mission follows an off-nadir pointing strategy targeting forest and vegetation applications in the mid-latitudes. For the mountain cryosphere, this could both be an advantage due to the increased coverage, and a disadvantage due to a lack of direct repeat measurements. In that case, some of the insights presen-

ted in this work will be useful also for the data provided by ICESat-2. With the current surge of cubesats, flocks of small satellites that ensure high spatial and temporal coverage (Poghosyan and Golkar, 2017), quasi-life metadata from daily global imagery or atmospheric measurements is becoming available and may be combined with ICESat-2 data. Accurate knowledge of the surface and atmosphere conditions during ICESat-2 data acquisition opens up for exciting new possibilities.

# References


Abdalati, W., Zwally, H.J., Bindschadler, R., Csatho, B., Farrell, S.L., Fricker, H.A., Harding, D., Kwok, R., Lefsky, M., Markus, T., Marshak, A., Neumann, T., Palm, S., Schutz, B., Smith, B., Spinhirne, J., Webb, C., 2010. The ICESat-2 laser altimetry mission. Proceedings of the IEEE 98, 735–751. doi:10.1109/JPROC.2009.2034765.

Abshire, J.B., Sun, X., Riris, H., Sirota, J.M., McGarry, J.F., Palm, S., Yi, D., Liiva, P., 2005. Geoscience laser altimeter system (GLAS) on the ICESat mission: On-orbit measurement performance. Geophysical Research Letters 32. doi:10.1029/2005GL024028.

Altena, B., Kääb, A., 2017. Elevation change and improved velocity retrieval using orthorectified optical satellite data from different orbits. Remote Sensing 9. doi:10.3390/rs9030300.

Arendt, A.A., Echelmeyer, K.A., Harrison, W.D., Lingle, C.S., Valentine, V.B., 2002. Rapid wastage of Alaska glaciers and their contribution to rising sea level. Science 297, 382–386. doi:10.1126/science.1072497.

Armitage, T.W.K., Ridout, A.L., 2015. Arctic sea ice freeboard from AltiKa and comparison with CryoSat-2 and Operation IceBridge. Geophysical Research Letters 42, 6724–6731. doi:10.1002/2015GL064823.

Bao, W., Liu, S., Wei, J., Guo, W., 2015. Glacier changes during the past 40 years in the West Kunlun Shan. Journal of Mountain Science 12, 344–357. doi:10.1007/s11629-014-3220-0.

Barton, D.K., 1984. A half century of radar. IEEE Transactions on Microwave Theory and Techniques 32, 1161–1170. doi:10.1109/TMTT.1984.1132828.

Berthier, E., Arnaud, Y., Baratoux, D., Vincent, C., Rémy, F., 2004. Recent rapid thinning of the "Mer de Glace" glacier derived from satellite optical images. Geophysical Research Letters 31. doi:10.1029/2004GL020706.

Berthier, E., Arnaud, Y., Vincent, C., Rémy, F., 2006. Biases of SRTM in high-mountain areas: Implications for the monitoring of glacier volume changes. Geophysical Research Letters 33. doi:10.1029/2006GL025862.

Berthier, E., Cabot, V., Vincent, C., Six, D., 2016. Decadal region-wide and glacier-wide mass balances derived from multi-temporal ASTER satellite digital elevation models. Validation over the Mont-Blanc area. Frontiers in Earth Science 4, 63. doi:10.3389/feart.2016.00063.

Berthier, E., Schiefer, E., Clarke, G.K.C., Menounos, B., Rémy, F., 2010. Contribution of Alaskan glaciers to sea-level rise derived from satellite imagery. Nature Geoscience 3, 92–95. doi:10.1038/ngeo737.

Berthier, E., Toutin, T., 2008. SPOT5-HRS digital elevation models and the monitoring of glacier elevation changes in North-West Canada and South-East Alaska. Remote Sensing of Environment 112, 2443–2454. doi:10.1016/j.rse.2007.11.004.

Berthier, E., Vincent, C., Magnússon, E., Gunnlaugsson, A.T., Pitte, P., Le Meur, E., Masiokas, M., Ruiz, L., Pálsson, F., Belart, J.M.C., Wagnon, P., 2014. Glacier topography and elevation changes derived from Pléiades sub-meter stereo images. The Cryosphere 8, 2275–2291. doi:10.5194/tc-8-2275-2014.

Bhardwaj, A., Sam, L., Akanksha, Martín-Torres, F.J., Kumar, R., 2016a. UAVs as remote sensing platform in glaciology: Present applications and future prospects. Remote Sensing of Environment 175, 196–204. doi:10.1016/j.rse.2015.12.029.

Bhardwaj, A., Sam, L., Bhardwaj, A., Martín-Torres, F.J., 2016b. Lidar remote sensing of the cryosphere: Present applications and future prospects. Remote Sensing of Environment 177, 125–143. doi:10.1016/j.rse.2016.02.031.

Bolch, T., Kulkarni, A., Kääb, A., Huggel, C., Paul, F., Cogley, J.G., Frey, H., Kargel, J.S., Fujita, K., Scheel, M., Bajracharya, S., Stoffel, M., 2012. The State and Fate of Himalayan Glaciers. Science 336, 310–314. doi:10.1126/science.1215828.

Born, G.H., Dunne, J.A., Lame, D.B., 1979. Seasat mission overview. Science 204, 1405–1406. doi:10.1126/science.204.4400.1405.

Brandt, O., Hawley, R.L., Dunse, T., Kohler, J., Hagen, J.O., Morris, E., Scott, J.B.T., Eiken, T., 2008. Comparison of airborne radar altimeter and ground-based Ku-band radar measurements on the ice cap Austfonna, Svalbard, in: 2008 IEEE International Geoscience and Remote Sensing Symposium, pp. IV 177–180. doi:10.1109/IGARSS.2008.4779686.

Brenner, A., Bentley, C., Csatho, B., Harding, D., Hofton, M., Minster, J., Roberts, L., Saba, J., Schutz, R., Thomas, R., Yi, D., Zwally, H., 2011. Derivation of range and range distributions from laser pulse waveform analysis for surface elevations, roughness, slope, and vegetation heights. GLAS Algorithm Theoretical Basis Document, Version 5.0. NASA Goddard Space Flight Center.

Brenner, A.C., DiMarzio, J.P., Zwally, H.J., 2007. Precision and accuracy of satellite radar and laser altimeter data over the continental ice sheets. IEEE Transactions on Geoscience and Remote Sensing 45, 321–331. doi:10.1109/TGRS.2006.887172.

Brown, M.E., Arias, S.D., Neumann, T., Jasinski, M.F., Posey, P., Babonis, G., Glenn, N.F., Birkett, C.M., Escobar, V.M., Markus, T., 2016. Applications for ICESat-2 data: From NASA's early adopter program. IEEE Geoscience and Remote Sensing Magazine 4, 24–37. doi:10.1109/MGRS.2016.2560759.

Brunt, K., Farrell, S.L., Escobar, V.M., 2013. ICESat-2: A next generation laser altimeter for space-borne determination of surface elevation, in: Proceedings of the 93rd American Meteorological Society Annual Meeting, Austin, Texas, USA.

Brunt, K.M., Neumann, T.A., Amundson, J.M., Kavanaugh, J.L., Moussavi, M.S., Walsh, K.M., Cook, W.B., Markus, T., 2016. MABEL photon-counting laser altimetry data in Alaska for ICESat-2 simulations and development. The Cryosphere 10, 1707–1719. doi:10.5194/tc-10-1707-2016.

Bühler, Y., Adams, M.S., Bösch, R., Stoffel, A., 2016. Mapping snow depth in alpine terrain with unmanned aerial systems (UASs): potential and limitations. The Cryosphere 10, 1075–1088. doi:10.5194/tc-10-1075-2016.

Bühler, Y., Marty, M., Egli, L., Veitinger, J., Jonas, T., Thee, P., Ginzler, C., 2015. Snow depth mapping in high-alpine catchments using digital photogrammetry. The Cryosphere 9, 229–243. doi:10.5194/tc-9-229-2015.

Burrows, J.P., Platt, U., Borrell, P., 2011. Tropospheric remote sensing from space, in: The Remote Sensing of Tropospheric Composition from Space. Springer. doi:10.1007/978-3-642-14791-3.

Capaldo, P., Nascetti, A., Porfiri, M., Pieralice, F., Fratarcangeli, F., Crespi, M., Toutin, T., 2015. Evaluation and comparison of different radargrammetric approaches for Digital Surface Models generation from COSMO-SkyMed, TerraSAR-X, RADARSAT-2 imagery: Analysis of Beauport (Canada) test site. ISPRS Journal of Photogrammetry and Remote Sensing 100, 60–70. doi:10.1016/j.isprsjprs.2014.05.007.

Cogley, J.G., 2012. Climate science: Himalayan glaciers in the balance. Nature 488, 468–469. doi:10.1038/488468a.

Collier, P., 2002. The impact on topographic mapping of developments in land and air survey: 1900–1939. Cartography and Geographic Information Science 29, 155–174. doi:10.1559/152304002782008440.

Collins, J., Riegler, G., Schrader, H., Tinz, M., 2015. Applying terrain and hydrological editing to tandem-x data to create a consumer-ready worlddem product. International Archives of Photogrammetry, Remote Sensing and Spatial Information Sciences 40, 1149–1154. doi:10.5194/isprsarchives-XL-7-W3-1149-2015.

Colvocoresses, A., 1982. An automated mapping satellite system (Mapsat). Photogrammetric Engineering and Remote Sensing 48, 1585–1591.

Dall, J., Madsen, S.N., Keller, K., Forsberg, R., 2001. Topography and penetration of the Greenland Ice Sheet measured with Airborne SAR Interferometry. Geophysical Research Letters 28, 1703–1706. doi:10.1029/2000GL011787.

Deems, J.S., Painter, T.H., Finnegan, D.C., 2013. Lidar measurement of snow depth: a review. Journal of Glaciology 59, 467–479. doi:10.3189/2013JoG12J154.

Degnan, J.J., 2002. Photon-counting multikilohertz microlaser altimeters for airborne and spaceborne topographic measurements. Journal of Geodynamics 34, 503–549. doi:10.1016/S0264-3707(02)00045-5.

Dehecq, A., Gourmelen, N., Shepherd, A., Cullen, R., Trouvé, E., 2013. Evaluation of CryoSat-2 for height retrieval over the Himalayan range, in: Proceedings of the CryoSat-2 third user workshop, Dresden, Germany, 12–14 March 2013.

Dehecq, A., Millan, R., Berthier, E., Gourmelen, N., Trouvé, E., Vionnet, V., 2016. Elevation changes inferred from TanDEM-X data over the Mont-Blanc area: Impact of the X-band interferometric bias. IEEE Journal of Selected Topics in Applied Earth Observations and Remote Sensing 9, 3870–3882. doi:10.1109/JSTARS.2016.2581482.

Dietz, A.J., Kuenzer, C., Gessner, U., Dech, S., 2012. Remote sensing of snow — a review of available methods. International Journal of Remote Sensing 33, 4094–4134. doi:10.1080/01431161.2011.640964.

Dozier, J., Bair, E.H., Davis, R.E., 2016. Estimating the spatial distribution of snow water equivalent in the world's mountains. Wiley Interdisciplinary Reviews: Water 3, 461–474. doi:10.1002/wat2.1140.

Escobar, V., Arias, S.D., Woo, L., Neumann, T., Jasinski, M., Brown, M., Turner, W., 2015. Ice, Cloud and land Elevation Satellite-2 2nd Applications Workshop. Technical Report. NASA Goddard Space Flight Center. URL: https://icesat.gsfc.nasa.gov/icesat2/applications/ICESat2_2ndApplicationsWorkshop_Report_Final_05August2015.pdf.

Farinotti, D., Longuevergne, L., Moholdt, G., Duethmann, D., Mölg, T., Bolch, T., Vorogushyn, S., Güntner, A., 2015. Substantial glacier mass loss in the Tien Shan over the past 50 years. Nature Geoscience 8, 716–722. doi:10.1038/ngeo2513.

Farr, T.G., Kobrick, M., 2000. Shuttle radar topography mission produces a wealth of data. Eos, Transactions American Geophysical Union 81, 583–585. doi:10.1029/E0081i048p00583.

Farr, T.G., Rosen, P.A., Caro, E., Crippen, R., Duren, R., Hensley, S., Kobrick, M., Paller, M., Rodriguez, E., Roth, L., Seal, D., Shaffer, S., Shimada, J., Umland, J., Werner, M., Oskin, M., Burbank, D., Alsdorf, D., 2007. The Shuttle Radar Topography Mission. Reviews of Geophysics 45. doi:10.1029/2005RG000183.

Ferretti, A., Monti-Guarnieri, A., Prati, C., Rocca, F., Massonet, D., 2007. InSAR principles-guidelines for SAR interferometry processing and interpretation (TM-19, February 2007). European Space Agency, ESTEC, Nordwijk, The Netherlands.

Fischer, L., Huggel, C., Kääb, A., Haeberli, W., 2013. Slope failures and erosion rates on a glacierized high-mountain face under climatic changes. Earth Surface Processes and Landforms 38, 836–846. doi:10.1002/esp.3355.

Fischer, L., Kääb, A., Huggel, C., Noetzli, J., 2006. Geology, glacier retreat and permafrost degradation as controlling factors of slope instabilities in a high-mountain rock wall: the Monte Rosa east face. Natural Hazards and Earth System Science 6, 761–772. doi:10.5194/nhess-6-761-2006.

Fischer, M., Huss, M., Hoelzle, M., 2015. Surface elevation and mass changes of all Swiss glaciers 1980–2010. The Cryosphere 9, 525–540. doi:10.5194/tc-9-525-2015.

Fleig, A.K., Andreassen, L.M., Barfod, E., Haga, J., Haugen, L.E., Hisdal, H., Melvold, K., Saloranta, T., 2013. Norwegian Hydrological Reference Dataset for Climate Change Studies. NVE report 2–2013. Norwegian Water Resources and Energy Directorate, Oslo, Norway.

Foresta, L., Gourmelen, N., Pálsson, F., Nienow, P., Björnsson, H., Shepherd, A., 2016. Surface elevation change and mass balance of Icelandic ice caps derived from swath mode CryoSat-2 altimetry. Geophysical Research Letters 43, 12,138–12,145. doi:10.1002/2016GL071485.

Frey, H., Paul, F., 2012. On the suitability of the SRTM DEM and ASTER GDEM for the compilation of topographic parameters in glacier inventories. International Journal of Applied Earth Observation and Geoinformation 18, 480–490. doi:10.1016/j.jag.2011.09.020.

Fricker, H.A., Borsa, A., Minster, B., Carabajal, C., Quinn, K., Bills, B., 2005. Assessment of ICESat performance at the salar de Uyuni, Bolivia. Geophysical Research Letters 32. doi:10.1029/2005GL023423.

Fricker, H.A., Padman, L., 2006. Ice shelf grounding zone structure from ICESat laser altimetry. Geophysical Research Letters 33. doi:10.1029/2006GL026907.

Fricker, H.A., Scambos, T., Bindschadler, R., Padman, L., 2007. An active subglacial water system in West Antarctica mapped from space. Science 315, 1544–1548. doi:10.1126/science.1136897.

Fu, L.L., Holt, B., 1982. Seasat views oceans and sea ice with synthetic-aperture radar. JPL publication 81–120. California Institute of Technology, Jet Propulsion Laboratory, Pasadena, California.

Gardelle, J., Berthier, E., Arnaud, Y., 2012a. Impact of resolution and radar penetration on glacier elevation changes computed from DEM differencing. Journal of Glaciology 58, 419–422. doi:10.3189/2012JoG11J175.

Gardelle, J., Berthier, E., Arnaud, Y., 2012b. Slight mass gain of Karakoram glaciers in the early twenty-first century. Nature Geoscience 5, 322–325. doi:10.1038/ngeo1450.

Gardelle, J., Berthier, E., Arnaud, Y., Kääb, A., 2013. Region-wide glacier mass balances over the Pamir-Karakoram-Himalaya during 1999–2011. The Cryosphere 7, 1263–1286. doi:10.5194/tc-7-1263-2013.

Gardner, A.S., Moholdt, G., Cogley, J.G., Wouters, B., Arendt, A.A., Wahr, J., Berthier, E., Hock, R., Pfeffer, W.T., Kaser, G., Ligtenberg, S.R.M., Bolch, T., Sharp, M.J., Hagen, J.O., van den Broeke, M.R., Paul, F., 2013. A reconciled estimate of glacier contributions to sea level rise: 2003 to 2009. Science 340, 852–857. doi:10.1126/science.1234532.

Gay, M., Ferro-Famil, L., 2016. Penetration depth of Synthetic Aperture Radar signals in ice and snow: an analytical approach, in: 4th Workshop on Remote Sensing and Modeling of Surface Properties, Grenoble, France.

Gesch, D., Oimoen, M., Danielson, J., Meyer, D., 2016. Validation of the ASTER global digital elevation model version 3 over the conterminous United States. International Archives of the Photogrammetry, Remote Sensing and Spatial Information Sciences XLI-B4, 143–148. doi:10.5194/isprs-archives-XLI-B4-143-2016.

Girod, L., Nuth, C., Kääb, A., 2016. Glacier volume change estimation using time series of improved ASTER DEMs. International Archives of the Photogrammetry, Remote Sensing and Spatial Information Sciences XLI-B8, 489–494. doi:10.5194/isprs-archives-XLI-B8-489-2016.

Girod, L., Nuth, C., Kääb, A., Etzelmüller, B., Kohler, J., 2017. Terrain changes from images acquired on opportunistic flights by SfM photogrammetry. The Cryosphere 11, 827–840. doi:10.5194/tc-11-827-2017.

Gleyzes, M.A., Perret, L., Kubik, P., 2012. Pléiades system architecture and main performances. International Archives of the Photogrammetry, Remote Sensing and Spatial Information Sciences XXXIX-B1, 537–542. doi:10.5194/isprsarchives-XXXIX-B1-537-2012.

Graham, L.C., 1974. Synthetic interferometer radar for topographic mapping. Proceedings of the IEEE 62, 763–768. doi:10.1109/PROC.1974.9516.

Gray, L., Burgess, D., Copland, L., Cullen, R., Galin, N., Hawley, R., Helm, V., 2013. Interferometric swath processing of Cryosat data for glacial ice topography. The Cryosphere 7, 1857–1867. doi:10.5194/tc-7-1857-2013.

Gurung, D.R., Maharjan, S.B., Shrestha, A.B., Shrestha, M.S., Bajracharya, S.R., Murthy, M.S.R., 2017. Climate and topographic controls on snow cover dynamics in the Hindu Kush Himalaya. International Journal of Climatology doi:10.1002/joc.4961.

Gwenzi, D., Lefsky, M.A., 2014. Prospects of photon counting lidar for savanna ecosystem structural studies. International Archives of the Photogrammetry, Remote Sensing and Spatial Information Sciences XL-1, 141–147. doi:10.5194/isprsarchives-XL-1-141-2014.

Harding, D.J., Carabajal, C.C., 2005. ICESat waveform measurements of within-footprint topographic relief and vegetation vertical structure. Geophysical Research Letters 32. doi:10.1029/2005GL023471.

Harding, D.J., Dabney, P., Yu, A.W., Valett, S.R., Timmons, E., 2015. SIMPL Measurements of Laser Light Penetration into Snow, Ice and Water: the 2015 Greenland Airborne Campaign in Support of ICESat-2. AGU Fall Meeting Abstracts 2015 .

Harris, C., Arenson, L.U., Christiansen, H.H., Etzelmüller, B., Frauenfelder, R., Gruber, S., Haeberli, W., Hauck, C., Hölzle, M., Humlum, O., Isaksen, K., Kääb, A., Kern-Lütschg, M.A., Lehning, M., Matsuoka, N., Murton, J.B., Nötzli, J., Phillips, M., Ross, N., Seppälä, M., Springman, S.M., Mühll, D.V., 2009. Permafrost and climate in Europe: Monitoring and modelling thermal, geomorphological and geotechnical responses. Earth-Science Reviews 92, 117–171. doi:10.1016/j.earscirev.2008.12.002.

Hirano, A., Welch, R., Lang, H., 2003. Mapping from ASTER stereo image data: DEM validation and accuracy assessment. ISPRS Journal of Photogrammetry and Remote Sensing 57, 356–370. doi:10.1016/S0924-2716(02)00164-8.

Horan, K.H., Kerekes, J.P., 2013. An automated statistical analysis approach to noise reduction for photon-counting lidar systems, in: 2013 IEEE International Geoscience and Remote Sensing Symposium, pp. 4336–4339. doi:10.1109/IGARSS.2013.6723794.

Howat, I.M., Smith, B.E., Joughin, I., Scambos, T.A., 2008. Rates of southeast Greenland ice volume loss from combined ICESat and ASTER observations. Geophysical Research Letters 35. doi:10.1029/2008GL034496.

Huang, T., Jia, L., Lu, J., Zhou, J., 2016. An improved method of using icesat altimetry data to extract Tibetan Plateau glacier thickness change rate, in: 2016 IEEE International Geoscience and Remote Sensing Symposium, pp. 7109–7112. doi:10.1109/IGARSS.2016.7730855.

Huss, M., 2013. Density assumptions for converting geodetic glacier volume change to mass change. The Cryosphere 7, 877–887. doi:10.5194/tc-7-877-2013.

Jaber, W.A., Floricioiu, D., Rott, H., 2016. Geodetic mass balance of the Patagonian icefields derived from SRTM and TanDEM-X data, in: 2016 IEEE International Geoscience and Remote Sensing Symposium, pp. 342–345. doi:10.1109/IGARSS.2016.7729082.

Jaber, W.A., Floricioiu, D., Rott, H., Eineder, M., 2013. Surface elevation changes of glaciers derived from SRTM and TanDEM-X DEM differences, in: 2013 IEEE International Geoscience and Remote Sensing Symposium, pp. 1893–1896. doi:10.1109/IGARSS.2013.6723173.

Jacob, T., Wahr, J., Pfeffer, W.T., Swenson, S., 2012. Recent contributions of glaciers and ice caps to sea level rise. Nature 482, 514–518. doi:10.1038/nature10847.

Jansson, P., Hock, R., Schneider, T., 2003. The concept of glacier storage: a review. Journal of Hydrology 282, 116–129. doi:10.1016/s0022-1694(03)00258-0.

Jasinski, M.F., Stoll, J.D., Cook, W.B., Ondrusek, M., Stengel, E., Brunt, K., 2016. Inland and near-shore water profiles derived from the high-altitude multiple altimeter beam experimental lidar (MABEL). Journal of Coastal Research 76, 44–55. doi:10.2112/SI76-005.

Jester, P.L., 2012. The ICESat/GLAS Instrument Operations Report. ICESat (GLAS) Science Processing Software Document Series NASA/TM–2012-208641 / Vol. 4. NASA Goddard Space Flight Center. Greenbelt, Maryland.

Kääb, A., 2002. Monitoring high-mountain terrain deformation from repeated air- and spaceborne optical data: examples using digital aerial imagery and ASTER data. ISPRS Journal of Photogrammetry and Remote Sensing 57, 39–52. doi:10.1016/S0924-2716(02)00114-4.

Kääb, A., 2005. Combination of SRTM3 and repeat ASTER data for deriving alpine glacier flow velocities in the Bhutan Himalaya. Remote Sensing of Environment 94, 463–474. doi:10.1016/j.rse.2004.11.003.

Kääb, A., 2005. Remote sensing of mountain glaciers and permafrost creep. Schriftenreihe Physische Geographie, Volume 48. ISBN 3 85543 244 9.

Kääb, A., 2008. Glacier volume changes using ASTER satellite stereo and ICESat GLAS laser altimetry. A test study on Edgeøya, eastern Svalbard. IEEE Transactions on Geoscience and Remote Sensing 46, 2823–2830. doi:10.1109/TGRS.2008.2000627.

Kääb, A., Berthier, E., Nuth, C., Gardelle, J., Arnaud, Y., 2012. Contrasting patterns of early twenty-first-century glacier mass change in the Himalayas. Nature 488, 495–498. doi:10.1038/nature11324.

Kääb, A., Treichler, D., Nuth, C., Berthier, E., 2015. Brief Communication: Contending estimates of 2003-2008 glacier mass balance over the Pamir-Karakoram-Himalaya. The Cryosphere 9, 557–564. doi:10.5194/tc-9-557-2015.

Kartverket, 2016. Terrengmodeller — land. Data description. The Norwegian Mapping Authority, Norway. Online, accessed 6 June 2016. URL: http://www.kartverket.no/data/kartdata/terrengmodeller/Terrengmodell-10-meters-grid/.

Kartverket, 2017. Nasjonal detaljert høydemodell. Data description. The Norwegian Mapping Authority, Norway. Online, accessed 22 March 2017. URL: http://www.kartverket.no/hoydemodell.

Kaser, G., Grosshauser, M., Marzeion, B., 2010. Contribution potential of glaciers to water availability in different climate regimes. Proceedings of the National academy of Sciences of the United States of America 107, 20223–20227. doi:10.1073/pnas.1008162107.

Ke, L., Ding, X., Song, C., 2015a. Estimation of mass balance of Dongkemadi glaciers with multiple methods based on multi-mission satellite data. Quaternary International 371, 58–66. doi:10.1016/j.quaint.2015.02.043.

Ke, L., Ding, X., Song, C., 2015b. Heterogeneous changes of glaciers over the western Kunlun Mountains based on ICESat and Landsat-8 derived glacier inventory. Remote Sensing of Environment 168, 13–23. doi:10.1016/j.rse.2015.06.019.

Korona, J., Berthier, E., Bernard, M., Rémy, F., Thouvenot, E., 2009. SPIRIT. SPOT 5 stereoscopic survey of polar ice: Reference images and topographies during the fourth International Polar Year (2007–2009). ISPRS Journal of Photogrammetry and Remote Sensing 64, 204–212. doi:10.1016/j.isprsjprs.2008.10.005.

Krieger, G., Moreira, A., Fiedler, H., Hajnsek, I., Werner, M., Younis, M., Zink, M., 2007. TanDEM-X: A satellite formation for high-resolution SAR interferometry. IEEE Transactions on Geoscience and Remote Sensing 45, 3317–3341. doi:10.1109/TGRS.2007.900693.

Kropáček, J., Neckel, N., Bauder, A., 2014. Estimation of Mass Balance of the Grosser Aletschgletscher, Swiss Alps, from ICESat Laser Altimetry Data and Digital Elevation Models. Remote Sensing 6, 5614. doi:10.3390/rs6065614.

Kwok, R., Cunningham, G., Hoffmann, J., Markus, T., 2016. Testing the ice-water discrimination and freeboard retrieval algorithms for the ICESat-2 mission. Remote Sensing of Environment 183, 13–25. doi:10.1016/j.rse.2016.05.011.

Kwok, R., Rothrock, D.A., 2009. Decline in Arctic sea ice thickness from submarine and ICESat records: 1958–2008. Geophysical Research Letters 36. doi:10.1029/2009GL039035.

Lange, K.L., Little, R.J.A., Taylor, J.M.G., 1989. Robust statistical modeling using the t distribution. Journal of the American Statistical Association 84, 881–896. doi:10.2307/2290063.

Larsen, C.F., Motyka, R.J., Arendt, A.A., Echelmeyer, K.A., Geissler, P.E., 2007. Glacier changes in southeast Alaska and northwest British Columbia and contribution to sea level rise. Journal of Geophysical Research: Earth Surface 112. doi:10.1029/2006JF000586.

Leberl, F., 1976. Imaging radar applications to mapping and charting. Photogrammetria 32, 75–100. doi:10.1016/0031-8663(76)90015-6.

Lefsky, M.A., 2010. A global forest canopy height map from the moderate resolution imaging spectroradiometer and the geoscience laser altimeter system. Geophysical Research Letters 37. doi:10.1029/2010GL043622.

Lentz, H., Braun, H.M., Younis, M., Fischer, C., Wiesbeck, W., Mavrocordatos, C., 2002. Concept and realization of an Airborne SAR/Interferometric Radar Altimeter System (ASIRAS), in: 2002 IEEE International Geoscience and Remote Sensing Symposium, pp. 3099–3101, vol. 6. doi:10.1109/IGARSS.2002.1027097.

Lettenmaier, D.P., Alsdorf, D., Dozier, J., Huffman, G.J., Pan, M., Wood, E.F., 2015. Inroads of remote sensing into hydrologic science during the WRR era. Water Resources Research 51, 7309–7342. doi:10.1002/2015WR017616.

Levinsen, J.F., Simonsen, S.B., Sørensen, L.S., Forsberg, R., 2016. The impact of DEM resolution on relocating radar altimetry data over ice sheets. IEEE Journal of Selected Topics in Applied Earth Observations and Remote Sensing 9, 3158–3163. doi:10.1109/JSTARS.2016.2587684.

Li, Z., Fang, H., Tian, L., Dai, Y., Zong, J., 2015. Changes in the glacier extent and surface elevation in Xiongcaigangri region, Southern Karakoram Mountains, China. Quaternary International 371, 67–75. doi:10.1016/j.quaint.2014.12.004.

Li, Z., Tian, L., Wu, H., Wang, W., Zhang, S., Zhang, J., Li, X., 2016. Changes in glacier extent and surface elevations in the Depuchangdake region of northwestern Tibet, China. Quaternary Research 85, 25–33. doi:10.1016/j.yqres.2015.12.005.

Liston, G.E., 2004. Representing subgrid snow cover heterogeneities in regional and global models. Journal of Climate 17, 1381–1397. doi:10.1175/1520-0442(2004)017<1381:RSSCHI>2.0.CO;2.

Luojus, K., Pulliainen, J., Takala, M., Derksen, C., Rott, H., Nagler, T., Solberg, R., Wiesmann, A., Metsamaki, S., Malnes, E., Bojkov, B., 2010. Investigating the feasibility of the Globsnow snow water equivalent data for climate research purposes, in: 2010 IEEE International Geoscience and Remote Sensing Symposium. doi:10.1109/IGARSS.2010.5741987.

Markus, T., Neumann, T., Martino, A., Abdalati, W., Brunt, K., Csatho, B., Farrell, S., Fricker, H., Gardner, A., Harding, D., Jasinski, M., Kwok, R., Magruder, L., Lubin, D., Luthcke, S., Morison, J., Nelson, R., Neuenschwander, A., Palm, S., Popescu, S., Shum, C., Schutz, B.E., Smith, B., Yang, Y., Zwally, J., 2017. The Ice, Cloud, and land Elevation Satellite-2 (ICESat-2): Science requirements, concept, and implementation. Remote Sensing of Environment 190, 260–273. doi:10.1016/j.rse.2016.12.029.

Marti, R., Gascoin, S., Berthier, E., de Pinel, M., Houet, T., Laffly, D., 2016. Mapping snow depth in open alpine terrain from stereo satellite imagery. The Cryosphere 10, 1361–1380. doi:10.5194/tc-10-1361-2016.

Marzeion, B., Leclercq, P.W., Cogley, J.G., Jarosch, A.H., 2015. Brief communication: Global reconstructions of glacier mass change during the 20th century are consistent. The Cryosphere 9, 2399–2404. doi:10.5194/tc-9-2399-2015.

Matsuo, K., Heki, K., 2010. Time-variable ice loss in Asian high mountains from satellite gravimetry. Earth and Planetary Science Letters 290, 30–36. doi:10.1016/j.epsl.2009.11.053.

Meier, M.F., Dyurgerov, M.B., Rick, U.K., O'Neel, S., Pfeffer, W.T., Anderson, R.S., Anderson, S.P., Glazovsky, A.F., 2007. Glaciers dominate eustatic sea-level rise in the 21st century. Science 317, 1064–1067. doi:10.1126/science.1143906.

Melvold, K., Skaugen, T., 2013. Multiscale spatial variability of lidar-derived and modeled snow depth on Hardangervidda, Norway. Annals of Glaciology 54, 273–281. doi:10.3189/2013AoG62A161.

Moholdt, G., Hagen, J.O., Eiken, T., Schuler, T.V., 2010a. Geometric changes and mass balance of the Austfonna ice cap, Svalbard. The Cryosphere 4, 21–34. doi:10.5194/tc-4-21-2010.

Moholdt, G., Nuth, C., Hagen, J.O., Kohler, J., 2010b. Recent elevation changes of Svalbard glaciers derived from ICESat laser altimetry. Remote Sensing of Environment 114, 2756–2767. doi:10.1016/j.rse.2010.06.008.

Molijn, R.A., Lindenbergh, R.C., Gunter, B.C., 2011. ICESat laser full waveform analysis for the classification of land cover types over the cryosphere. International Journal of Remote Sensing 32, 8799–8822. doi:10.1080/01431161.2010.547532.

Müller, K., 2011. Microwave penetration in polar snow and ice: Implications for GPR and SAR. Dissertation submitted to the Faculty of Mathematics and Natural Sciences, No. 1090. Department of Geosciences, University of Oslo, Norway. ISSN 1501-7710.

Neckel, N., Kropáček, J., Bolch, T., Hochschild, V., 2014. Glacier mass changes on the Tibetan Plateau 2003–2009 derived from ICESat laser altimetry measurements. Environmental Research Letters 9. doi:10.1088/1748-9326/9/1/014009.

NSIDC, 2012. GLAS Altimetry HDF5 Product Usage Guide. Technical Report. National Snow and Ice Data Center. URL: http://nsidc.org/data/docs/daac/glas_altimetry/pdf/NSIDC_AltUserGuide_Rel33-hdf5.pdf.

NSIDC, 2016. Attributes for ICESat Laser Operations Periods: Latest Release. Data description. National Snow and Ice Data Center. University of Colorado, Boulder, Colorado, USA. Online, accessed 30 October 2016. URL: ftp://sidads.colorado.edu/pub/DATASETS/nsidc0587_ICESAT_GLAS_LTA/Section3_Product_Documentation/glas_laser_ops_attrib.pdf.

Nuth, C., 2011. Quantification and interpretation of glacier elevation changes. Dissertation submitted to the Faculty of Mathematics and Natural Sciences, No. 1062. Department of Geosciences, University of Oslo, Norway. ISSN 1501-7710.

Nuth, C., Kääb, A., 2011. Co-registration and bias corrections of satellite elevation data sets for quantifying glacier thickness change. The Cryosphere 5, 271–290. doi:10.5194/tc-5-271-2011.

NVE, 2016. Climate indicator products. Online glacier database. Norwegian Water Resources and Energy Directorate. Online, accessed 31 May 2016. URL: http://glacier.nve.no/viewer/CI/.

Palm, S.P., Yang, Y., Spinhirne, J.D., Marshak, A., 2011. Satellite remote sensing of blowing snow properties over Antarctica. Journal of Geophysical Research: Atmospheres 116. doi:10.1029/2011JD015828.

Papasodoro, C., Royer, A., Langlois, A., Berthier, E., 2016. Potential of RADARSAT-2 stereo radargrammetry for the generation of glacier DEMs. Journal of Glaciology 62, 486–496.

Paul, F., Haeberli, W., 2008. Spatial variability of glacier elevation changes in the Swiss Alps obtained from two digital elevation models. Geophysical Research Letters 35. doi:10.1029/2008GL034718.

Phan, H.V., Lindenbergh, R., Menenti, M., 2017. Assessing orographic variability in glacial thickness changes at the Tibetan Plateau using ICESat laser altimetry. Remote Sensing 9. doi:10.3390/rs9020160.

Poghosyan, A., Golkar, A., 2017. Cubesat evolution: Analyzing cubesat capabilities for conducting science missions. Progress in Aerospace Sciences 88, 59–83. doi:10.1016/j.paerosci.2016.11.002.

Pritchard, H.D., Arthern, R.J., Vaughan, D.G., Edwards, L.A., 2009. Extensive dynamic thinning on the margins of the Greenland and Antarctic ice sheets. Nature 461, 971–975. doi:10.1038/nature08471.

Pritchard, H.D., Ligtenberg, S.R.M., Fricker, H.A., Vaughan, D.G., van den Broeke, M.R., Padman, L., 2012. Antarctic ice-sheet loss driven by basal melting of ice shelves. Nature 484, 502–505. doi:10.1038/nature10968.

Rabus, B., Eineder, M., Roth, A., Bamler, R., 2003. The shuttle radar topography mission — a new class of digital elevation models acquired by spaceborne radar. ISPRS Journal of Photogrammetry and Remote Sensing 57, 241–262. doi:10.1016/S0924-2716(02)00124-7.

Rankl, M., Braun, M., 2016. Glacier elevation and mass changes over the central Karakoram region estimated from TanDEM-X and SRTM/X-SAR digital elevation models. Annals of Glaciology 57, 273–281. doi:10.3189/2016AoG71A024.

Reitebuch, O., Lemmerz, C., Nagel, E., Paffrath, U., Durand, Y., Endemann, M., Fabre, F., Chaloupy, M., 2009. The airborne demonstrator for the direct-detection doppler wind lidar ALADIN on ADM-Aeolus. PartI: Instrument design and comparison to satellite instrument. Journal of Atmospheric and Oceanic Technology 26, 2501–2515. doi:10.1175/2009JTECHA1309.1.

Richardson, S.D., Reynolds, J.M., 2000. An overview of glacial hazards in the Himalayas. Quaternary International 65–66, 31–47. doi:10.1016/S1040-6182(99)00035-X.

Riegler, G., Hennig, S., Weber, M., 2015. WorldDEM — a novel global foundation layer. International Archives of Photogrammetry, Remote Sensing and Spatial Information Sciences 40, 183.

Rignot, E., Echelmeyer, K., Krabill, W., 2001. Penetration depth of interferometric synthetic-aperture radar signals in snow and ice. Geophysical Research Letters 28, 3501–3504. doi:10.1029/2000GL012484.

Rodriguez, E., Morris, C.S., Belz, J.E., 2006. A global assessment of the SRTM performance. Photogrammetric Engineering & Remote Sensing 72, 249–260. doi:10.14358/PERS.72.3.249.

Rott, H., 2009. Advances in interferometric synthetic aperture radar (InSAR) in earth system science. Progress in Physical Geography 33, 769–791. doi:10.1177/0309133309350263.

Rott, H., Mätzler, C., 1987. Possibilities and limits of synthetic aperture radar for snow and glacier surveying. Annals of Glaciology 9, 195–199. doi:10.3198/1987AoG9-1-195-199.

Rott, H., Sturm, K., Miller, H., 1993. Active and passive microwave signatures of Antarctic firn by means of field measurements and satellite data. Annals of Glaciology 17, 337–343. doi:10.3198/1993AoG17-1-337-343.

Scambos, T.A., Bohlander, J.A., Shuman, C.A., Skvarca, P., 2004. Glacier acceleration and thinning after ice shelf collapse in the Larsen B embayment, Antarctica. Geophysical Research Letters 31. doi:10.1029/2004GL020670.

Schenk, T., Csatho, B., 2012. A new methodology for detecting ice sheet surface elevation changes from laser altimetry data. IEEE Transactions on Geoscience and Remote Sensing 50, 3302–3316. doi:10.1109/TGRS.2011.2182357.

Schiefer, E., Menounos, B., Wheate, R., 2007. Recent volume loss of British Columbian glaciers, Canada. Geophysical Research Letters 34. doi:10.1029/2007GL030780.

Schutz, B.E., Zwally, H.J., Shuman, C.A., Hancock, D., DiMarzio, J.P., 2005. Overview of the ICESat Mission. Geophysical Research Letters 32. doi:10.1029/2005GL024009.

Sen, P.K., 1968. Estimates of the regression coefficient based on Kendall's tau. Journal of the American Statistical Association 63, 1379–1389. doi:10.2307/2285891.

Shangguan, D.H., Bolch, T., Ding, Y.J., Kröhnert, M., Pieczonka, T., Wetzel, H.U., Liu, S.Y., 2015. Mass changes of Southern and Northern Inylchek Glacier, Central Tian Shan, Kyrgyzstan, during 1975 and 2007 derived from remote sensing data. The Cryosphere 9, 703–717. doi:10.5194/tc-9-703-2015.

Shimada, M., Tadono, T., Rosenqvist, A., 2010. Advanced land observing satellite (ALOS) and monitoring global environmental change. Proceedings of the IEEE 98, 780–799. doi:10.1109/JPROC.2009.2033724.

Slobbe, D., Lindenbergh, R., Ditmar, P., 2008. Estimation of volume change rates of Greenland's ice sheet from ICESat data using overlapping footprints. Remote Sensing of Environment 112, 4204 –4213. doi:10.1016/j.rse.2008.07.004.

Spinhirne, J.D., Palm, S.P., Hart, W.D., Hlavka, D.L., Welton, E.J., 2005. Cloud and aerosol measurements from GLAS: Overview and initial results. Geophysical Research Letters 32. doi:10.1029/2005GL023507.

Surazakov, A.B., Aizen, V.B., 2006. Estimating volume change of mountain glaciers using SRTM and map-based topographic data. IEEE Transactions on Geoscience and Remote Sensing 44, 2991–2995. doi:10.1109/TGRS.2006.875357.

Swatantran, A., Tang, H., Barrett, T., DeCola, P., Dubayah, R., 2016. Rapid, high-resolution forest structure and terrain mapping over large areas using single photon lidar. Scientific Reports 6. doi:10.1038/srep28277.

Tachikawa, T., Hato, M., Kaku, M., Iwasaki, A., 2011a. Characteristics of ASTER GDEM version 2, in: 2011 IEEE International Geoscience and Remote Sensing Symposium, pp. 3657–3660. doi:10.1109/IGARSS.2011.6050017.

Tachikawa, T., Kaku, M., Iwasaki, A., Gesch, D.B., Oimoen, M.J., Zhang, Z., Danielson, J.J., Krieger, T., Curtis, B., Haase, J., Abrams, M., Carabajal, C., 2011b. ASTER Global Digital Elevation Model Version 2 — summary of validation results. Technical Report. URL: http://pubs.er.usgs.gov/publication/70005960.

Tadono, T., Nagai, H., Ishida, H., Oda, F., Naito, S., Minakawa, K., Iwamoto, H., 2016. Generation of the 30 m-mesh global digital surface model by ALOS PRISM. International Archives of the Photogrammetry, Remote Sensing and Spatial Information Sciences XLI-B4, 157–162. doi:10.5194/isprs-archives-XLI-B4-157-2016.

Takaku, J., Tadono, T., Tsutsui, K., 2014. Generation of high resolution global DSM from ALOS PRISM. International Archives of Photogrammetry, Remote Sensing and Spatial Information Sciences 40, 243–248. doi:10.5194/isprsarchives-XL-4-243-2014.

Theil, H., 1950. A rank-invariant method of linear and polynomial regression analysis. Parts I, II, III. Proceedings of the Koninklijke Nederlandse Akademie van Wetenschappen 53, 386–392, 521–525, 1397–1412.

Toth, C., Jóźków, G., 2016. Remote sensing platforms and sensors: A survey. ISPRS Journal of Photogrammetry and Remote Sensing 115, 22–36. doi:10.1016/j.isprsjprs.2015.10.004.

Toutin, T., 2001. Elevation modelling from satellite visible and infrared (VIR) data. International Journal of Remote Sensing 22, 1097–1125. doi:10.1080/01431160117862.

Toutin, T., 2002. Impact of terrain slope and aspect on radargrammetric DEM accuracy. ISPRS Journal of Photogrammetry and Remote Sensing 57, 228–240. doi:10.1016/S0924-2716(02)00123-5.

Toutin, T., 2004. Review article: Geometric processing of remote sensing images: models, algorithms and methods. International Journal of Remote Sensing 25, 1893–1924. doi:10.1080/0143116031000101611.

Toutin, T., 2006. Generation of DSMs from SPOT-5 in-track HRS and across-track HRG stereo data using spatiotriangulation and autocalibration. ISPRS Journal of Photogrammetry and Remote Sensing 60, 170–181. doi:10.1016/j.isprsjprs.2006.02.003.

Toutin, T., 2008. ASTER DEMs for geomatic and geoscientific applications: a review. International Journal of Remote Sensing 29, 1855–1875. doi:10.1080/01431160701408477.

Toutin, T., Blondel, E., Clavet, D., Schmitt, C., 2013. Stereo radargrammetry with Radarsat-2 in the Canadian Arctic. IEEE Transactions on Geoscience and Remote Sensing 51, 2601–2609. doi:10.1109/TGRS.2012.2211605.

Toutin, T., Gray, L., 2000. State-of-the-art of elevation extraction from satellite SAR data. ISPRS Journal of Photogrammetry and Remote Sensing 55, 13 – 33. doi:10.1016/S0924-2716(99)00039-8.

Urban, T.J., Schutz, B.E., Neuenschwander, A.L., 2008. A survey of ICESat coastal altimetry applications: Continental coast, open ocean island, and inland river. Terrestrial, Atmospheric & Oceanic Sciences 19, 1–19. doi:10.3319/TAO.2008.19.1-2.1(SA).

Van Niel, T.G., McVicar, T.R., Li, L., Gallant, J.C., Yang, Q., 2008. The impact of misregistration on SRTM and DEM image differences. Remote Sensing of Environment 112, 2430–2442. doi:10.1016/j.rse.2007.11.003.

Vijay, S., Braun, M., 2016. Elevation change rates of glaciers in the Lahaul-Spiti (Western Himalaya, India) during 2000–2012 and 2012–2013. Remote Sensing 8, 1038. doi:10.3390/rs8121038.

Viviroli, D., Dürr, H.H., Messerli, B., Meybeck, M., Weingartner, R., 2007. Mountains of the world, water towers for humanity: Typology, mapping, and global significance. Water Resources Research 43. doi:10.1029/2006WR005653.

WGMS, 2016. Fluctuations of Glaciers Database. Digital data. World Glacier Monitoring Service, Zurich, Switzerland. doi:10.5904/wgms-fog-2016-08.

Wingham, D., Francis, C., Baker, S., Bouzinac, C., Brockley, D., Cullen, R., de Chateau-Thierry, P., Laxon, S., Mallow, U., Mavrocordatos, C., Phalippou, L., Ratier, G., Rey, L., Rostan, F., Viau, P., Wallis, D., 2006. CryoSat: A mission to determine the fluctuations in Earth's land and marine ice fields. Advances in Space Research 37, 841–871. doi:10.1016/j.asr.2005.07.027.

Winker, D.M., Couch, R.H., McCormick, M.P., 1996. An overview of LITE: NASA's Lidar In-space Technology Experiment. Proceedings of the IEEE 84, 164–180. doi:10.1109/5.482227.

Winker, D.M., Vaughan, M.A., Omar, A., Hu, Y., Powell, K.A., Liu, Z., Hunt, W.H., Young, S.A., 2009. Overview of the CALIPSO Mission and CALIOP Data Processing Algorithms. Journal of Atmospheric and Oceanic Technology 26, 2310–2323. doi:10.1175/2009JTECHA1281.1.

Yamaguchi, Y., Kahle, A.B., Tsu, H., Kawakami, T., Pniel, M., 1998. Overview of Advanced Spaceborne Thermal Emission and Reflection Radiometer (ASTER). IEEE Transactions on Geoscience and Remote Sensing 36, 1062–1071. doi:10.1109/36.700991.

Yi, D., Zwally, H.J., Sun, X., 2005. ICESat measurement of Greenland ice sheet surface slope and roughness. Annals of Glaciology 42, 83–89. doi:10.3189/172756405781812691.

Yi, S., Sun, W., 2014. Evaluation of glacier changes in high-mountain Asia based on 10 year GRACE RL05 models. Journal of Geophysical Research: Solid Earth 119, 2504–2517. doi:10.1002/2013JB010860.

Zebker, H.A., Villasenor, J., 1992. Decorrelation in interferometric radar echoes. IEEE Transactions on Geoscience and Remote Sensing 30, 950–959. doi:10.1109/36.175330.

Zink, M., Bachmann, M., Brautigam, B., Fritz, T., Hajnsek, I., Moreira, A., Wessel, B., Krieger, G., 2014. TanDEM-X: The new global DEM takes shape. IEEE Geoscience and Remote Sensing Magazine 2, 8–23. doi:10.1109/MGRS.2014.2318895.

Zwally, H., Schutz, B., Abdalati, W., Abshire, J., Bentley, C., Brenner, A., Bufton, J., Dezio, J., Hancock, D., Harding, D., Herring, T., Minster, B., Quinn, K., Palm, S., Spinhirne, J., Thomas, R., 2002. ICESat's laser measurements of polar ice, atmosphere, ocean, and land. Journal of Geodynamics 34, 405–445. doi:10.1016/S0264-3707(02)00042-X.

Zwally, H., Schutz, R., Hancock, D., Dimarzio, J., 2012. GLAS/ICESat L2 Global Land Surface Altimetry Data, Versions 33/34, GLAH14. Dataset. NASA DAAC at the National Snow and Ice Data Center, Boulder, Colorado USA. doi:10.5067/ICESAT/GLAS/DATA207.

Zwally, H.J., Jun, L., Brenner, A.C., Beckley, M., Cornejo, H.G., Dimarzio, J., Giovinetto, M.B., Neumann, T.A., Robbins, J., Saba, J.L., Donghui, Y., Wang, W., 2011. Greenland ice sheet mass balance: distribution of increased mass loss with climate warming; 2003–07 versus 1992–2002. Journal of Glaciology 57, 88–102. doi:10.3189/002214311795306682.

# List of Abbreviations

**ALOS** Advanced Land Observing Satellite

**ASTER** Advanced Spaceborne Thermal Emission and Reflection Radiometer

**ATLAS** Advanced Topographic Laser Altimeter System

**B/H ratio** base-to-height ratio

**CALIPSO** Cloud-Aerosol Lidar and Infrared Pathfinder Satellite Observations

**DEM** Digital Elevation Model

**DGPS** differential GPS

**dh** elevation difference

**dh/dt** surface elevation change over time

**DSM** Digital Surface Model

**ERS** European Remote Sensing

**ESA** European Space Agency

**GCP** Ground Control Point

**GDEM** Global Digital Elevation Model

**GLAS** Geoscience Laser Altimeter System

**GNSS** Global Navigation Satellite System

**GPS** Global Positioning System

**GRACE** Gravity Recovery and Climate Experiment

**HMA** High Mountain Asia

**ICESat** Ice, Cloud and land Elevation Satellite

**IMU** Internal Measurement Unit

**InSAR** Interferometric Synthetic Aperture Radar

**MABEL** Multiple Altimeter Beam Experimental Lidar

**NASA** U.S. National Aeronautics and Space Administration

**NIR** near-infrared

**NSIDC** U.S. National Snow and Ice Data Center

**NVE** Norwegian Water Resources and Energy Directorate

**POCA** Point of Closest Approach

**PRISM** Panchromatic Remote-sensing Instrument for Stereo Mapping

**RMSE** root mean square error

**SAR** Synthetic Aperture Radar

**SfM** Structure from Motion

**SIRAL** Synthetic Aperture Interferometric Radar Altimeter

**SPIRIT** SPOT-5 stereoscopic survey of Polar Ice: Reference Images and Topographies

**SPOT** Satellite Pour l'Observation de la Terre

**SRTM** Shuttle Radio Topography Mission

**SWE** snow water equivalent

**SWIR** short-wave infrared

**TIN** triangular irregular network

**TIR** thermal infrared

**TP** Tibetan Plateau

**UAV** unmanned aerial vehicles

**VNIR** visible and near-infrared

# Part II

# Journal Publications

I

# Publication I

D. Treichler and A. Kääb:
**ICESat laser altimetry over small mountain glaciers**
*The Cryosphere*, 10, 2129–2146, 2016.
doi:10.5194/tc-10-2129-2016

The Cryosphere, 10, 2129–2146, 2016
www.the-cryosphere.net/10/2129/2016/
doi:10.5194/tc-10-2129-2016


The Cryosphere Open Access EGU

# ICESat laser altimetry over small mountain glaciers

**Désirée Treichler and Andreas Kääb**

Institute of Geosciences, University of Oslo, P.O. Box 1047, 0316 Oslo, Norway

*Correspondence to:* Désirée Treichler (desiree.treichler@geo.uio.no)

Received: 28 December 2015 – Published in The Cryosphere Discuss.: 26 January 2016
Revised: 6 July 2016 – Accepted: 28 July 2016 – Published: 16 September 2016

**Abstract.** Using sparsely glaciated southern Norway as a case study, we assess the potential and limitations of ICESat laser altimetry for analysing regional glacier elevation change in rough mountain terrain. Differences between ICESat GLAS elevations and reference elevation data are plotted over time to derive a glacier surface elevation trend for the ICESat acquisition period 2003–2008. We find spatially varying biases between ICESat and three tested digital elevation models (DEMs): the Norwegian national DEM, SRTM DEM, and a high-resolution lidar DEM. For regional glacier elevation change, the spatial inconsistency of reference DEMs – a result of spatio-temporal merging – has the potential to significantly affect or dilute trends. Elevation uncertainties of all three tested DEMs exceed ICESat elevation uncertainty by an order of magnitude, and are thus limiting the accuracy of the method, rather than ICESat uncertainty. ICESat matches glacier size distribution of the study area well and measures small ice patches not commonly monitored in situ. The sample is large enough for spatial and thematic subsetting. Vertical offsets to ICESat elevations vary for different glaciers in southern Norway due to spatially inconsistent reference DEM age. We introduce a per-glacier correction that removes these spatially varying offsets, and considerably increases trend significance. Only after application of this correction do individual campaigns fit observed in situ glacier mass balance. Our correction also has the potential to improve glacier trend significance for other causes of spatially varying vertical offsets, for instance due to radar penetration into ice and snow for the SRTM DEM or as a consequence of mosaicking and merging that is common for national or global DEMs. After correction of reference elevation bias, we find that ICESat provides a robust and realistic estimate of a moderately negative glacier mass balance of around $-0.36 \pm 0.07$ m ice per year. This regional estimate agrees well with the heterogeneous but overall negative in situ glacier mass balance observed in the area.

## 1 Introduction

The role of mountain glaciers and snow as sources for drinking water, irrigation, and hydropower is getting increasing attention, not least due to the significant population increase and economic development in a number of mountain regions and surrounding lowlands (Jansson et al., 2003; Viviroli et al., 2007). Retreat of mountain glaciers is also a major cause of eustatic sea level rise (Gardner et al., 2013), but the response of some large glacierized systems to climatic changes is still poorly quantified, especially in regions with large climatic variability. The glacier regions least represented in long-term in situ glacier monitoring programmes are those with the largest ice volumes (Zemp et al., 2015), which are less inhabited and difficult to access and, therefore, are not well studied. Regional estimates of ice loss recently gained importance, not least for assessing the current and future contribution of water stored in land ice masses to sea level rise (Gardner et al., 2013; Jacob et al., 2012; Marzeion et al., 2012; Radić et al., 2014; Radić and Hock, 2011) and for quantifying current run-off contribution from glacier imbalance (Kääb et al., 2015) or changes in the upstream cryosphere (e.g. Bliss et al., 2014; Immerzeel et al., 2010). Remotely sensed data are of special value in remote mountain regions where measurements such as in situ mass balance measurements are sparse or lacking completely.

Elevation data from the Geoscience Laser Altimeter System (GLAS) on board the NASA Ice, Clouds, and Land Elevation Satellite (ICESat) provides what is likely the most consistent global elevation measurement currently available (Nuth and Kääb, 2011). The use of this data to derive thick-

ness changes of Arctic ice caps is well established (Nuth et al., 2010; Moholdt et al., 2010; Bolch et al., 2013; Nilsson et al., 2015; Slobbe et al., 2008). Kääb et al. (2012) have shown that, when combined with reference heights from a digital elevation model (DEM), ICESat data can successfully be used to derive regional-scale glacier mass balance even in rough topographies such as the Himalayas. Subsequently, ICESat elevation measurements combined with the Shuttle Radar Topography Mission (SRTM) DEM were used to estimate sea level rise contributions from mountain glaciers globally (Gardner et al., 2013), regionally in high-mountain Asia (Neckel et al., 2014; Kääb et al., 2015) and even for local glacier mass balance studies in the Kunlun Shan (Ke et al., 2015) and the Alps (Kropáček et al., 2014).

The increased public interest in glacier retreat, not least due to its effects on water resources stored in mountain glaciers, requires that the performance of ICESat over such terrain is carefully evaluated and associated error sources are well characterized. This is especially important given that using ICESat data over mountain topography is at (or even exceeds) the limits of what the mission was designed for. As a case study for this purpose we chose the mountains of southern Norway. With its comparably small and sparse glaciers, situated within a varied topographic setting of both steep and gentle mountains, we consider the region as a representative case for the limits of applicability of ICESat data for analysing changes of mountain glaciers. In contrast to large, remote areas like high-mountain Asia, the climatic framework and glacier responses are relatively well known and measured in southern Norway, and accurate, up-to-date glacier masks and a high-resolution reference DEM are available.

Specifically, we aim to address the following questions in our study.

- What prerequisites and conditions need to be fulfilled to make ICESat-derived elevation changes over a certain area a valid method to assess glacier volume changes?
- Is the ICESat track density high enough for the sparse glacier cover in the study region, and are the point samples along ICESat profiles representative of the whole glacier population in southern Norway?
- Can a realistic elevation trend be retrieved for the years 2003–2009 (glacier volume loss), and is it possible to detect climate-related patterns, namely the spatial transition from maritime towards more continental glaciers with increasing distance to the coast?
- What is the minimum region size with respect to glacier density for ICESat GLAS data to ensure statistically significant results? Are realistic annual glacier thickness changes visible over a sufficiently sampled single glacier?

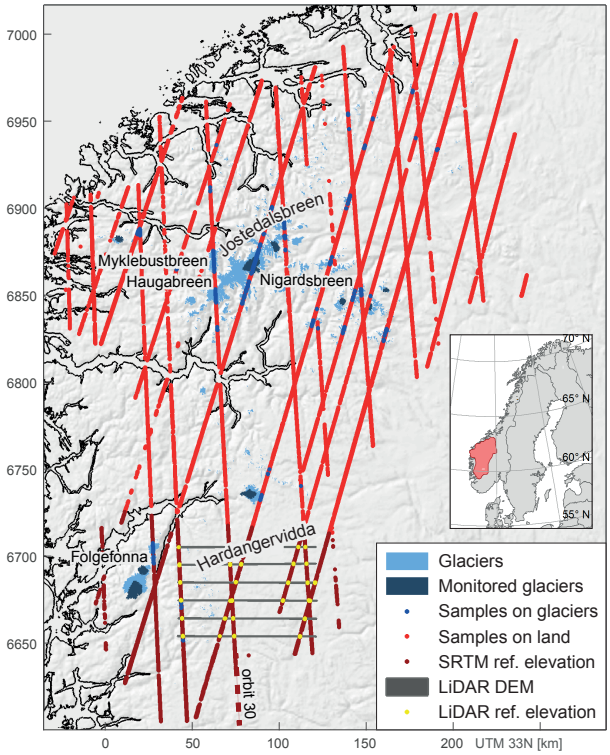


**Figure 1.** ICESat samples over glaciers and stable ground (land) in southern Norway. Only used footprints are displayed (no footprints on clouds or water). Glaciers with ongoing monitoring by NVE are emphasized.

- How do the findings compare to observed glaciological and geodetic glacier mass measurements?
- How does the reference DEM influence the quality of the results, and how can the footprint reference elevation best be modelled?

## 2 Study site and data

### 2.1 Southern Norway

The study area referred to here as southern Norway extends over an area of 100 000 km$^2$ at 59–63° latitude. It comprises all areas of the Scandinavian Mountains south of Trondheim that are within a 20-km buffer around the glaciers (Fig. 1). While very steep, especially at fjord flanks, the study area consists of both rounded and rough mountains but also includes high-elevation plateaus such as Hardangervidda. The climate of the study area is governed by a west–east gradient from a maritime climate at the coast with high precipitation amounts to dryer conditions further east in the rain shadow of the Scandinavian Mountains (Melvold and Skaugen, 2013). This is also reflected in measured glacier net balance magnitudes (Kjøllmoen et al., 2011). The Norwe-

gian glacier area has recently been mapped by the Norwegian Water Resources and Energy Directorate (NVE) based on Landsat imagery from 1999 to 2006 (Andreassen and Winsvold, 2012; Winsvold et al., 2014; digital data available from NVE, 2016; or the Global Land Ice Measurements from Space (GLIMS) database: GLIMS and NSIDC, 2012). Glaciers cover 1522 $km^2$ or roughly 1.5 % of our study area. This includes 1575 ice bodies ranging from small perennial ice patches of just over 0.01 $km^2$ in size to the largest outlet glaciers ($> 40\,km^2$) of the Jostedalsbreen ice cap. Fifty percent of the glacierized surface in southern Norway consists of glaciers with $< 5\,km^2$ spatial extension and 20 % of the glacier area of ice patches smaller than $< 1\,km^2$. Some maritime glaciers advanced in the 1990s while glaciers located in more continental climate showed mainly frontal retreat (Nesje et al., 2008; Andreassen et al., 2005). After a culmination in 2000, most of the monitored glaciers in Norway experienced net mass deficit (Kjøllmoen et al., 2011; Andreassen et al., 2016).

### 2.2 ICESat

ICESat GLAS was a single-beam spaceborne laser altimeter operational between February 2003 and October 2009, sampling the surface elevation of the Earth within roughly 70 m footprints during two to three observation periods each year of about 1 month each (Schutz et al., 2005). The laser footprints have 172 m spacing along-track, and approximately 42 km cross-track spacing between 91-day repeat reference orbits at 61° latitude (Fig. 1). Cross-track spacing increases at lower latitudes, making polar areas in principle more favourable for ICESat applications. Note that our study area already lies in the polar acquisition mask of the ICESat mission at $> 59°$ N, where the off-nadir pointing mode enabled near repeats of the tracks (ca. ±150 m), in contrast to a nominal orbit repeat precision of ±1000 m for midlatitudes (Schutz et al., 2005). In accordance with what Kääb et al. (2012) found to be the most suitable product for mountain glacier analyses, the ICESat data set used was GLAS/ICESat L2 Global Land Surface Altimetry HDF5 data (GLAH14), release 33 (Zwally et al., 2012). For GLAH14, elevation values were not changed between releases 33 and 34 (NSIDC, 2014). The data contain quality attributes and elevation corrections for each footprint. These attributes include a waveform saturation flag (attribute sat_corr_flag) to indicate saturation of the sensor when recording the returned pulse and a correction for the potential bias in extracted elevations from these saturated waveforms (attribute d_satElevCorr). The flags and corrections are intended for improving elevation accuracy on ice sheets (the original main purpose of the mission) and are not necessarily valid in rough mountain topography (NSIDC, 2012).

### 2.3 Reference data

The reference elevation data sets used are the national DEMs provided by the Norwegian Mapping Authority (further referred to as Kartverket) in 10 and 20 m spatial resolution (http://data.kartverket.no). In mountain areas, the Kartverket DEMs are based on source data at 1 : 50 000 map scale including elevation contours at 20 m equidistance, resulting in a nominal absolute vertical accuracy of ±4–6 m (defined as the standard deviation of elevation; Kartverket, 2016). Using the source date stamp of elevation contours as a proxy, the age of the DEMs was found to be highly variable geographically, ranging from 1978 to 2009 on southern Norwegian glaciers, and from 1961 to 2011 on non-glacierized areas.

For the Hardangervidda area and up to approximately 60.3° N, the global DEM from the Shuttle Radar Topography Mission (SRTM, Farr and Kobrick, 2000) is available at 3 arcsec resolution (corresponding to 93 m in $y$, and 45 m in $x$ direction at 60° N) from the U.S. Geological Survey (https://dds.cr.usgs.gov/srtm/; NASA JPL, 2013). The SRTM DEM used here is based on C-band radar data acquired in February 2000 and consists of a composite of four or more overpasses at latitudes that far north (Farr et al., 2007). The absolute vertical accuracy of the mission is stated as 16 m (defined as 1.6 times the standard deviation of the error budget throughout the entire mission; Rabus et al., 2003) but found to be in the range of a few metres compared to ICESat elevations (Carabajal and Harding, 2006). The SRTM DEM featured as the reference DEM of choice for previous ICESat glacier trend analyses (e.g. Gardner et al., 2013; Kääb et al., 2012). Unfortunately, it does not cover glaciers visited by more than one ICESat overpass in southern Norway. Thus, in this study, the SRTM non-void filled elevation data only serves as alternative reference DEM for land samples.

For parts of the non-glacierized Hardangervidda plateau, high-resolution lidar DEMs were provided by NVE (Melvold and Skaugen, 2013). The data consist of six east–west-oriented 80 km-long stripes of 500 m width and cell size of 2 m, flown on 21 September 2008 (minimum snow cover, leaf-off conditions). Data sets were available as high-resolution gridded DEMs. From comparison to a kinematic ground GPS survey carried out in April 2008, Melvold and Skaugen (2013) found the absolute elevation errors of the lidar data set to range from −0.95 to +0.51 m, with a mean error of 0.012 m and a standard deviation of 0.12 m.

Yearly net surface mass balance estimates from in situ measurements of eight glaciers within the study area (see the NVE report series "Glaciological investigations in Norway"; Kjøllmoen et al., 2011) were used as a reference for glacier behaviour during the ICESat acquisition period. The data series are the product of the recent homogenization of in situ measurements with geodetic measurements (Andreassen et al., 2016) and are available from http://glacier.nve.no/viewer/CI (NVE, 2016).

## 3 Methods

ICESat data points from the end of the hydrological year (autumn campaigns) are treated as a statistical sample of glacier surface elevations in southern Norway. We follow the double differencing method described by Kääb et al. (2012) where differences between ICESat elevations and a reference DEM (hereafter referred to as dh) are analysed. Direct comparison of ICESat elevations of different years, as done for larger Arctic glaciers and ice caps (plane-fitting methods, e.g. Howat et al., 2008; Moholdt et al., 2010), is not possible for small mountain glaciers. These methods assume a constant slope of the ice surface within the spatial variability of ICESat repeat ground tracks, which is not given for small mountain glaciers. The use of a reference DEM instead takes into account the more complex surface topography of small glaciers. When compared to elevations from a reference data set of a different source date, the dh will be negative if the surface has lowered over time between the DEM source date and ICESat acquisition time, and positive if the surface has risen. Differences should be zero if the surface elevation was constant, such as over stable ground. Uncertainties in elevation measurements of both data sets, not least as a result of rough terrain within the $\sim 70$ m circular ICESat footprint, raise the need for sufficiently large statistical samples to reduce the effect of random errors. The evolution of dh over time is used to investigate surface elevation change trends over the ICESat acquisition period 2003–2008. (The 2009 autumn campaign is excluded due to low spatial coverage before complete ICESat failure.) Note that ICESat captures a signal of volumetric balance that results from surface elevation changes rather than mass change directly. The same is also the case where geodetic mass balances are obtained from DEM differencing, which is a widely used method. Comparison of ice surface elevation change trends with in situ measurements provided in metres water equivalent (m w.e.) requires unit conversion that depends on ice density. To validate the ICESat-derived trends, we back-converted the in situ data using the same density as NVE used for mass to volume conversion of geodetic data (Andreassen et al., 2016). It is based on the findings of Huss (2013), who suggested a value of $850 \pm 60\,\mathrm{kg\,m^{-3}}$ as an average integrated over an entire glacier. (See also the discussion and density scenarios in the Supplement of Kääb et al., 2012.)

### 3.1 Pre-processing and filtering of ICESat data

ICESat surface elevations (height above reference ellipsoid) were converted to Norwegian height above mean sea level, in accordance with national DEM elevations. The ca. 170 000 data points within the study area were classified into ice and land footprints using the glacier outlines provided by NVE. Footprints lying partially on glaciers, i.e. with footprint centre locations within 40 m of NVE glacier borders (both in- and outside original outlines), were classified as ice borders and excluded from further analysis. Apart from avoiding a mixed land/ice elevation signal from partly ice-covered 70 m footprints this also accounts for the spatial uncertainty of glacier outlines and their potential change over time. For glacier analyses, spring and summer campaigns were excluded to avoid biased trends due to yearly varying snow heights (see argumentation in Kääb et al., 2012, 2015), and the 2009 autumn campaign was excluded due to insufficient spatial coverage caused by weakening of the laser over time. To account for differences in spatial distribution and potential elevation changes due to onset of snowfall, the split autumn campaign of October 2008 (laser 3K, ran out of power before the campaign was completed) and December 2008 (laser 2D, completion of the autumn 2008 campaign) were treated separately where appropriate. Land footprints on fjords and lakes were filtered out using shoreline data provided by the Norwegian Mapping Authority, as water levels may vary (tides, hydropower reservoirs).

Reference DEMs were corrected for elevation bias and spatially co-registered with ICESat (see Sect. 3.2). Reference elevations for each footprint were extracted from the DEMs by different statistical means: footprint centre elevation, mean, median, mode (rounded to the metre/decimetre for the Kartverket/lidar DEMs), inverse distance-weighted (IDW, linear weighing, i.e. power 1), and bilinear interpolation of elevation of DEM grid cells within an assumed circular footprint with 35 m radius (i.e. four grid cells for SRTM, 12 for Kartverket 20 m, 38 for Kartverket 10 m and $\sim 960$ for the lidar DEM).

The elevation differences between ICESat and the Kartverket DEM were analysed to denote a cut-off threshold for maximum elevation differences. Mean dh were found to be $\sim -0.5$ m for land, and $\sim -2$ m for ice samples (i.e. ICESat elevations are lower than reference elevations over glaciers). Using bootstrapping methods and histogram analysis for thresholds between 50 and 250 m for $|\,\mathrm{dh}\,|$, we found that a cut-off threshold of $\pm 100$ m dh effectively removed cloud measurements. Footprints with $|\,\mathrm{dh}\,| >$ threshold were excluded from all further analyses. The conservative threshold allows for uncertainty in elevation measurements of both data sets (land and ice), while allowing for slightly skewed dh distributions. It ensures all negative dh from glacier surface lowering between DEM acquisition date and ICESat elevation measurements are included while removing footprints on clouds (false positive dh).

Robust linear regression (we used Matlab's robustfit function with default parameterization) through all individual samples was performed to find a linear trend for surface elevation change over time. Robust methods iteratively reweigh least squares to find and exclude outliers until regression coefficients converge. For our ice trends we found that ca. 2–3 % of the samples received weight 0 and were thus essentially removed as outliers. As an alternative trend estimate, we used the gamlss package in R (www.gamlss.org) to perform regression using a fitted $t$ distribution. The $t$ fit

accounts for a larger number of outliers in our distribution of dh (Fig. 2) compared to a normal distribution (Lange et al., 1989).

### 3.2 Subpixel shifts and corrections applied to the reference DEMs

Based on dh of autumn campaign land samples, elevation bias, and spatial shifts between ICESat and the reference DEMs were quantified. The non-systematic spatial shifts of subpixel magnitude and biases were corrected where possible. No corrections were applied to the lidar DEM. For the Kartverket and SRTM DEMs, directions and magnitudes of the shifts seemed to vary highly, also within single DEM tiles. Automated co-registration using the methods of Nuth and Kääb (2011) was performed to correct an overall 20 m shift south and −2.6 m vertical offset of the SRTM DEM, compared to ICESat. However, additional shifts and biases that seem present in subunits of the SRTM DEM could not be corrected. For the Kartverket DEMs, dh were found to be elevation-dependent (more negative with increasing elevation above sea level $H$). The relationship is in the order of decimetres per 100 m elevation and applies to both the 10 and 20 m DEM as both are based on the same source data. To account for this vertical bias, a correction term $c_H$ was applied to individual elevation values of both Kartverket DEMs:

$$c_H = 0.882 - 0.00158 \cdot H. \quad (1)$$

Automated co-registration of the individual nominal Kartverket DEM tiles ($50 \times 50$ km and $100 \times 100$ km for the 10/20 m DEMs respectively) was not applied systematically as it did not result in an overall positive effect. This is due to overlying shifts of (unknown) production subunits within single tiles in different directions. To account for the apparently consistent vertical offsets in some areas, correction terms for each individual nominal tile ($c_{\text{tile}}$) and the indicative source date ($c_{\text{date}}$) of the Kartverket DEM were computed (after $c_H$ correction). For each nominal DEM tile the median land difference between ICESat and the Kartverket DEM was removed; alternatively the same was done for each temporal unit of the Kartverket DEM. Both corrections are meant to remove vertical spatio-temporal biases and bias patterns in the reference DEM. The values of the corrections correspond to the median dh of all filtered land footprints at minimum snow cover (autumn campaigns only) per tile and date and are in the order of ±1 m per tile, and ±5 m per date respectively. Potential physical causes such as vertical uplift due to post-glacial rebound in Scandinavia are in the order of decimetres for the last half century and cannot explain the large differences between ICESat and reference elevations on land surfaces. As a proxy for the reference DEM source date per ICESat footprint we used the time stamp of the closest elevation contour line to each footprint (elevation contours are the most important input data set the Kartverket DEMs are based on; Kartverket, personal communication, 2013). However, these correction terms are an approximate only. Spatially confined units with unique source data/firm update dates do not strictly exist and the total DEM is thus a product of spatio-temporal merging (Kartverket, personal communication, 2013), not untypical for DEMs from national mapping agencies.

For glaciers, spatially varying DEM source dates add additional uncertainty. Surface elevation difference between Kartverket DEM acquisition and the first ICESat acquisitions varies for individual glaciers, resulting in different (additional) offsets for each glacier. A correction term $c_{\text{glac}}$ for this effect was computed from the median dh of ice samples at the time of minimum snow cover (autumn campaigns only) for each individual glacier, as classified using the NVE glacier inventory. The values of $c_{\text{glac}}$ range from −20 to +15 m and reflect mainly vertical glacier changes between the DEM and ICESat dates in this study. For other areas, potentially other vertical biases from DEM production, such as height datums or signal penetration, could be addressed in a similar way. The latter are not relevant for the photogrammetric methods behind the Kartverket DEM, but may be relevant for radar wave penetration within the SRTM DEM.

### 3.3 Sample representativeness and trend sensitivity

In order to relate measured dh to actual net glacier mass balance, the ICESat sample has to mirror key characteristics of the area/terrain with respect to glacier driving processes. We assessed the representativeness of the ICESat glacier sample for the study area in terms of average elevation, slope, aspect, spatial distribution of the footprints, glacier size, and age of the reference DEM. Representativeness with respect to terrain parameters was tested by comparing the sample distribution to the respective distributions of all glaciers in southern Norway (we used all Kartverket DEM cells within the glacier mask). This was done both for the entire ICESat sample and for individual campaigns. Consistency in terms of reference DEM age distribution per campaign was assessed using the source date of the closest contour line for each sample as a proxy. Additionally, the size of the glaciers sampled by ICESat was compared to the entire glacier population of southern Norway.

To assure robustness of fitted glacier surface elevation difference trends, the effect of different data subsets and elevation corrections applied to either of the data sets were assessed. Subsets were created by including/excluding (a) sets of footprints, as those classified as ice border, with specific DEM time stamps, or samples flagged as fully saturated (attribute sat_corr_flag ≥ 3); (b) spatial subsets, e.g. of glaciers east and west of the main water divide; and (c) entire campaigns. The elevation corrections assessed include ICESat saturation elevation correction (attribute d_satElevCorr) in addition to the correction terms per Kartverket DEM tile/source date/glacier described above ($c_{\text{tile}}$, $c_{\text{date}}$, $c_{\text{glac}}$). Very intentionally, we did not divide our samples into footprints only in the accumulation or ablation parts of the

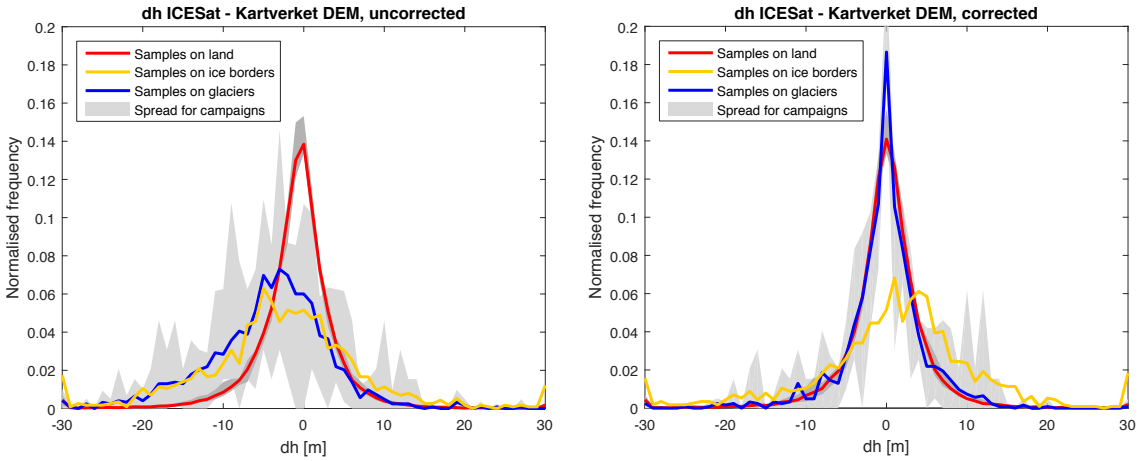


**Figure 2.** dh of land and ice (autumn campaigns 2003–2008) for the uncorrected Kartverket 10 m DEM elevations (left) and with DEM elevation corrections ($c_{\text{tile}}$, $c_H$) and per-glacier correction ($c_{\text{glac}}$) applied (right). The grey spreads shows the range of distributions for ice (wide spread, light grey) and land dh (narrow spread, darker grey) of individual campaigns.

glaciers respectively. In order to capture a signal that translates into geodetic mass balance, it is essential to sample the entire glacier to consider both surface elevation changes from ice melt/gain and dynamic glacier flow. If this is not ensured, the condition of mass continuity is violated, and it would thus be physically incorrect to draw conclusions on glacier mass balance based on surface elevation trends from a subset of samples in the ablation/accumulation areas only. The influence of separating footprints over ice and snow/firn for separate density scenarios is discussed in Kääb et al. (2012).

## 4 Results

### 4.1 ICESat sample overview

Roughly 75 % of the nearly 170 000 ICESat footprints over southern Norway contains valid information of the Earth's surface elevation (125 312 samples after removal of footprints on clouds and water surfaces, see Table S1 in the Supplement). Thereof, 2.6 % lie fully on glaciers (vs. an additional 0.9 % that were classified as ice borders). For glacier analyses, considering autumn campaigns only, a total of 1268 ice and 48 854 land samples remain. These numbers are reduced by 2.8 % (ice) and 1.6 % (land) only by excluding the weak autumn 2009 campaign. Dh of the remaining samples rarely exceed ±10 m. The dh are $t$ distributed with a narrower peak but heavier tails compared to a normal distribution. Before application of the correction terms to the Kartverket reference DEM, the dh distributions of ice and ice border samples are considerably wider and in average more negative than land dh (Fig. 2, left). After application of $c_H$, $c_{\text{tile}}$ and $c_{\text{glac}}$ correction terms, 94 and 95 % of the ice, and land autumn samples respectively, but only 80 % of ice border autumn samples show less than 10 m absolute elevation difference between ICESat and the (corrected) Kartverket 10 m DEM elevations (Fig. 2, right).

The spatial distribution and number of ICESat samples is not constant over time and decreases to as little as 10 % of the number of samples of the autumn 2003 campaign, which includes most samples of all campaigns (427 ice samples). In autumn 2009, only 35 ice samples (vs. 792 land samples) remain over southern Norway. Other autumn campaigns with very small sample numbers are 2005 (65 ice samples) and 2008 (24 and 24 ice samples for the October and December campaigns respectively). These periods with particularly few samples correspond to campaigns with few orbits flown (2008, 2009) or heavy cloud coverage (2005).

Of the ice samples, 128 lie on glaciers that were only sampled during a single autumn campaign. After the application of $c_{\text{glac}}$, any glacier elevation change signal from these single overpass samples is cancelled out. The majority of these (113) occurred during the autumn 2003 campaign due to a transition between two different orbit patterns in the middle of the campaign (Schutz et al., 2005). The single overpass samples with on average 0 m dh may thus flatten out derived trends and were excluded where appropriate.

### 4.2 Representativeness of ICESat glacier sample

The entire ICESat glacier sample appears representative in terms of elevation, aspect, slope, spatial distribution, and glacier area of the glaciers sampled (Fig. 3 and Fig. S1 in the Supplement). Compared to the frequency histogram of the entire glacierized surface in southern Norway, ICESat slightly oversamples east-facing glaciers and underrepresents the glacierized area in the south-western parts of the area of interest due to the orbits not covering the Folgefonna ice cap (Fig. 1). However, these deviations are of the same magnitude or less than deviations of the frequency his-

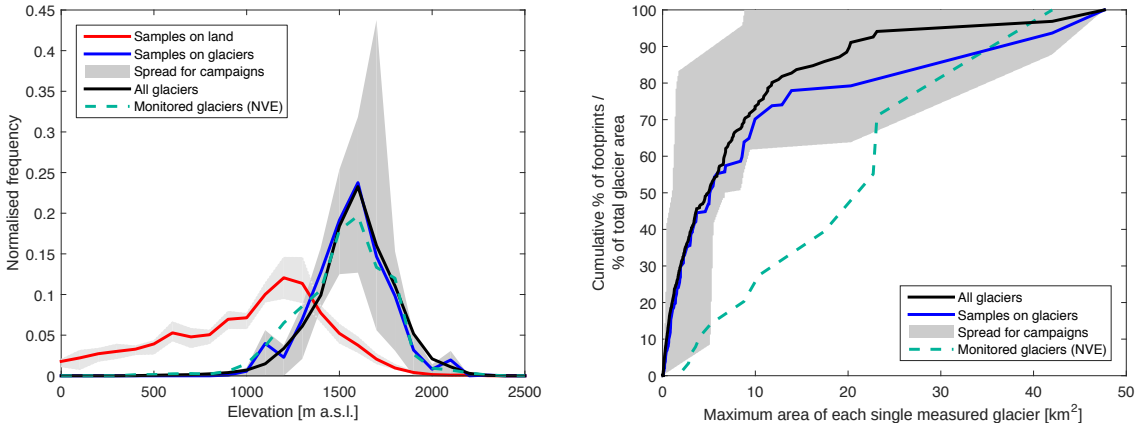


**Figure 3.** Representativeness of 2003–2008 ICESat autumn campaign samples in terms of footprint elevation (left) and area of glaciers sampled (right), compared to the entire glacierized surface in southern Norway and monitored glacierized surface (mass balance program by NVE). The grey spread encompasses the distributions of single ICESat autumn campaigns; where it is wide, the difference between individual campaigns is the largest. Reading example for glacier area comparison: 50 % of the entire glacierized surface in southern Norway is made out of glaciers $< 5\,\mathrm{km}^2$, 50 % of the glacierized surface where NVE runs a mass balance program is made of glaciers $< 23\,\mathrm{km}^2$, and 50 % of all ICESat autumn ice samples lie on glaciers $< 5.1\,\mathrm{km}^2$.

tograms of the glacierized area monitored in situ by NVE. Of the individual campaigns (autumn campaigns 2003–2008 shown within the grey spread), those with the fewest samples deviate the most, but still follow the distribution of the full data set. Variability between campaigns is largest (wide grey spread) for easting, also for land samples, due to the sensitivity of the sample to exclusion of entire orbits (due to shorter campaigns/cloudy weather). The two autumn 2008 campaigns are only representative if combined, as only a subset of orbits was flown in October and December. The autumn 2009 campaign was found to include ice samples for one overpass only (orbit 30, Fig. 1), resulting in sampling of only Myklebustbreen and Haugabreen, an outlet glacier of the Jotunheimen ice cap. All other campaigns have 5–13 different orbits with glacier samples. Severe spatial concentration and poor representation of southern Norwegian glaciers confirmed that also for our study area, the entire autumn 2009 campaign should be excluded from further analyses.

Of the 1575 ice bodies in southern Norway, 96 or 6.1 % are hit by at least one footprint of our filtered ICESat ice sample. While not the same glaciers are sampled each year, for all autumn campaigns except for 2009, footprints are spread on 17 (2008) to 77 (2003) different glaciers across the study area. Our ICESat footprints seem to capture small ice bodies according to their relative share of the total glacierized area: 47 % of the samples lie on glaciers smaller than $5\,\mathrm{km}^2$, 17 % on ice bodies $< 1\,\mathrm{km}^2$ (Fig. 3, right). Only the (combined) autumn 2008 campaign samples no glacier $> 12\,\mathrm{km}^2$, and the ice bodies sampled in December 2008 are distinctively smaller than those sampled in October in 2008. The smallest glacier within the NVE mass balance programme in the area is $2.2\,\mathrm{km}^2$ large.

### 4.3 Error sources and corrections for ICESat and DEM elevations

Elevation errors in the DEMs were found to exceed ICESat footprint elevation uncertainty as well as the magnitude of corrections available in the ICESat products. ICESat elevation corrections from effects of waveform saturation (attribute d_satElevCorr) are in the range of decimetres; all other elevation corrections within the data set are even smaller. Application of ICESat correction terms had no notable effect on dh distributions. The relative share of saturated samples (parameter satCorrFlag $\geq 3$ in the data set) varies between 5 and 40 % for the different campaigns and is up to 15 % higher for ice than for land. In contrast to the findings of Kääb et al. (2012) for high-mountain Asia, we found the number of saturated samples to decrease over time to as little 0–2 % for the last three acquisition campaigns (laser 2D-2F). Filtering increased the relative share of saturated samples by on average 5 %, and mean absolute dh (after filtering) are smaller for saturated footprints than for non-saturated ones (95 % confidence) for both land and ice, whether or not saturation correction was applied to the dh. Saturated samples were therefore not removed from the data set for trend computation, and saturation correction was not applied.

In contrast to the ICESat elevation values that seem robust without any corrections, elevation correction terms applied to the Kartverket reference DEMs significantly narrowed dh distributions (Fig. 2, right). The elevation-dependent correction term $c_H$ successfully removed skewness towards more negative dh in dh distributions, and per-glacier correction $c_{\mathrm{glac}}$ clearly caused a major reduction in ice dh. The correction terms $c_{\mathrm{tile}}$ and $c_{\mathrm{date}}$ were found to be interchangeable

and resulted in minor improvements only on land and ice dh distributions. For single footprints, uncertainty in reference DEM elevation is on the order of metres.

Looking at single footprints, reference DEM elevations differ by decimetres to metres between the different statistical measurements (mean, bilinear interpolation, etc.) applied to DEM grid cells within the ICESat footprint, for one and the same DEM. The method chosen matters most for the SRTM DEM with only four contributing cells, but differences resulting from the chosen elevation extraction method – from the perspective of a single footprint – are also higher for the high-resolution lidar DEM with ca. 960 contributing cells than for the 10/20 m Kartverket DEMs. However, for larger sample numbers, these differences cancel out and dh distributions for reference elevations from the same DEM, but different elevation extraction methods, are approximately the same (Fig. 4). Summarizing statistical methods appear to produce slightly narrower dh distributions than centre DEM elevations only but the difference between the curves is not significant. Mode elevations differ most from reference elevations computed by the other methods, also for the 2 m lidar DEM. We based our further analyses on median DEM elevations per footprint, or bilinear interpolation in the case of the low-resolution SRTM DEM.

Reference elevations between DEMs from different sources varied greatly. For the 184 autumn samples on Hardangervidda where all four reference DEMs were available, the lidar DEM matched ICESat elevations closest with a mean vertical offset of 0.03 m and a narrow dh distribution (Fig. 4). Elevation differences from the co-registered SRTM DEM are skewed with a heavier tail towards negative dh. Distributions of the (corrected) Kartverket DEMs, dating back to the 1970s in eastern parts of the Hardangervidda, are particularly wide for this subset of samples, including an average vertical offset of −1.3 m. For other spatial subsets, widths and vertical offsets of dh distributions of the SRTM and Kartverket DEMs vary to the same degree in a seemingly random way. Distributions of dh based on the 10 vs. 20 m Kartverket DEMs were the same, also for other spatial subsets, and no improvement in elevation precision per footprint could be found from the finer grid resolution.

Analysis of the DEM source dates for ice samples of the different campaigns (Fig. 5) shows the representativeness of our sample in terms of Kartverket reference DEM age distribution. Seventy percent of the samples have reference elevations from 2008 to 2009 (further termed "post-2000"), and only approximately 20 and 10 % date back to the 1990s and 1980s ("pre-2000") respectively. Only two campaigns divert from this distribution: in autumn 2005, 60 % of the ice samples have old reference DEMs, and in 2009, all ice samples have very recent reference elevations from 2008 to 2009. For the split autumn 2008 campaign, all but one of the October samples fall on reference DEMs from 2008, while 80 % of the December samples have pre-2000 DEMs. If using uncorrected Kartverket DEM elevations, pre-2000 dh are significantly more negative (mean dh: −7.3 m) than post-2000 dh (−3.1 m). The per-glacier correction $c_{\mathrm{glac}}$ completely reconciles the two distributions as seen in Fig. 2. Note that $c_{\mathrm{glac}}$ treats glaciers as spatial units with consistent source data set. Where this is not given – and parts of a glacier surface are mapped on different dates or with different methods – the correction will be only partially effective.

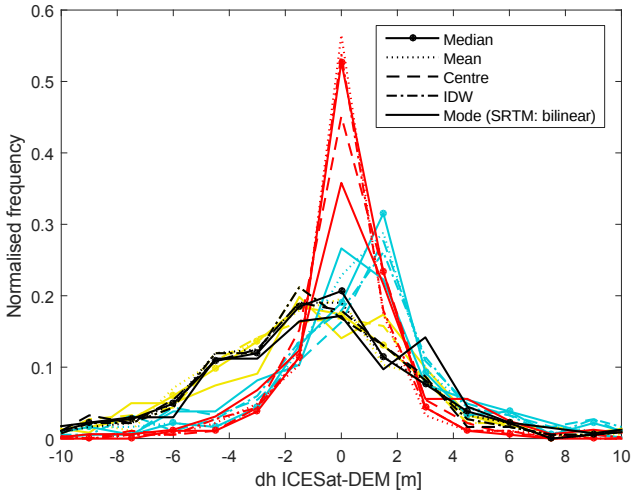


**Figure 4.** Graph shows dh from different reference DEMs and statistical measures to summarize elevations within footprints (184 land samples): lidar 2 m (red), Kartverket 10 m (black) and 20 m (yellow), SRTM ∼ 90 m (blue, bilinear interpolation shown instead of mode).

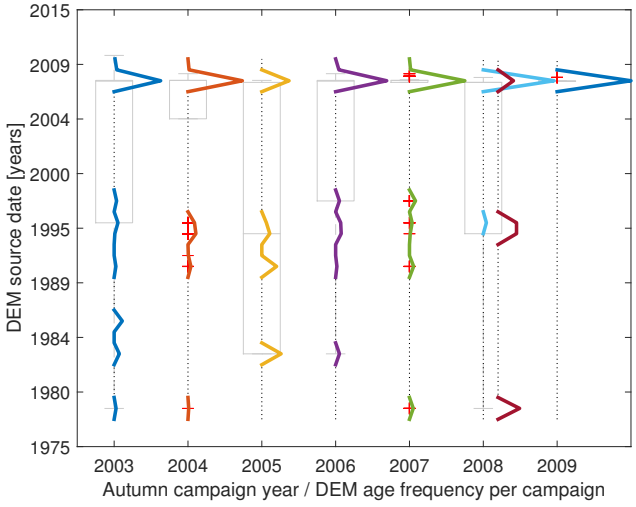


**Figure 5.** DEM source date distributions for ICESat autumn campaign samples on glaciers. The box plots emphasize the average DEM age per campaign while the frequency histograms (coloured curves) reflect the relative DEM age distributions. In 2008, the October (blue) and December (brown) campaigns are shown separately (frequency histogram) and grouped (box plot).

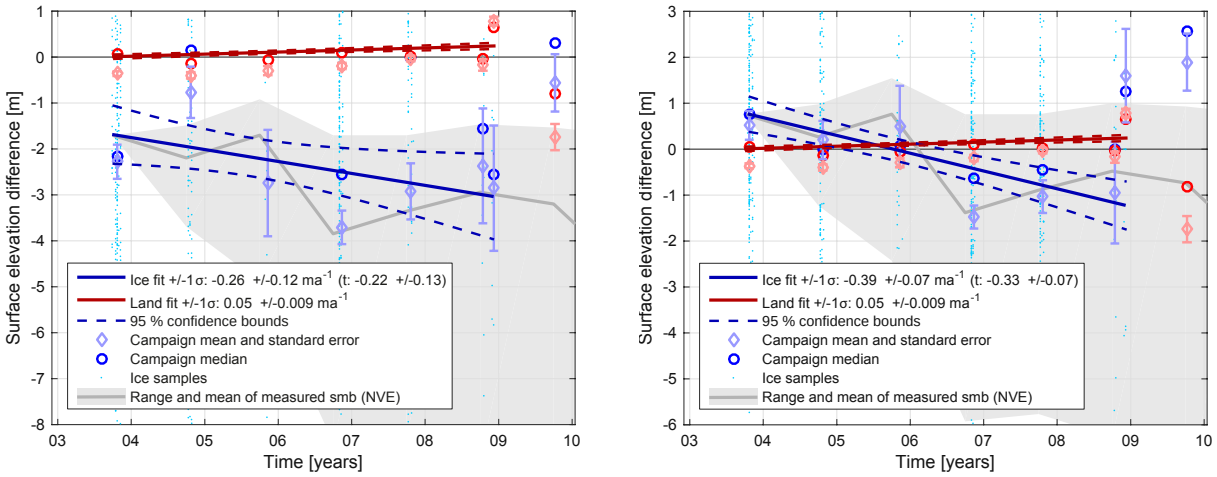


**Figure 6.** Surface elevation difference trends for land (red) and ice (blue) samples respectively, for autumn campaigns 2003–2008. Left: per-tile and -elevation corrections ($c_{\text{tile}}$, $c_H$) applied, 1233 samples. Right: per-tile, -elevation and -glacier correction ($c_{\text{glac}}$) applied, 1105 samples. Trends are computed from individual dh samples using robust linear regression. Campaign median and mean ± standard error per campaign and class are shown to indicate the variability in dh per campaign. The grey spread corresponds to the measured range of cumulative surface mass balances of eight glaciers in the area, reconverted to ice volume changes using a density of 850 kg m$^{-3}$ (Andreassen et al., 2016), and their area-weighted mean. The data provided by NVE are based on in situ and geodetic measurements.

### 4.4 Glacier thickness trends

We find a glacier surface elevation change of $-0.39\,\text{m a}^{-1} \pm 0.07$ standard error ($1\sigma$) for the years 2003–2008 (Fig. 6, right) with all corrections to DEM elevations applied when samples on glaciers covered by only a single autumn overpass were excluded. The trend slope decreases slightly to $-0.34 \pm 0.062\,\text{m a}^{-1}$ when such single-overpass samples are included. Using a $t$ fit instead, we found trends in general to be less sloping than robust trends for the same sample/set of applied corrections, and obtained alternative ice trend estimates of $-0.33 \pm 0.07$ and $-0.27 \pm 0.061\,\text{m a}^{-1}$ on the same data sets. Campaign means are more negative than campaign medians, which indicates slightly skewed dh distributions for both ice and land samples. Land campaign means/medians follow the near-zero trend as computed from all individual samples very closely ($0.05 \pm 0.009\,\text{m a}^{-1}$, $t$ fit: $0.04 \pm 0.009\,\text{m a}^{-1}$). An exception to that is the December 2008 campaign which indicates surface rise in contrast to the October 2008 campaign due to onset of winter snowfall at higher elevations. Exclusion of the December 2008 campaign effectively sets the land trend to zero and renders the ice trend more negative. On the other hand, however, the December ice samples are required for the autumn 2008 campaign to be representative (see Sect. 4.1). Correction of December samples for increasing snow depth (estimated from October to December land dh differences per elevation) also removes the land trend, but does not affect the ice trend. If the per-glacier dh correction $c_{\text{glac}}$ is not applied, the ice trend is reduced and uncertainty increases to $-0.26 \pm 0.12\,\text{m a}^{-1}$ ($t$ fit: $-0.22 \pm 0.13\,\text{m a}^{-1}$). This decrease of thickness loss rate is due to the mixing of older and newer dates of the reference DEM that introduces biased dh and thus dilutes trends. Without the correction, ice campaign medians/means of uncorrected samples do not follow the assumed linear trend well and the standard errors of the campaign means just about overlap with 95 % trend confidence bounds (Fig. 6, left). Deviation and uncertainty are largest for campaigns with few samples and non-representative DEM age distribution: 2005, October/December 2008 (split), and 2009 (excluded from trends). If ICESat trends were fitted through campaign medians instead of individual samples, these biased/non-representative campaigns would get the same weight as all other campaigns and, consequently, have more power to alter the derived trend. This stresses that ICESat trends over glaciers should be computed based on the entire footprint sample, not based on campaign statistics (e.g. median dh) that give campaigns disproportionate weight compared to the actual number of samples included in that campaign.

After applying the per-glacier vertical correction $c_{\text{glac}}$ to the ice dh, means/medians of single campaigns follow the pattern of NVE's in situ mass balance measurements remarkably well. The range of cumulative net surface mass balances, converted to surface elevation changes (Huss, 2013) of eight glaciers in the study area, is shown as a grey spread in Fig. 6. Note that these data are a product of the recent homogenization of in situ data of Norwegian glaciers with geodetic measurements (Andreassen et al., 2016) and thus differs from more positive glacier mass balance curves published earlier. For some of the studied glaciers, the data ho-

mogenization suggests stronger mass loss and no or more moderate mass surplus for the glaciers with positive cumulative surface mass balance in the studied time period. Campaign means are shifted up with the ice trend line crossing 0 m dh in autumn 2005 which corresponds to zero-elevation difference between ICESat and reference DEM considering decreasing sample numbers (autumn 2005 corresponds to the mean date of all ICESat samples used). Noteworthy is the 2005 autumn campaign which – only after correction – fits well with the reported positive net balance for five out of ten measured glaciers (Kjøllmoen et al., 2006). The 2009 campaign does not follow the trend or the in situ measurements, regardless of the application of $c_{\mathrm{glac}}$, In situ measurements suggest moderately negative net surface mass balances for that year (Kjøllmoen et al., 2010).

The slopes of both land and ice trends are not significantly affected ($< \pm 0.01\,\mathrm{m\,a^{-1}}$ change in trend slope) by either DEM correction terms ($c_H$, $c_{\mathrm{tile}}$ and $c_{\mathrm{date}}$), the use of alternative statistical measures to extract DEM elevations per footprint, or the application of saturation correction to ICESat elevations. Exclusion of saturated samples and application of saturation correction to the remaining dh flattens out ice trend slopes by $0.03\,\mathrm{m\,a^{-1}}$ and increases uncertainty (see Table 1). Including ice border samples only affects the ice trend if $c_{\mathrm{glac}}$ is not applied, but does not increase trend significance despite the increased sample number. If winter campaigns are included, the ice trend becomes considerably more negative ($-0.43 \pm 0.066\,\mathrm{m\,a^{-1}}$, $t$ fit: $-0.41 \pm 0.070\,\mathrm{m\,a^{-1}}$. The same accounts for fitting a trend through winter campaign samples only ($-0.42 \pm 0.092$, $t$ fit: $-0.41 \pm 0.097\,\mathrm{m\,a^{-1}}$). Note that for comparability between winter and autumn trends single overpass samples are not excluded in the numbers here. The 2003 winter campaign had a different orbit pattern to later campaigns (Schutz et al., 2005). We found yearly varying snow heights of between 3 and 7 m on glaciers, and the maximum values in winter 2005 correspond well to the overall strongly positive winter mass balance of that particular year (Kjøllmoen et al., 2006). Ice trend slopes are considerably more sensitive to all changes in sample composition described above if $c_{\mathrm{glac}}$ is not applied.

Continental glaciers east of the water divide show a more negative trend than coastal glaciers. The same is true for small (area $< 5\,\mathrm{km^2}$) vs. large glaciers, and ice samples with pre-2000 vs. post-2000 reference DEM. The latter corresponds to an arbitrary subset in size (with a tendency of older reference DEMs for smaller glaciers) and spatial distribution of glaciers rather than a selection based on any physically meaningful criteria. The increases in trend slope amount to 50–150 % between these respective subset pairs (Table 1). However, we could not find a significant relationship between dh magnitude and distance to coast. Exclusion/inclusion of entire campaigns was found to affect trends only for campaigns at either end of the ICESat acquisition period.

Note that subsets of samples of only accumulation/ablation zones, as well as certain elevation or slope classes, would also result in different trends (not shown). Such sample subsets can obviously not fulfil the requirement of representativeness for the entire glacier area and are thus not comparable to in situ glacier mass balance measurements. Glaciers that are not in balance adjust their geometry via glacier flow, which causes additional surface elevation changes that may be different for the accumulation and ablation parts of a glacier. Only sampling of the entire glacier(s) ensures that both elevation changes due to surface mass balance as well as glacier dynamics are included in the volumetric mass balance signal measured by ICESat.

The problem of biased trends due to non-representative spatial sampling by ICESat is illustrated well by the spatially clumped autumn 2009 campaign. The only glaciers that are sampled in 2009 have a strongly positive trend (Fig. 7, $+0.47 \pm 011\,\mathrm{m\,a^{-1}}$, in total 181 samples from Myklebustbreen and Haugabreen for autumn campaigns 2003–2009). While this trend is based on fewer campaigns (missing data in 2005 and 2007, only 3 and 7 samples for the 2004/08 campaigns respectively), the trend slope is not unrealistic (2.05/0.14 m w.e. cumulative balance before/after data homogenization for nearby Nigardsbreen in 2003–2009; Kjøllmoen et al., 2009; Andreassen et al., 2016). The ICESat sample on these glaciers is representative (also for single campaigns) in terms of elevation, slope, aspect, and spatial distribution (within a single track that roughly follows the glacier flow line) compared to the entire glacier area of Myklebustbreen/Haugabreen from the reference DEM. The reference DEM for this area was updated in 2008, resulting in a positive offset of the ice campaign mean in autumn 2009 (Fig. 6). The fact that these glaciers are not at all representative for the cumulative mass balance of the entire glacier population in southern Norway explains the large offset of the 2009 campaign mean to the 2003–2008 ICESat trend.

## 5 Discussion

### 5.1 Representativeness

When combined with reference elevations from a DEM, ICESat data provide realistic estimates for glacier surface elevation change in southern Norway. However, our results bring out the importance of ensuring representativeness of the sample as well as good control over biases in reference elevations.

The ICESat sample has to be representative not only in terms of terrain and topographic characteristics that govern glacier behaviour but also data quality aspects that vary spatially. Parameters with coarse spatial patterns have the largest biasing potential. Consequently, reference DEM quality and age, glacier area, and severe variations in spatial distribution of the samples were found to potentially have the largest

**Table 1.** Trends and trend standard error (SE), as computed from different subsets and corrections applied to the data set ($c_H$, $c_{\text{tile}}$ and $c_{\text{glac}}$ are applied unless specified otherwise). Footprints on glaciers sampled only during one autumn campaign are excluded except for the subsets marked with an asterisk, i.e. * corresponds to all 2003–2008 (autumn) ice samples. In bold are final estimates for the whole of southern Norway. Italicized are values for land samples.

| Data set | Correction/subset | Robust trend | SE ($1\sigma$) | Samples | $t$ trend | SE ($1\sigma$) |
|---|---|---|---|---|---|---|
| ice | ($c_H$, $c_{\text{glac}}$, only $>1$ overpass) | **−0.39** | **0.07** | **1105** | **−0.33** | **0.07** |
| land | ($c_H$, $c_{\text{tile}}/c_{\text{date}}$) | ***+ 0.05*** | ***0.009*** | ***48 089*** | ***+ 0.04*** | ***0.009*** |
| ice | ($c_H$, $c_{\text{glac}}$) all ice samples* | **−0.34** | **0.062** | **1233** | **−0.27** | **0.061** |
| ice | $c_{\text{glac}}$ not applied* | −0.26 | 0.12 | 1233 | −0.22 | 0.13 |
| ice | Dec 2008 excluded | −0.44 | 0.072 | 1085 | −0.37 | 0.071 |
| land | *Dec 2008 excluded* | *−0.003* | *0.010* | *44 568* | *−0.004* | *0.010* |
| ice | Corr Dec 2008 | −0.4 | 0.07 | 1105 | −0.34 | 0.069 |
| land | *Corr Dec 2008* | *+0.001* | *0.009* | *48 089* | *−0.003* | *0.009* |
| ice | Incl 2009 | −0.25 | 0.065 | 1140 | −0.22 | 0.066 |
| land | *Incl 2009* | *+0.03* | *0.008* | *48 854* | *+0.03* | *0.008* |
| ice | *Sat_corr* applied, saturated samples excluded | −0.35 | 0.072 | 1001 | −0.3 | 0.075 |
| ice | East of water divide | −0.55 | 0.14 | 242 | −0.54 | 0.14 |
| ice | West of water divide | −0.36 | 0.08 | 863 | −0.29 | 0.08 |
| ice | Pre-2000 DEM source date | −0.72 | 0.16 | 298 | −0.64 | 0.17 |
| ice | Post-2000 DEM source date | −0.29 | 0.076 | 807 | −0.26 | 0.076 |
| ice | Including ice border samples | −0.36 | 0.07 | 1541 | −0.33 | 0.07 |
| ice | Including winters 2003–2008* | −0.43 | 0.066 | 2536 | −0.41 | 0.070 |
| ice | Only winters 2003–2008* | −0.42 | 0.092 | 1303 | −0.41 | 0.097 |
| ice | Samples on glaciers $>5\,\text{km}^2$ | −0.28 | 0.089 | 621 | −0.26 | 0.091 |
| ice | Samples on glaciers $<5\,\text{km}^2$ | −0.53 | 0.11 | 484 | −0.43 | 0.11 |
| ice | Myklebustbreen/Haugabreen (2003–2009) | +0.47 | 0.11 | 181 | +0.47 | 0.12 |

impact on glacier trend estimates. This sensitivity is a direct result of interference of the non-uniform glacier behaviour within the study area with the (coarse) spatial pattern of these influencing parameters. In contrast, parameters that vary much more spatially such as elevation, slope, or aspect were found to be of less concern. Also smaller sample subsets are representative in that respect. Campaigns with low sample numbers and spatial clumping are most prone to biases. Owing to the rapidly decreasing laser power, campaigns towards the end of the acquisition period are most affected. However, severe cloud cover and subsequent exclusion of too many orbits can result in poor spatial distribution also for other campaigns. An example for this is the autumn 2005 campaign in southern Norway for which the only few ice samples mostly lie on old reference DEMs.

When relating ICESat trends to traditional glaciological measurements it is important to keep in mind that the subset of in situ monitored glaciers and the glaciers covered by our ICESat sample might not be fully comparable. Differences in estimated mass/volume changes are therefore likely to not (only) be caused by the methods used, but are rather a result of different sample composition. This is in line with the findings of e.g. Zemp et al. (2015) or Cogley (2009), who assign differences in mass budgets as from glaciological vs. geodetic measurements to sample composition rather than method-inherent causes. We find that with ICESat's random spatial sampling (with respect to glacier locations), we also capture many small ice bodies and snow patches. The share of samples, in terms of the area of the ice bodies on which single footprints lie, accurately reflects the size distribution of all glaciers and ice patches of the total glacierized surface

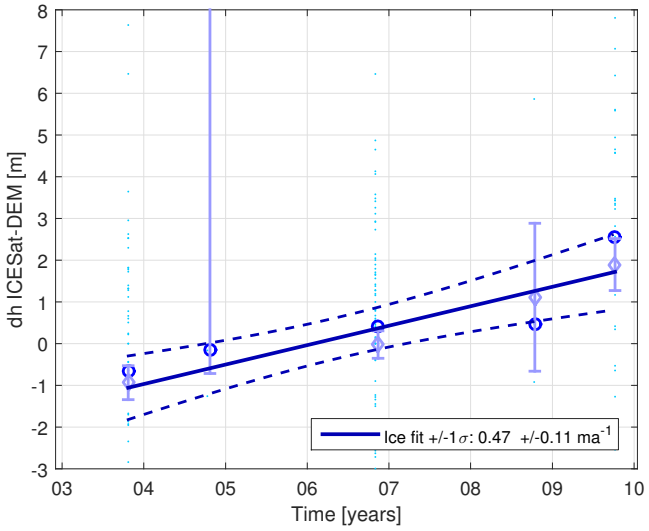


**Figure 7.** The autumn 2003–2009 trend for samples only on those glaciers that are covered by the autumn 2009 campaign (Myklebustbreen and Haugabreen) is strongly positive. The large error bars in 2004 and 2008 result from the very low campaign sample numbers of only three and seven samples respectively.

in southern Norway. While such small ice patches are commonly not monitored in situ, they are likely to be equally affected by climate change if not even more sensitive (Bahr and Radić, 2012; Fischer et al., 2014). Subsequent differences in glacier volume/mass changes as derived from ICESat, compared to traditional glaciological methods on selected valley glaciers, might therefore not agree if upscaled to the entire glacier population of a study area (Bahr and Radić, 2012).

The moderately negative glacier surface elevation change trends for the years 2003–2008 fit well with overall negative net cumulative mass balance series from glaciological measurements on glaciers in southern Norway. Trend slopes are robust against applied corrections or changes in sample composition as long as representativeness of the sample is guaranteed. Given the highly heterogeneous behaviour of Norwegian glaciers and the varying age of some parts of the reference DEM, both the measured dh (up to 20 m) and the resulting trend confidence intervals are within an expected range. We find that smaller glaciers, and glaciers to the (dryer) east of the water divide, experienced stronger changes than larger and coastal glaciers. This is in agreement with the individual reactions of the monitored glaciers in southern Norway to the increasing atmospheric temperatures during the last decade.

To fill gaps from missing campaigns or to increase spatial resolution of estimated glacier trends, other authors have tried to obtain an alternative trend estimate fitted through winter ice samples (e.g. Gardner et al., 2013). However, our results for southern Norway show that ICESat is sensitive to – and even able to reproduce – yearly varying snow depths, and our glacier surface elevation change trends are more negative for winter ice samples. Even though the difference between the winter and autumn trends is not significant in our study, the standard error of the winter trend is 50 % larger which reflects the uncertainty added from yearly/spatially varying snow depths. Moreover, the different orbit pattern of the winter 2003 campaign (and first phase of autumn 2003 campaign) compared to all following campaigns may cause problems with representativeness and spatial distribution of the samples, especially if spatially varying elevation corrections such as our per-glacier correction $c_{\mathrm{glac}}$ are applied. Our results therefore advise against including winter samples in glacier trend analyses. We also recommend including only footprints lying entirely on glaciers, i.e. excluding footprints that we classified as ice border samples. The signal from mixed ice/land footprints adds unnecessary uncertainty to the derived trends that does not justify the increased sample numbers.

Regarding the example of Myklebustbreen, we show that it may be possible to detect trends even for single glaciers. Unfortunately, no mass balance measurements exist to verify the positive surface elevation change found for this glacier. How confident we can be in such a local trend depends on appropriate temporal and spatial coverage. Our results show that the applicability of ICESat in arbitrary glacierized regions does not depend on a single factor only. Likewise, the minimum region size needed to derive valid estimates on glacier surface elevation change from ICESat cannot be expressed as a hard threshold but depends on a combination of factors specific to each area: glacier density and ICESat track density (i.e. sample size), representativeness of the ICESat sample, and homogeneity of the glacier signal within the study (sub-) region. In general, ICESat track density increases with latitude, making areas closer to the poles more favourable for ICESat studies. However, size and spatial distribution of glaciers as well as less cloud cover in dryer areas may result in large enough sample numbers even in small mountain regions at lower latitudes – as long as the representativeness condition is fulfilled. Representativeness of the sample may also be given for lower sample numbers than we found in southern Norway, where a glacier population is more homogeneous with respect to its topographic setting as well as mass balance changes/surface elevation trends. Spatially varying effects such as from DEM elevation bias or highly non-uniform glacier behaviour within the study area require larger sample numbers – and thus larger region sizes – to account for the introduced uncertainty. In that regard, southern Norway may not be an ideal location to test the limits of ICESat applicability, and in other mountain regions with more consistent reference DEMs even smaller study areas may potentially yield valid ICESat glacier surface elevation change estimates.

### 5.2 Glacier trend sensitivity

Given the temporal variability in annual surface mass balances from long-term in situ measurements, the glacier sur-

face elevation change derived from ICESat data is not likely to represent a long-term trend. Our results are only representative for the development within the 5 years covered. It is in general not recommended to extrapolate trends derived from such a short time interval, neither for ICESat-derived trends, nor mass balance series in general.

Trend slopes are considerably less sensitive to missing/biasing campaigns in the middle of the ICESat acquisition period than to campaigns missing at either end. Inclusion of the non-representative 2009 campaign which diverges strongly from the assumed linear trend (corresponding to an assumed constant mass balance) significantly alters the trend slope. The considerable trend slope differences for our various sample subsets show that trends are even more sensitive to changes in sample composition or applied corrections when sample numbers are small.

For our data, we found that robust fitting methods, as used by e.g. Kääb et al. (2012) for ICESat glacier trends, result in comparable but somewhat steeper trend estimates as when fitting a $t$ distribution to the data. The error estimates of both methods overlap for all subsets/sets of corrections applied to the data set, thus the trends are not significantly different. A $t$ fit better captures the heavier tails of the sample distribution and includes the uncertainties in the data within the statistical model used to compute the fit. The iteratively lowered weighing of samples within the robust fitting technique (which assumes a normal distribution) results in a similar effect – although one can argue that the weights assigned to outliers are so small that data points that do not fit the trend essentially are removed, and thus sample numbers reduced. Consequently, according to Street et al. (1988), error estimates for the robust methods might not be correct. However, given that most outliers indeed correspond to erroneous measurement of either ICESat or reference elevations, exclusion of these samples from trend estimates might be desirable. We found that error estimates of both methods are very similar, and differences resulting from the different trend fitting approaches are of the same order as caused by changes to the sample composition or due to application of correction factors. We thus prefer to leave the question of whether robust or $t$ fits are more appropriate to derive elevation trends from ICESat open.

### 5.3 The role of DEM quality and elevation errors

Of all correction factors applied, the correction for constant offsets on glaciers introduced by DEM age ($c_{\mathrm{glac}}$) deserves special attention as it considerably increased the statistical significance of glacier surface elevation trends. Not only is the trend standard error halved, but the correction also makes the trend slope much more robust to changes in sample composition/elevation corrections. The correction thus captures and eliminates errors in the data set that have a far bigger effect on trends than, for example, different fitting techniques. By applying $c_{\mathrm{glac}}$ we see an increase in trend slope even though the correction decreases ice dh. The fact that single campaigns fit measured mass balance after application of the correction strongly indicates that this correction is important for accurately capturing glacier surface elevation development within the studied time period. The estimated glacier surface elevation trend of the sample, without accounting for DEM age offsets, is not significantly different from the former trend estimate, but the wider confidence interval, trend sensitivity, and large offsets of single campaigns are a clear sign that not all error sources were accounted for in the uncorrected data set. It also illustrates the importance of representativeness very well in terms of factors that may not be immediately obvious, such as spatially varying vertical offsets in the reference data. Note that a correction for "DEM age" as done here has a different significance for glaciers compared to stable ground. On glaciers that change their surface elevation over time, the spatially varying bias we see in our data set is likely to indeed be caused by different DEM ages. On top of that, other spatially varying biases due to mosaicking of data from different sources may add additional bias to glaciers. On land surfaces, the contrary is the case and the latter type of bias would usually play the main role – while the age of the reference DEM is negligible except for areas and timescales where, e.g. vertical uplift due to post-glacial rebound causes relevant age-dependent bias.

Where the correction is applied to spatial units with changing elevation – such as on glaciers – a certain consistency and repetition in spatial sampling is needed. The surface change signal contribution from a glacier sampled only by one overpass is removed by the $c_{\mathrm{glac}}$ correction. While we found that the error from keeping the single overpass samples in our trend estimates is smaller than the uncertainty from not applying $c_{\mathrm{glac}}$ we recommend removing these samples as the introduced bias corresponds to a systematic flattening of the trend. It should be kept in mind that for winter trends (summer trends on the southern hemisphere) this might affect most, if not all, of the March 2003 campaign samples due to the different ground track pattern of that campaign.

Correction of per-glacier offset is only possible in our study because the glaciers seem to mostly correspond to spatial units of consistent DEM age in Norway. The correction factor is independent of (not available) metadata for data quality and does not correspond to nor help to correct offsets of the surrounding terrain. In our case, zero-land trend, therefore, does not guarantee the absence of a time-dependent bias for glacier samples (with different distribution in terms of source date stamp). The assumption of a constant vertical offset per glacier is not necessarily valid everywhere, e.g. Swiss glaciers were not considered as unities in the mosaicking of airborne DEM acquisition flight lines but sometimes cut right across (M. Hölzle, personal communication, 2015). This resulted in differently timed outlines and elevation data for parts of the same glacier, further complicating DEM differencing with historic DEMs in the Alps, as done by Fischer et al. (2015). We faced similar challenges in our attempts

to co-register ICESat and the reference DEMs. The spatial units (tiles or source time stamp of elevation contours) available to us did not correspond entirely with spatial units of data origin that would exhibit a constant spatial shift or elevation error. Other DEMs for larger areas, and especially national DEMs, are likely to contain similar inherent errors as we found for the Kartverket DEM, and Fischer et al. (2015) for historic Swiss DEMs, as they all consist of a patchwork of source data sets with various time stamps – especially in remote areas. Metadata on elevation data sources are rarely available, and DEMs might have been (post-) processed to optimize characteristics other than high elevation accuracy, for instance smoothness or realistic visual appearance.

Global DEMs, such as the ASTER GDEMs or the upcoming TanDEM-X DEM, might also be a composite of numerous units of unknown or different age or elevation biases. While the radar-based elevations from the SRTM were acquired within a short time frame which eliminates DEM age error, the DEM still remains a patchwork from acquisitions from different overpasses, and elevation differences to ICESat elevations were found to vary spatially (e.g. Carabajal and Harding, 2006). Van Niel et al. (2008) found that shifts of subpixel magnitude result in artificially generated elevation differences of the same magnitude as the actual, measured elevation differences between the SRTM and national higher-resolution DEMs for two mountainous test sites in Australia and China. As an additional source of uncertainty for radar-based DEMs when serving as reference elevation, radar penetration into snow and ice is estimated to be in the range of several metres (Gardelle et al., 2012; Kääb et al., 2015) and can be considered to be another type of spatial pattern to which our per-glacier correction could be of benefit. However, further analyses on this end would be necessary, given the strong gradients and differences in snow/ice consistency between accumulation and ablation zones of a glacier that make radar penetration vary strongly even within a single glacier (Dall et al., 2001; Müller, 2011; Rignot et al., 2001).

ICESat GLAS data come with numerous correction terms which might signal uncertainty in the elevation values. For saturation correction, which is in the order of decimetres, we showed that the effect is negligible over rough mountain terrain and does not affect our results. Moreover, the saturation flag does not necessarily correspond with lower quality data over mountainous terrain, neither on ice nor land surfaces. The correction might not capture the effect of waveform saturation over such terrain appropriately. It is not generally recommended for land surfaces (NSIDC, 2012), and the error potentially resulting from waveform saturation is in the order of decimetres only. However, Molijn et al. (2011) found a larger occurrence of saturated samples at the transition from (rough) glacier-free terrain to (flat) glacier surfaces in the Dry Valleys in Antarctica. This can be explained with the adaptive gain setting of ICESat's GLAS instrument: the gain of the sensor is dynamically adjusted based on the recorded signal (NSIDC, 2012) and might not adapt fast enough for an abrupt change in the recorded waveform shapes between a footprint on dark, rough rocks and a flat, bright ice surface. A preferred occurrence of saturated samples and subsequent elevation error at glacier margins, where surface elevation changes are likely more pronounced, could potentially lead to a systematic bias in ICESat-derived glacier surface elevation change trends. In our study area we could not detect a systematic pattern in the spatial distribution of the saturated samples or where ICESat passes over glacier margins and experiences a land/ice surface type change. We believe that this is due to the small size of mountain glaciers and the rough surface topography both on land and glaciers (compared to large Antarctic outlet glaciers) that never really allowed the sensor to settle for a certain gain. Nevertheless, from the findings of Molijn et al. (2011) we cannot exclude that there is potential for a systematic bias from waveform saturation at ice/land transitions in other areas, and we recommend considering this possibility when applying our method in an arbitrary glacier region.

Likewise, other available corrections and biases of even smaller magnitude, such as intercampaign bias ($< 8$ cm, Hofton et al., 2013), the optional range increment for land samples (d_ldRngOff), and the GmC correction introduced in GLAS data of release 34 are of negligible importance compared to corrections applied to the reference DEM elevations. However, it cannot be excluded that these corrections might become relevant if a reference DEM without vertical bias were available, which would eliminate the current main error source.

On stable ground, the problem of time-dependent elevation differences due to surface elevation change is not present, but the artificial dh resulting from subpixel shifts or elevation-dependent errors were still found to compete with real, measured differences between the DEMs. This mainly has implications on the size of spatial and temporal units needed to aggregate footprints to get meaningful results. The example of Hardangervidda illustrates the potential of results on a local scale for areas with good quality reference elevations. Thereby, spatial resolution of the reference DEM is of less importance than the absence of (spatially varying) shifts or other biases in the data, resulting in narrower dh distributions of the low-resolution SRTM DEM compared to the Kartverket DEM, which seems to be of poorer quality in this area. However, the DEM resolution has to be small enough to appropriately capture the local relief variations. In more rugged terrain with large elevation variation within a single footprint, the spatial resolution of the DEM would likely play a more important role than on rather flat areas like Hardangervidda. We found the reference DEM rather than ICESat to limit more localized results that would reflect spatial variation or patterns of glacier change within the study area.

For glacier trend applications, the time to collect better reference DEMs for improved retrospect ICESat analyses has likely passed where glaciers experienced large changes in volume over the past decade. Still, the biases in the old ref-

erence DEMs of our study, originating from 10 to 20 years prior to the ICESat acquisition period, obviously became detectable and quantifiable. This fact underlines that ICESat data fully bear the potential to serve as a sample of glacier surface elevations in the 2000s even for areas where we currently do not yet have very accurate reference DEMs.

## 6 Conclusion

For the example of southern Norway, we show that ICESat elevations normalized to a reference DEM are fully capable of providing robust and realistic glacier surface elevation trends for the years 2003–2008 in mountainous terrain with scattered small- and medium-size glaciers. We estimate an average ice surface elevation change of $-0.39 \pm 0.07$ m (robust fit) and $-0.33 \pm 0.07$ m ($t$ fit) ice per year in 2003–2008 for southern Norwegian glaciers. Our estimate corresponds very well to the area-weighted average of observed cumulative mass balances from in situ and geodetic mass balance measurements on eight glaciers in the study area.

Despite sparse glacier cover of the study area, the coarse spatial sample of ICESat represents southern Norwegian glaciers accurately in terms of elevation, slope, aspect, spatial location, and area of the glaciers. Representativeness of the sample is also given for individual campaigns, and is a prerequisite for robust trend results. Non-representative campaigns have the potential to alter trends. Especially in terms of glacier area, ICESat samples reflect the size distribution of all glaciers in southern Norway considerably better than the (predominantly large) glaciers included in the in situ mass balance network in Norway.

The number of ICESat footprints on glaciers (1233 after filtering) within the study area was found to be large enough to allow for spatial and thematic subsampling. The considerable differences between trends from different sample subsets reflect the wide range of observed cumulative mass balances in the study area. Reasonably, we see a more negative elevation trend of continental and small glaciers compared to coastal or large glaciers respectively. Our glacier elevation change trends thus capture very varied glacier behaviour within the study area, and also depict glaciers with positive mass balance, as seen for Myklebustbreen and Hansebreen. On this example, we show that it may be possible to detect trends even for single well-covered glaciers, but with increased uncertainty due to spatially clumped sampling and missing data for some campaigns.

The applicability of ICESat in arbitrary glacierized regions depends on a combination of factors rather than a minimum region or sample size. The number of samples is determined by glacier density in relation to ICESat track density and the topography/climate-determined fraction of valid elevation measurements in the study region. Their representativeness, however, depends on the homogeneity of both the glacier topographic setting and their mass balance signal within the study area, as well as other spatially varying effects such as from DEM elevation bias. These factors are inherent for each region (and reference DEM) and will affect the sample/area size needed for a valid surface elevation change estimate. Uncertainties in reference DEM elevations exceed ICESat uncertainties by a magnitude. Elevation bias of unknown spatial units of the three assessed reference DEMs add noise that match or exceed measured elevation differences. These biases result from subpixel horizontal and vertical shifts, elevation-dependent bias, and varying source time stamps of the reference DEM of up to 20 years prior to ICESat acquisition. If not accounted for, spatially varying biases in combination with varying sample distribution over time may not cancel out and can affect the results by causing false trends. Representativeness of the sample in terms of such spatially varying bias in the reference DEM was found to be more important (and less given) than for terrain parameters like elevation or aspect. Due to their coarse spatial pattern, the DEM errors add varying but systematic bias in contrast to the random effects from geographic ICESat footprint distribution.

We developed a new per-glacier correction to harmonize the effect of age-dependent offsets between ICESat and the patchy reference DEM of unknown, but spatially varying source date. This correction greatly increased the statistical significance and robustness of our glacier change trend, and single campaigns also fit measured mass balance after application of the correction. For national or global DEMs in other regions, we see large potential from this correction or modified versions of it, for reducing glacier trend uncertainty related to spatio-temporal biases, such as from imperfect mosaicking, orbit inaccuracies, or radar penetration.

Our study shows that ICESat analyses in mountain terrain are currently limited by the reference DEMs rather than ICESat performance. ICESat provides an accurate sample of global glacier surface elevations in the 2000s. There is still large potential, even several years after the mission ended, for new upcoming DEMs to improve ICESat analysis in retrospect (e.g. TanDEM-X, new mapping agency DEMs). After its launch, ICESat2, with its denser cross- and along-track sampling and improved performance over rough surfaces (Kramer, 2015), will have the capability to provide an even more detailed, accurate, and valuable sample of glacier surface elevations using the methods outlined here.

## 7 Data availability

All data sources are given in Sect. 2.

**The Supplement related to this article is available online at doi:10.5194/tc-10-2129-2016-supplement.**

*Author contributions.* Désirée Treichler designed the study, performed data analyses, and prepared the manuscript. Andreas Kääb designed the study and edited the manuscript.

*Acknowledgements.* The study was funded by the European Research Council under the European Union's Seventh Framework Programme (FP/2007–2013)/ERC grant agreement no. 320816, the ESA project Glaciers_cci (4000109873/14/I-NB) and the Department of Geosciences, University of Oslo. We are very grateful to NASA and USGS for free provision of the ICESat data and the SRTM DEM respectively, to the Norwegian mapping agency for their topographic DEMs, and to the Norwegian Water Resources and Energy Directorate for glacier outlines, mass balance data, and the Hardangervidda lidar DEM.

Edited by: G. H. Gudmundsson
Reviewed by: R. C. Lindenbergh and one anonymous referee

## References

Andreassen, L. M. and Winsvold, S. H. (Eds.): Inventory of Norwegian glaciers, NVE Rapport 38, Norges Vassdrags- og energidirektorat, 236 pp., 2012.

Andreassen, L. M., Elvehøy, H., Kjøllmoen, B., Engeset, R. V., and Haakensen, N.: Glacier mass-balance and length variation in Norway, Ann. Glaciol., 42, 317–325, doi:10.3189/172756405781812826, 2005.

Andreassen, L. M., Elvehøy, H., Kjøllmoen, B., and Engeset, R. V.: Reanalysis of long-term series of glaciological and geodetic mass balance for 10 Norwegian glaciers, The Cryosphere, 10, 535–552, doi:10.5194/tc-10-535-2016, 2016.

Bahr, D. B. and Radić, V.: Significant contribution to total mass from very small glaciers, The Cryosphere, 6, 763–770, doi:10.5194/tc-6-763-2012, 2012.

Bliss, A., Hock, R., and Radić, V.: Global response of glacier runoff to twenty-first century climate change, J. Geophys. Res.-Earth, 119, 717–730, doi:10.1002/2013jf002931, 2014.

Bolch, T., Sørensen, L. S., Simonsen, S. B., Mölg, N., Machguth, H., Rastner, P., and Paul, F.: Mass loss of Greenland's glaciers and ice caps 2003–2008 revealed from ICESat laser altimetry data, Geophys. Res. Lett., 40, 875–881, doi:10.1002/grl.50270, 2013.

Carabajal, C. C. and Harding, D. J.: SRTM C-Band and ICESat Laser Altimetry Elevation Comparisons as a Function of Tree Cover and Relief, Photogr. Sci. Eng., 72, 287–298, 2006.

Cogley, J. G.: Geodetic and direct mass-balance measurements: comparison and joint analysis, Ann. Glaciol., 50, 96–100, 2009.

Dall, J., Madsen, S. N., Keller, K., and Forsberg, R.: Topography and penetration of the Greenland Ice Sheet measured with Airborne SAR Interferometry, Geophys. Res. Lett., 28, 1703–1706, doi:10.1029/2000gl011787, 2001.

Farr, T. G. and Kobrick, M.: Shuttle radar topography mission produces a wealth of data, Eos T. A. Geophys. Un., 81, 583–585, doi:10.1029/EO081i048p00583, 2000.

Farr, T. G., Rosen, P. A., Caro, E., Crippen, R., Duren, R., Hensley, S., Kobrick, M., Paller, M., Rodriguez, E., Roth, L., Seal, D., Shaffer, S., Shimada, J., Umland, J., Werner, M., Oskin, M., Burbank, D., and Alsdorf, D.: The Shuttle Radar Topography Mission, Rev. Geophys., 45, RG2004, doi:10.1029/2005rg000183, 2007.

Fischer, M., Huss, M., Barboux, C., and Hoelzle, M.: The new Swiss Glacier Inventory SGI2010: relevance of using high-resolution source data in areas dominated by very small glaciers, Arct. Antarct. Alp. Res., 46, 933–945, doi:10.1657/1938-4246-46.4.933, 2014.

Fischer, M., Huss, M., and Hoelzle, M.: Surface elevation and mass changes of all Swiss glaciers 1980–2010, The Cryosphere, 9, 525–540, doi:10.5194/tc-9-525-2015, 2015.

Gardelle, J., Berthier, E., and Arnaud, Y.: Impact of resolution and radar penetration on glacier elevation changes computed from DEM differencing, J. Glaciol., 58, 419–422, doi:10.3189/2012JoG11J175, 2012.

Gardner, A. S., Moholdt, G., Cogley, J. G., Wouters, B., Arendt, A. A., Wahr, J., Berthier, E., Hock, R., Pfeffer, W. T., Kaser, G., Ligtenberg, S. R. M., Bolch, T., Sharp, M. J., Hagen, J. O., van den Broeke, M. R., and Paul, F.: A Reconciled Estimate of Glacier Contributions to Sea Level Rise: 2003 to 2009, Science, 340, 852–857, doi:10.1126/science.1234532, 2013.

GLIMS and NSIDC: GLIMS Glacier Database, Version 1, NSIDC: National Snow and Ice Data Center, Boulder, Colorado USA, doi:10.7265/N5V98602, 2005, updated 2012.

Hofton, M. A., Luthcke, S. B., and Blair, J. B.: Estimation of ICESat intercampaign elevation biases from comparison of lidar data in East Antarctica, Geophys. Res. Lett., 40, 5698–5703, doi:10.1002/2013gl057652, 2013.

Howat, I. M., Smith, B. E., Joughin, I., and Scambos, T. A.: Rates of southeast Greenland ice volume loss from combined ICESat and ASTER observations, Geophys. Res. Lett., 35, L17505, doi:10.1029/2008gl034496, 2008.

Huss, M.: Density assumptions for converting geodetic glacier volume change to mass change, The Cryosphere, 7, 877–887, doi:10.5194/tc-7-877-2013, 2013.

Immerzeel, W. W., van Beek, L. P. H., and Bierkens, M. F. P.: Climate Change Will Affect the Asian Water Towers, Science, 328, 1382–1385, doi:10.1126/science.1183188, 2010.

Jacob, T., Wahr, J., Pfeffer, W. T., and Swenson, S.: Recent contributions of glaciers and ice caps to sea level rise, Nature, 482, 514–518, doi:10.1038/nature10847, 2012.

Jansson, P., Hock, R., and Schneider, T.: The concept of glacier storage: a review, J. Hydrol., 282, 116–129, doi:10.1016/S0022-1694(03)00258-0, 2003.

Kääb, A., Berthier, E., Nuth, C., Gardelle, J., and Arnaud, Y.: Contrasting patterns of early twenty-first-century glacier mass change in the Himalayas, Nature, 488, 495–498, doi:10.1038/nature11324, 2012.

Kääb, A., Treichler, D., Nuth, C., and Berthier, E.: Brief Communication: Contending estimates of 2003–2008 glacier mass balance over the Pamir–Karakoram–Himalaya, The Cryosphere, 9, 557–564, doi:10.5194/tc-9-557-2015, 2015.

Kartverket: Terrengmodeller – land, Kartverket; available at: http://www.kartverket.no/Kart/Kartdata/Terrengmodeller/Terrengmodell-10-meters-grid/, last accessed: 6 June 2016.

Ke, L., Ding, X., and Song, C.: Heterogeneous changes of glaciers over the western Kunlun Mountains based on ICESat and Landsat-8 derived glacier inventory, Remote Sens. Environ., 168, 13–23, doi:10.1016/j.rse.2015.06.019, 2015.

Kjøllmoen, B., Andreassen, L. M., Engeset, R. V., Elvehøy, H., Jackson, M., and Giesen, R. H.: Glaciological investigations in Norway in 2005, edited by: Kjøllmoen, B., Norwegian Water Resources and Energy Directorate (NVE), Oslo, Norway, NVE Report 2 2006, 99 pp., 2006.

Kjøllmoen, B., Andreassen, L. M., Elvehøy, H., Jackson, M., Giesen, R. H., and Tvede, A. M.: Glaciological investigations in Norway in 2008, edited by: Kjøllmoen, B., Norwegian Water Resources and Energy Directorate (NVE), Oslo, Norway, NVE Report 2 2009, 80 pp., 2009.

Kjøllmoen, B., Andreassen, L. M., Elvehøy, H., Jackson, M., and Giesen, R. H.: Glaciological investigations in Norway in 2009, edited by: Kjøllmoen, B., Norwegian Water Resources and Energy Directorate (NVE), Oslo, Norway, NVE Report 2, 85 pp. + app., 2010.

Kjøllmoen, B., Andreassen, L. M., Elvehøy, H., Jackson, M., and Giesen, R. H.: Glaciological investigations in Norway in 2010, edited by: Kjøllmoen, B., Norwegian Water Resources and Energy Directorate (NVE), Oslo, Norway, NVE Report 3, 89 pp. + app., 2011.

Kramer, H. J.: ICESat-2 (Ice, Cloud and land Elevation Satellite-2), available at: https://directory.eoportal.org/web/eoportal/satellite-missions/i/icesat-2, last access: 20 November 2015.

Kropáček, J., Neckel, N., and Bauder, A.: Estimation of Mass Balance of the Grosser Aletschgletscher, Swiss Alps, from ICESat Laser Altimetry Data and Digital Elevation Models, Remote Sens., 6, 5614, doi:10.3390/rs6065614, 2014.

Lange, K. L., Little, R. J. A., and Taylor, J. M. G.: Robust Statistical Modeling Using the T-Distribution, J. Am. Stat. Assoc., 84, 881–896, doi:10.2307/2290063, 1989.

Marzeion, B., Jarosch, A. H., and Hofer, M.: Past and future sea-level change from the surface mass balance of glaciers, The Cryosphere, 6, 1295–1322, doi:10.5194/tc-6-1295-2012, 2012.

Melvold, K. and Skaugen, T.: Multiscale spatial variability of lidar-derived and modeled snow depth on Hardangervidda, Norway, Ann. Glaciol., 54, 273–281, doi:10.3189/2013AoG62A161, 2013.

Moholdt, G., Nuth, C., Hagen, J. O., and Kohler, J.: Recent elevation changes of Svalbard glaciers derived from ICESat laser altimetry, Remote Sens. Environ., 114, 2756–2767, doi:10.1016/j.rse.2010.06.008, 2010.

Molijn, R. A., Lindenbergh, R. C., and Gunter, B. C.: ICESat laser full waveform analysis for the classification of land cover types over the cryosphere, Int. J. Remote Sens., 32, 8799–8822, doi:10.1080/01431161.2010.547532, 2011.

Müller, K.: Microwave penetration in polar snow and ice: Implications for GPR and SAR, PhD thesis, Department of Geosciences, University of Oslo, Norway, 2011.

NASA JPL: NASA Shuttle Radar Topography Mission Global 30 arc second, NASA LP DAAC, doi:10.5067/MEaSUREs/SRTM/SRTMGL30.002, 2013.

Neckel, N., Kropáček, J., Bolch, T., and Hochschild, V.: Glacier mass changes on the Tibetan Plateau 2003–2009 derived from ICESat laser altimetry measurements, Environ. Res. Lett., 9, 014009, doi:10.1088/1748-9326/9/1/014009, 2014.

Nesje, A., Bakke, J., Dahl, S. O., Lie, Ø., and Matthews, J. A.: Norwegian mountain glaciers in the past, present and future, Global Planet. Change, 60, 10–27, doi:10.1016/j.gloplacha.2006.08.004, 2008.

Nilsson, J., Sandberg Sørensen, L., Barletta, V. R., and Forsberg, R.: Mass changes in Arctic ice caps and glaciers: implications of regionalizing elevation changes, The Cryosphere, 9, 139–150, doi:10.5194/tc-9-139-2015, 2015.

NSIDC: GLAS Altimetry HDF5 Product Usage Guide, NASA DAAC at the National Snow and Ice Data Center, Boulder, Colorado USA, 2012.

NSIDC: GLAS/ICESat L1 and L2 Global Altimetry Data, Version 34, NASA DAAC at the National Snow and Ice Data Center, Boulder, Colorado USA, available at: http://nsidc.org/data/docs/daac/glas_icesat_l1_l2_global_altimetry.gd.html, 2014.

NVE: Glacier outlines, Norges Vassdrags- og energidirektorat, digital data available at: https://www.nve.no/hydrology/glaciers/glacier-data, last access: 28 August 2016.

Nuth, C. and Kääb, A.: Co-registration and bias corrections of satellite elevation data sets for quantifying glacier thickness change, The Cryosphere, 5, 271–290, doi:10.5194/tc-5-271-2011, 2011.

Nuth, C., Moholdt, G., Kohler, J., Hagen, J. O., and Kääb, A.: Svalbard glacier elevation changes and contribution to sea level rise, J. Geophys. Res., 115, doi:10.1029/2008jf001223, 2010.

NVE: Climate indicator products, Norwegian Water Resources and Energy Directorate, online glacier database, available at: http://glacier.nve.no/viewer/CI/ (last access: 31 May 2016), 2016.

Rabus, B., Eineder, M., Roth, A., and Bamler, R.: The shuttle radar topography mission – a new class of digital elevation models acquired by spaceborne radar, ISPRS J. Photogramm., 57, 241–262, doi:10.1016/S0924-2716(02)00124-7, 2003.

Radić, V. and Hock, R.: Regionally differentiated contribution of mountain glaciers and ice caps to future sea-level rise, Nat. Geosci., 4, 91–94, doi:10.1038/Ngeo1052, 2011.

Radić, V., Bliss, A., Beedlow, A. C., Hock, R., Miles, E., and Cogley, J. G.: Regional and global projections of twenty-first century glacier mass changes in response to climate scenarios from global climate models, Clim. Dynam., 42, 37–58, doi:10.1007/s00382-013-1719-7, 2014.

Rignot, E., Echelmeyer, K., and Krabill, W.: Penetration depth of interferometric synthetic-aperture radar signals in snow and ice, Geophys. Res. Lett., 28, 3501–3504, doi:10.1029/2000gl012484, 2001.

Schutz, B. E., Zwally, H. J., Shuman, C. A., Hancock, D., and DiMarzio, J. P.: Overview of the ICESat Mission, Geophys. Res. Lett., 32, L21S01, doi:10.1029/2005gl024009, 2005.

Slobbe, D. C., Lindenbergh, R. C., and Ditmar, P.: Estimation of volume change rates of Greenland's ice sheet from ICESat data using overlapping footprints, Remote Sens. Environ., 112, 4204–4213, doi:10.1016/j.rse.2008.07.004, 2008.

Street, J. O., Carroll, R. J., and Ruppert, D.: A Note on Computing Robust Regression Estimates via Iteratively Reweighted Least Squares, Am. Stat., 42, 152–154, doi:10.2307/2684491, 1988.

Van Niel, T. G., McVicar, T. R., Li, L., Gallant, J. C., and Yang, Q.: The impact of misregistration on SRTM and DEM image differences, Remote Sens. Environ., 112, 2430–2442, doi:10.1016/j.rse.2007.11.003, 2008.

Viviroli, D., Dürr, H. H., Messerli, B., Meybeck, M., and Weingartner, R.: Mountains of the world, water towers for humanity: Typology, mapping, and global significance, Water Resour. Res., 43, W07447, doi:10.1029/2006wr005653, 2007.

Winsvold, S. H., Andreassen, L. M., and Kienholz, C.: Glacier area and length changes in Norway from repeat inventories, The Cryosphere, 8, 1885–1903, doi:10.5194/tc-8-1885-2014, 2014.

Zemp, M., Frey, H., Gärtner-Roer, I., Nussbaumer, S. U., Hoelzle, M., Paul, F., Haeberli, W., Denzinger, F., Ahlstrøm, A. P., Anderson, B., and others: Historically unprecedented global glacier decline in the early 21st century, J. Glaciol., 61, 745–762, doi:10.3189/2015JoG15J017, 2015.

Zwally, H. J., Schutz, R., Bentley, C., Bufton, J., Herring, T., Minster, J., Spinhirne, J., and Thomas, R.: GLAS/ICESat L2 Global Land Surface Altimetry Data (HDF5), Version 33, GLAH14, NASA DAAC at the National Snow and Ice Data Center, Boulder, Colorado USA, doi:10.5067/ICESAT/GLAS/DATA207, 2012.

# Part III

# Appendix

# Appendix A

# Co-authored publications, proceedings and presentations

## Co-authored publications

Kääb, A., Treichler, D., Nuth, C., and Berthier, E., 2015. Brief Communication: Contending estimates of 2003–2008 glacier mass balance over the Pamir–Karakoram–Himalaya. The Cryosphere, vol. 9, pp. 557–564. doi:10.5194/tc-9-557-2015.

## Proceedings

Treichler, D., Kääb, A., and Melvold, K., 2016. Across spatial scales: Snow depth from satellite and airborne LiDAR combined. Proceedings of the 2nd Virtual Geoscience Conference, Bergen, Norway, 21–23 September 2016. [Poster]

## Conference presentations (first-author only)

Treichler, D., Kääb, A., Salzmann, N., and Shea, J., 2016. Recent glacier changes in High Mountain Asia: A spatially diverse pattern. General Assembly of the American Geoscience Union (AGU), San Francisco, USA, 12–16 December 2016. [Presentation]

Treichler, D., Kääb, A., 2015. Snow depth estimates from ICESat laser data — a case study in southern Norway. IGS Nordic Branch Meeting, Copenhagen, Denmark, 29–31 October 2015. [Presentation]

Treichler, D., Kääb, A., Nuth, C., and Berthier, E., 2015. Hydrological implications of glacier mass changes in High Mountain Asia derived from ICESat laser altimetry. International Glaciological Society (IGS) International Symposium on Glaciology in High-Mountain Asia, Kathmandu, Nepal, 2–6 March 2015. [Presentation]

Treichler, D., and Kääb, A., 2014. Potential and limitations of ICESat over small mountain glaciers. General Assembly of the AGU, San Francisco, USA, 15–19 December 2014. [Presentation]

Treichler, D., and Kääb, A., 2013. Potential of ICESat data for glacier mass balance trend estimation in Southern Norway. IGS Nordic Branch Meeting, Lammi, Finland, 31 October–2 November 2013. [Presentation]

## Invited presentations

Treichler, D., Kääb, A., Nuth, C., and Berthier, E. 2015. Glacier surface elevation trends from ICESat: potential and pitfalls — Norway and High Mountain Asia. Department of Geosciences, University of Fribourg, Fribourg, Switzerland, 2 June 2015.

Treichler, D., Kääb, A., Nuth, C., and Berthier, E. 2016. HMA's glaciers seen by a space laser — potential and pitfalls of continental-scale remote sensing. Brown bag seminar, International Centre for Integrated Mountain Development (ICIMOD), Kathmandu, Nepal, 8 April 2016.